UIDE

Powered by
Arizona State University

ING. AUTOMOTRIZ

Trabajo integración Curricular previa a la obtención del título de Ingeniería en Mecánica Automotriz

AUTORES:
Bilaña Ortega Jasón Mateo
Monar Rodríguez Johan Gabriel

TUTOR:
Ing. Juan Carlos Rubio Terán, MBA

Análisis de las variables brillo y color en pintura automotriz, provocados por efectos de los solventes, bajo norma ASTM D523.

QUITO – ECUADOR | 2023

CERTIFICACIÓN DE AUTORÍA

Nosotros, Bilaña Ortega Jasón Mateo, Monar Rodríguez Johan Gabriel, declaramos bajo juramento, que el trabajo aquí descrito es de nuestra autoría; que no ha sido presentado anteriormente para ningún grado o calificación profesional y que se ha consultado la bibliografía detallada.

Cedemos nuestros derechos de propiedad intelectual a la Universidad Internacional del Ecuador, para que sea publicado y divulgado en internet, según lo establecido en la Ley de Propiedad Intelectual, su reglamento y demás disposiciones legales.

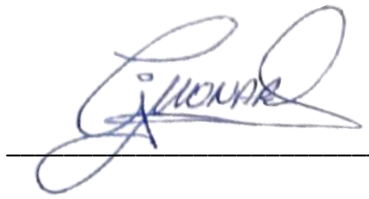

Bilaña Ortega Jasón Mateo

Monar Rodríguez Johan Gabriel

APROBACIÓN DEL TUTOR

Yo, **Ing. Juan Carlos Rubio Terán**, certifico que conozco a los autores del presente trabajo, siendo el responsable exclusivo tanto de su originalidad y autenticidad, como de su contenido.

_____

Ing. Juan Carlos Rubio, MBA

DEDICATORIA

Esta tesis es dedicada para mi bisabuelo Pedro Tonato, a mis abuelos Segundo Ortega y Magdalena Tonato que los considero mis padres, inculcando en mi valores y fortalezas, para alcanzar y luchar por cada una de mis metas, mis padres biológicos Edwin Bilaña y Angélica Ortega, mis hermanos Jhonier y Kirenia Bilaña, mi tía Norma Ortega y hermana Wendy Topa que siempre estuvieron en el camino de esta gran pasión con varios momentos de alegría, tristeza y éxito, gracias por ser, estar y ser ese apoyo incondicional, tengo el gran honor de pertenecer a esta familia, por más difícil que se tornara la situación, estuvieron con sus palabras de aliento y motivación a terminar de conseguir este tan anhelado sueño, por ultimo quiero dedicar este trabajo para todos aquellos que sueñan con ser profesionales en la rama de la mecánica automotriz.

Bilaña Ortega Jasón Mateo

DEDICATORIA

Dedicó este trabajo y toda mi carrera universitaria en la UIDE primeramente a Dios que es mi guía, mi fortaleza y siempre está conmigo en las buenas y en las malas.

Dedico todo mi esfuerzo a mi padre que me acompañó casi en toda mi carrera. pero ahora él está con Dios viéndome desde el cielo, apoyándome, ayudándome a crecer poco a poco, él siempre estuvo muy orgulloso de que un día me graduaría de Ingeniero Automotriz, pero por cuestiones de la vida no me puede acompañar en este gran logro, pero sé que desde cielo está muy orgulloso de mi.

Monar Rodríguez Johan Gabriel,

AGRADECIMIENTOYO

Quiero empezar agradeciendo a dios por brindarme la oportunidad de culminar mi carrera, a la Universidad Internacional del Ecuador UIDE en especial a la escuela de mecánica automotriz por abrirme las puertas y brindarme la oportunidad de continuar con este gran sueño, a mis padres, hermanos y familia en general que estuvieron presentes en cada momento de este maravilloso camino que culmina con este trabajo de investigación.

Bilaña Ortega Jasón Mateo

AGRADECIMIENTOYO

Finalmente quiero agradecer este nuevo alcance de mi vida, la culminación de mi trabajo a mi madre, a mis hermanos, a mi hijo y a mi novia quienes estuvieron conmigo para superar el dolor de perder a mi padre y poderme incentivar a culminar mi carrera hoy gracias a todos estoy cumpliendo un sueño más de vida.

Monar Rodríguez Johan Gabriel

INDICE DE CONTENIDO

DECLARATORIA ii
CERTIFICACION iii
APROBACION DEL TUTOR..... iv
DEDICATORIA v
AGRADECIMIENTO vi
ÍNDICE DE CONTENIDO viii
RESUMEN 1

1. INTRODUCCIÓN 2
2. MARCO TEÓRICO 7
3. MATERIALES 8
4. TOMA DE DATOS 11
5. PROCEDIMIENTO DE INGRESO HHO 12
6. CONCLUSIONES 19
7. REFERENCIAS BIBLIOGRÁFICAS 20

ANEXOS
INTRODUCCIÓN.....

1. ANEXO 1 23

ANEXOS MARCO TEORICO

1. ANEXO 2 60

ANEXO MATERIALES Y METODOS

1. ANEXO 1.....77
2. ANEXO 2 85
3. ANEXO 3 98
4. ANEXO 4 99

ANÁLISIS DE LAS VARIABLES BRILLO Y COLOR EN PINTURA AUTOMOTRIZ, PROVOCADOS POR EFECTOS DE LOS SOLVENTES, BAJO NORMA ASTM D523.

Ing. Juan Carlos Rubio Terán. MBA[1],Bilaña Ortega Jasón.[3], Monar Rodríguez Johan.[4]

[1] Ingeniería Automotriz - Universidad, Titulo Obtenido, email, jrubio@uide.edu.ec Quito – Ecuador
[3] Ingeniería Automotriz - Universidad Internacional del Ecuador, jabilañaor@uide.edu.ec
[3] Ingeniería Automotriz - Universidad Internacional del Ecuador, jomonarro@uide.edu.ec
Quito - Ecuador

RESUMEN

Este estudio se centra en el análisis de las variables de brillo y color en pintura automotriz, específicamente en relación con los efectos provocados por los solventes, siguiendo las pautas de la norma ASTM D523. La pintura automotriz es crítica para la apariencia y durabilidad de los vehículos, y factores como brillo y color son de gran importancia estética y de realce.

En la **introducción**, se destaca la relevancia de la calidad visual en la industria automotriz y se plantea la hipótesis de que los solventes podrían influir en las propiedades de brillo y color de la pintura. La **metodología** emplea la norma ASTM D523 para evaluar el brillo a partir de la medición de la reflectancia de la superficie y el color mediante análisis espectrofotométrico. Se someten muestras de pintura a diferentes tipos de solventes manteniendo la misma pintura base y color para determinar en esencia la incidencia en brillo y color.

Los **resultados** revelan una correlación significativa entre los diferentes tipos de solventes y la disminución del brillo de la pintura, así como cambios en los valores de color. Con el cambio de tipo de solvente, se observa una disminución gradual del brillo y una posible alteración en la tonalidad del color. Además, se identifican patrones consistentes de cambio en función del tipo de solvente utilizado.

En **conclusión**, este estudio evidencia que los solventes influyen de manera significativa en las propiedades de brillo y color de la pintura automotriz, lo que podría tener implicaciones en la calidad percibida del vehículo. Estos hallazgos destacan la importancia de un manejo cuidadoso de los solventes en el proceso de pintura automotriz y proporcionan información valiosa para la mejora de los estándares de **calidad en la industria automotriz.**

Palabras clave: Solventes, brillo, cambio de color, ASTM D523, pruebas, influencia alteraciones.

ABSTRACT

This study focuses on the analysis of gloss and color variables in automotive paint, specifically in relation to the effects caused by solvents, following the guidelines of the ASTM D523 standard. Automotive paint is critical to the appearance and durability of vehicles, and factors such as gloss and color are of great aesthetic importance.

In the introduction, the relevance of visual quality in the automotive industry is highlighted and it is hypothesized that solvents could influence the gloss and color properties of paint. The **methodology** uses ASTM D523 to assess gloss from surface reflectance measurement and color by spectrophotometric analysis. Paint samples are subjected to different types of solvents while maintaining the same base paint and color to essentially determine the incidence of gloss and color.

The **results** reveal a significant correlation between the different types of solvents and the decrease in paint gloss, as well as changes in color values. With the change of type of solvent, a gradual decrease in gloss and a possible alteration in the color tone is observed. In addition, consistent patterns of change are identified based on the type of solvent used.

In **conclusion**, this study shows that solvents significantly influence the gloss and color properties of automotive paint, which could have implications for the perceived quality of the vehicle. These findings highlight the importance of careful solvent management in the automotive painting process and provide valuable information for improving quality standards in the automotive industry.

Keywords: Solvents, gloss, color change, ASTM D523, tests, influence alterations.

INTRODUCCIÓN

El estudio analiza la necesidad de muchos usuarios así como la demanda de los concesionarios en entregar la mejor calidad y la satisfacción de sus cliente, las circunstancias actuales hace que se incluyan otros agentes del sector, así como las aseguradoras que dejando de lado la calidad pretenden ajustar los márgenes de ingresos tratan de bajar los costos y esto repercute en la calidad del trabajo final, siendo la calidad de materiales el elemento diferenciador para que puedan alcanzar esas metas y por obvias razones al termino del trabajo en el vehículo tenga muchas variaciones de coloración , brillo entre otras que los clientes perciben, las más recurrentes que los clientes mencionan tiene que ver con la intensidad del brillo, no es el mismo siendo más opaco que el original, la repintada no tiene el mismo color, existen diferencias entre el original y la pieza remplazada o repintada, o lo que no duran lo mismo siendo este uno de los menos recurrentes, que el brillo al corto tiempo se hace opaco, estos reclamos hacen pensar que las variantes que pueda incidir para generar el estudio y por qué existen esas variaciones.

La evaluación de las variables de brillo y color en pintura automotriz, que son una consecuencia de la acción de solventes, del tipo solvente o el tipo de laca que se utiliza para el repintado automotriz siendo esencial para garantizar la calidad estética y funcional de los vehículos. Este estudio busca analizar los efectos de los solventes en estas propiedades, siguiendo la norma ASTM D523.

Es importante resaltar que la calidad de la pintura no está en tela de duda para este estudio, se considera una pintura de alta calidad, así mismo la base de la pintura utilizada, para la investigación se presenta características de gran calidad, resaltando estos dos factores para la durabilidad así como para la estética final del proceso de pintado, él estudio se basa

en la incidencia que tienen los solventes al ser utilizados en las pinturas, ya que estos difieren en calidad, la misma que se relaciona con el precio de venta y al final afectan produciendo variaciones en el trabajo final pintado automotriz de los vehículos, determinando que los solventes pueden alterar significativamente el brillo, el color y la durabilidad de la pintura, el trabajo de investigación determina dos de los tres parámetros expuestos que son el incidencia en el brillo y la afectación en el color.

La metodología implica la preparación de muestras de pintura automotriz aplicadas en tres probetas de pruebas (planchas metálicas similares a la chapa de un vehículo) y su aplicación con diferentes tipos de solventes. La validación del brillo se realiza mediante la reflectancia "La reflectancia es el fenómeno en que un espectro de la luz es reflejado por la superficie de un objeto. El grado en que esto sucede depende del material del objeto pues determinados elementos absorben cierto espectro del rango luminoso mientras reflejan otro. El color reflejado es el que vemos" **Sárosi, Zoltán & Knapp, Wolfgang & Kunz, Andreas & Wegener, Konrad. (2010)** con la utilización de herramientas específicas para su efecto, y el análisis espectrofotométrico se emplea para evaluar los cambios en el color. Se llevan a cabo pruebas bajo condiciones controladas, siguiendo los lineamientos de la norma ASTM D523.

Figura #1 Ejemplos de índices de reflectancia de algunos materiales.

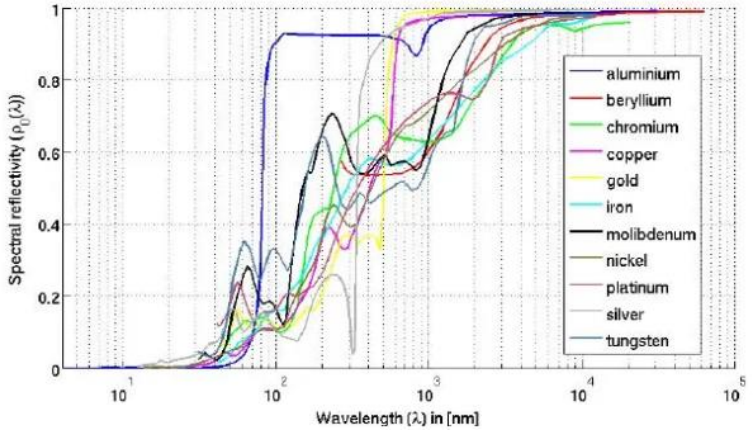

Fuente, Sárosi, Zoltán & Knapp, Wolfgang & Kunz, Andreas & Wegener, Konrad. (2010)

Los resultados revelan patrones significativos: a medida que aumenta la concentración de solventes, se observa una disminución gradual del brillo de la pintura, lo que puede influir en la apariencia del vehículo. Además, se detectan variaciones en los valores de color, lo que sugiere una alteración en la tonalidad. Los tipos de solventes también muestran efectos específicos en las propiedades evaluadas.

En conclusión, este estudio demuestra que los solventes ejercen un impacto considerable en las propiedades de brillo y color de la pintura automotriz, lo que subraya la necesidad de un manejo cuidadoso de estos productos químicos en la industria. Estos resultados ofrecen información crucial para mejorar la calidad y la durabilidad de la pintura en la utilización de vehículos, contribuyendo a la satisfacción del cliente y al mantenimiento de estándares superiores en la industria automotriz.

Marco Teórico

El análisis de las variables de brillo y color en pintura automotriz, influenciadas por los efectos de los solventes, es crucial para garantizar la calidad y apariencia de los vehículos. El brillo y el color son aspectos clave en la satisfacción del cliente y la percepción de calidad en la industria automotriz. La investigación se basa en la norma ASTM D523, que proporciona pautas estandarizadas para evaluar estas propiedades.

Los solventes son parte fundamental en el proceso químico de la pintura automotriz, al ser parte de la formula incide en el proceso de pintado o repintado, de la misma forma que afecta la calidad del terminado y tiempo de vida útil, sin dejar de mano que muchos de los solventes tienen un grado elevado de contaminación ambiental, es por ello que hoy en día se utilizan solventes de base de agua para mitigar los daños que se generan por el pintado o repintado a la naturaleza.

El trabajo de los solventes es dispersar o disolver los componentes como pigmentos, resinas o solidos de las pinturas para convertirlos en una solución liquida que se la pueda dispersar sobre una superficie uniforme y cubra con facilidad la zona aplicada, la selección de un adecuado solvente que no solo sea compatible con la base de la pintura permite que se logre la viscosidad adecuada de compuesto, permitiendo un proceso sencillo de aplicación, del solvente también depende la capacidad de secado y características como el brillo, intensidad del color y que el color no cambie su tonalidad.

La mayor parte de los solventes son derivados de los hidrocarburos entre ellos los aromáticos y alifáticos, pueden ser alcoholes, ésteres y cetonas, cada solvente tiene características específicas que juegan un papel preponderante en la formulación y en las características con referencia al rendimiento de la pintura. Por citar un ejemplo los solventes en base a hidrocarburos aromáticos son muy empleados por su capacidad de disolver una gran gama de resinas.

Los solventes no solo tienen incidencia en la formulación, aplicación y rendimientos, adicional a ello tienen implicaciones importantes en la contaminación ambiental, en el proceso de pintado las evaporaciones de los solventes aportan contaminantes al aire como los (COV) que adicional a la contaminación ambiental pueden tener efectos negativos para la salud de las personas que realizan el trabajo. “Los compuestos orgánicos volátiles (VOCs, por sus siglas en inglés) se emiten como gases por ciertos sólidos o líquidos. Los VOCs incluyen una variedad de sustancias químicas, algunas de las cuales pueden tener efectos adversos en la salud a corto y a largo plazo” **Agencia De Protección Ambiental De Los Estados Unidos (EPA), 2015**

La intensa búsqueda mundial en tratar de bajar cualquier tipo de contaminación ambiental o que afecte a la salud de los humanos ha hecho que se desarrollen solventes en base a base de agua que ya no desprende (VOC) que son más amigables con el medio ambiente y de que tienen un impacto menor para las personas. “"el desarrollo de pinturas más respetuosas con el medio ambiente es una tendencia importante en la industria de la pintura, y el solvente desempeña un papel crucial en este esfuerzo**" Hsu y Yu (2018)**

La metodología comprende la preparación de muestras de pintura automotriz y su exposición a diferentes tipos de solventes, emulando condiciones reales de uso. El brillo se mide mediante la reflectancia, evaluando cómo la intensidad de la luz reflejada cambia en función de los solventes. Para el análisis del color, se emplea la espectrofotometría, midiendo las diferencias en la absorbancia de longitudes de onda específicas.

Figura #2 Reflectancia.

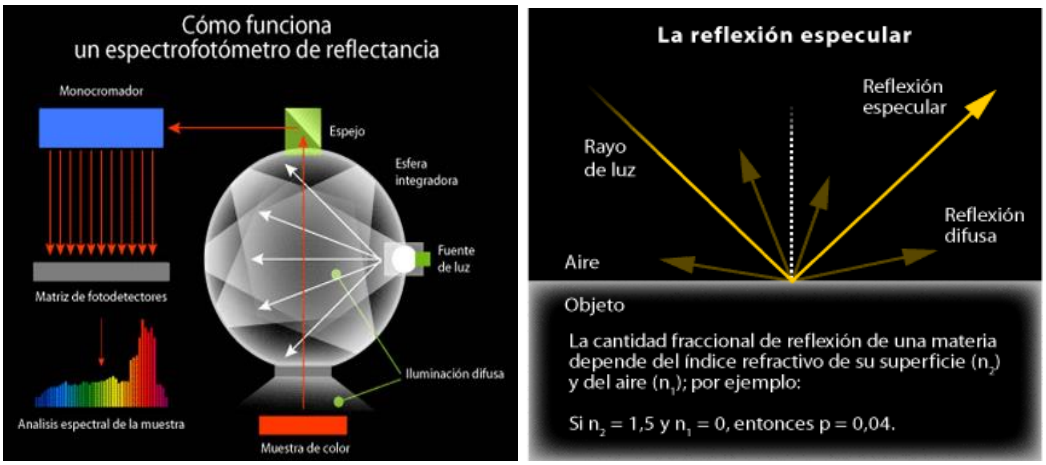

Fuente, Stephen Westland, febrero de 2001

Los resultados destacan que el aumento en la concentración de solventes conduce a una disminución del brillo en la pintura. Esta pérdida de brillo podría afectar negativamente la apariencia del vehículo. Además, se observan alteraciones en los valores de color, indicando cambios en la tonalidad de la pintura. Los tipos de solventes también generan efectos específicos en las propiedades evaluadas.

En resumen, este estudio demuestra que los solventes tienen un impacto significativo en las características de brillo y color de la pintura automotriz. La norma ASTM D523 proporciona un marco confiable para evaluar estas propiedades de manera estandarizada. Estos hallazgos respaldan la importancia de controlar y seleccionar los solventes utilizados en la producción de pintura automotriz para garantizar la calidad visual y la satisfacción del cliente en la industria automotriz.

Se describirá conceptos de la información necesaria para la estructura del artículo, enfocado en el tema a estudiar, es importante tener información de libros actualizados.

MATERIALES Y MÉTODOS

Planchas de acero de uso automotriz, Las tres placas metálicas son la base para la aplicación de todo el proceso de pintura y la realización de las pruebas, las dimensiones son 15cm largo x 10cm de ancho x 2mm de espesor, permite mite hacer el tratamiento del metal previo a la aplicación y adicional a ello permitirá hacer las pruebas respectivas de brillo y color.

Figura #3 Placas de ensayo.

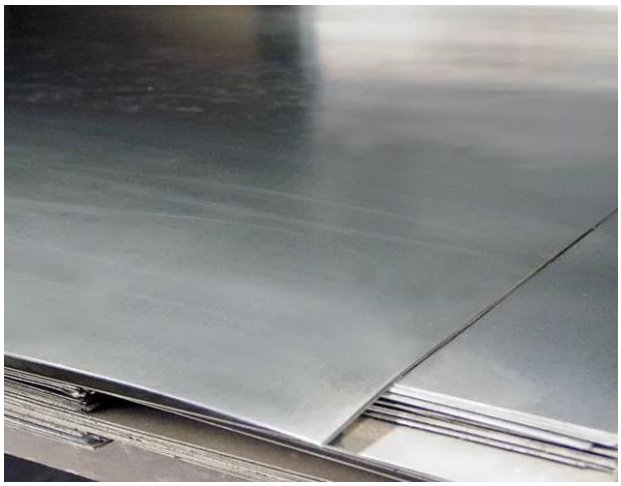

Fuente: Autores, 2023

Las placas son muestras de un segmento pequeño del vehículo, estas planchas de prueba son sometidas de inicio a la preparación de las mismas, la figura presenta en imágenes que no están aptas para su utilización al momento de la compra, las placas permiten la difusión de los diferentes procesos de pintura, así posterior al secado estas placas permites obtener los datos del estudio y son una evidencia de la investigación.

Resina o ligante, "La composición de una pintura determina su comportamiento en el momento de ser aplicada y el acabado final que presentará" **Locctite Teroson, 2015**. De la calidad de la resina depende de igual forma la adherencia y la calidad de la película de pintura que se deposita sobre ella, en la jerga automotriz se la conoce como fondo.

Figura #4 Resina adherente.

Fuente; Preparación autores, 2023

Pigmento "El pigmento es el compuesto encargado de cumplir una función determinada dentro de la composición de una pintura de carrocería, principalmente, dar un color, una textura o un efecto concreto" **Locctite Teroson, 2015**. Es la parte de la pintura que permite dar el color, la robustez y el espesor mayoritario, para los ensayos el color

seleccionado es rojo, esto se debe a que el uno de los colores con más conflictos de los clientes seguido del color negro, es por ello la toma la selección del color, como dato adicional dentro de los pigmentos hay algunas subdivisiones que permiten dar cuerpo a la pintura denominados de carga, de cubrición para darle un efecto de opacidad para resaltar los rasgos cromáticos, especiales para dar efectos como son los efectos metálicos, los perlados, los mismos cromados y efectos camaleón que depende del reflejo de la luz que los ilumina.

Figura #5 Pigmento de pruebas


Fuente, Autores, 2023

"**El disolvente** es el compuesto que le confiere una determinada fluidez a la pintura" **Locctite Teroson, 2015,** más conocidos como solventes de pintura es la parte primordial de estudio es la que permite que la pintura se aplique de forma uniforme en toda la superficie a cubrir, es la encarga de brindar una textura liza en la superficie

Medidor de Espesor de revestimiento de pintura permite determinar si las capas de pintura en las láminas de prueba sufren distorsión en la medida por los diferentes disolventes. Es una herramienta que tiene un rango de 0 – 1250 micras y lo que mide es el acho de la película de pintura.

Figura #6 Medidor de Espesor pintura

Fuente, Nicety Factory, 2022.

Medidor de brillo HOJILA GM-268 Medidor de brillo 20º 60º 85º Glossmeter con rango de 0.1~200 GU instrumento de ensayo para realizar la medida de brillo, mediante la utilización del equipo se determina la cantidad de brillo que cada placa refleja de acuerdo con el tipo de solvente, el equipo cumple con la norma ASTM D523 establecida para el estudio, adicional a ello permite identificar si la calidad de los disolventes va de la mano con el precio.

Figura #7 Medidor de brillo.

Fuente autores, 2023.

Norma ASTM D523 "ASTM D523 cubre la medición del brillo especular de muestras no metálicas para geometrías de medidor de brillo de 60º, 20º y 85º" **ASTM International, 2015** La metodología es experimental donde se ajusta a un proceso ya establecido que permite hacer un análisis estadístico comparativo y deductivo de los datos arrojados por los instrumentos de medida.

Resultados y Discusión

El analizar el brillo dentro del proceso de pintura con tres tipos de disolventes con calidades diferentes es poder determinar cómo éstos afectan en el terminado final de la pintura haciendo que la intensidad de brillo se afecta, siendo que los elementos constitutivos de fondo, pintura y barniz son los mismos con las mismas disoluciones en porcentajes y solo queda como elemento diferenciador el solvente y la calidad del mismo. Estos solventes en las mismas condiciones que con el brillo afectan también de una forma directa en la coloración es decir estos permite que se vea afectado la intensidad del color por lo que estudio permite verificar la variación del mismo con los diferentes solventes.

El estudio empieza en el corte y preparación de las planchas (3) donde se trabaja el proceso de pintura, mismas que deben ser tratadas para eliminar cualquier tipo de oxidación, impurezas o grasas que no permita que la pintura pueda incorporarse a ella o que con el tiempo puedan expulsar la capa adherida. Para ello se revisa que no tenga partes con presencia de oxidación, se hace la limpieza con disolventes para la eliminación de grasas adheridas que ayudan a evitar la oxidación del metal, posterior se realiza el proceso de lijado con una lija gruesa para la eliminación de grumos, pasando a una lija fina que deja la superficie lista para la imprimación de pintura, previo a la imprimación se realiza una última limpieza con disolvente para eliminar cualquier residuo que haya quedado.

Figura #8 Placas de metal para

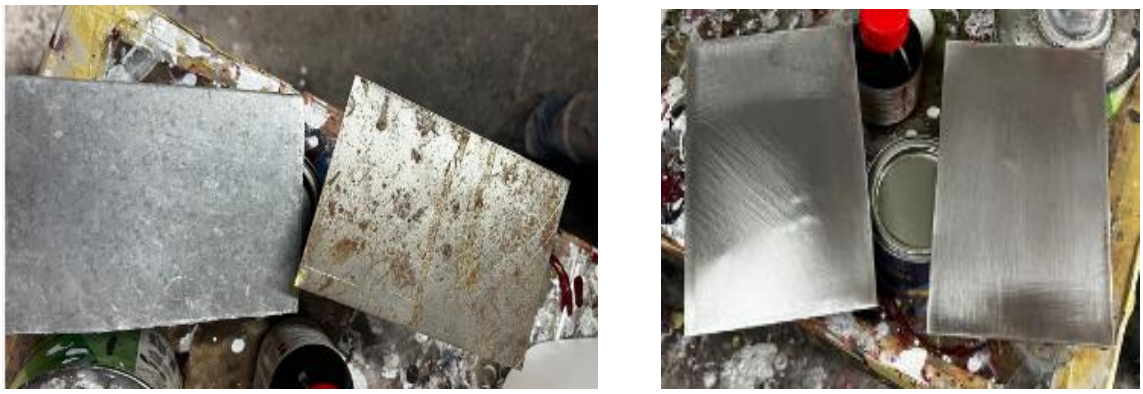

Fuente Autores, 2023.

Es importante recalcar que las placas de pruebas van a utilizar compontes en común como el fondo o resina, el pigmento o pintura, la laca o brillo y lo que no van a compartir y será particular en cada placa es el disolvente que es objeto de estudio en la investigación, como dato adicional los solventes son de distintas calidades y precios, sin que estos sean contraproducentes con su compatibilidad.

Con las placas lista se prepara la resina o fondo, cabe destacar que la resina necesita de un disolvente para su aplicación, la primera placa tiene el disolvente de menores prestaciones y así sucesivamente las dos placas subsiguientes van mejorando las prestaciones hasta llegar a la calidad superior, se prepara un base de resina o fonda para cada placa, la relación de porcentaje de concentración entre resina y disolvente son las mimas para todas las preparaciones, dejando claro que la variable del brillo y espesor final dependa exclusivamente de la calidad del solvente para esta investigación, si bien es cierto el proceso de pintura es manual y depende de la habilidad del pintor se ha tomado los parámetros necesarios para que sean lo más específicos posibles, la aplicación de la resina, del pigmento y de la laca se la hace en tres pasos, entre cada uno hay un proceso de secado.

Figura #9 Resina adherente.

Fuente, Autores 2023

La preparación de pigmento o pintura como se lo conoce en el mundo del repintado automotriz de igual forma no llega solo para su aplicación sino necesita de un disolvente para su aplicación, de la experiencia de los pintores se conoce que la cantidad de solvente va un poco de la mano de su experticia, algunos manifiestan que es mejor una cantidad mayor de disolvente que eso permite un secado más rápido y otros dicen que con un poco menos de lo recomendado porque da una capa más espesa y un mejor acabado, esto solo son comentarios de taller, es por esto que en el estudio se coloca por volumen (peso) el pigmento y el solvente para no dejar sesgos en el terminado final.

Figura #10 Aplicación del pigmento (pintura).

Fuente, Autores, 2023.

La laca o brillo de igual manera se aplica con disolvente, es por ello que el disolvente tiene una importancia primordial en el terminado, con la aplicación de la laca se termina con el proceso de pintado, posterior a ellos se presentan las placas para las medicas respectivas de acuerdo a lo planteado en la investigación, cabe señalar que cada aplicación tienen tres intervenciones hasta llegar al objetivo y en cada proceso de secado se sometió a las placas a un temperatura por lámparas de secado para que proceso de secado tengan los mismos parámetros.

Figura #11 Placas terminadas

Fuente; Autores,2023

Para el proceso de medición de las placas en primer lugar deben estar secas por completo, posterior a ello y con las placas identificadas se toma las lecturas de espesor de la pintura en cada una ellas, para genera un parámetro de comparación de las tres placas de prueba, la lectura de placa se la realiza por siete tomas para ya que se realiza con el método ANOVA para obtener el promedio y la varianza para establecer que las medidas sean correctas, al ser herramientas electrónicas y que su grado de precisión es muy alto los valores tomados son los mismos y se reflejan en la tabla.

Figura #12 Medición de espesor de pintura.

Fuente, Autores,2023

Las medidas encontradas se las tabula para el análisis comparativo entre las muestras del ensayo y definir su espesor.

Tabla #2 Datos de espesor de muestras.

LECTURA ESPESOR PINTURA EN MICRAS							
Placa	Lectura 1	Lectura 2	Lectura 3	Lectura 4	Lectura 5	Lectura 6	Lectura 7

Placa Disolvente 1	61	61	61	61	61	61	61
Placa Disolvente 2	59	59	59	59	59	59	59
Placa Disolvente 3	90	90	90	90	90	90	90

Fuente, Autores, 2023

Tablas #3 Resultados.

Grupos	*Cuenta*	*Suma*	*Promedio*	*Varianza*
Placa Disolvente 1	7	427	61,00	0,00
Placa Disolvente 2	7	413	59,00	0,00
Placa Disolvente 3	7	630	90,0	0,00

Fuente Autores, 2023

Los datos evidencia que el espesor de las placas pese a la utilización de los mismos insumos salvo el disolvente no son los mismos, y que aun así la calidad no determina el espesor que guarde relación con la calidad, se nota que con el disolvente de menos calidad tenemos un espesor superior al segundo, pero por debajo del tercero, la creencia hace pensar que a más espesor de la placa de pintura mejor duración y calidad, esto se confunde con el número de capas que se aplica, para el estudio se dio tres capas en cada proceso.

Los datos no siguen una lógica creciente o descendiente que se esperaría, si alternados, esto supondría que se deber a factores como la técnica del aplicador, la uniformidad de la superficie a pintar o la calidad de la pintura misma, al cuidar los detalles que evitan las condiciones de error del técnico, o de la superficie a pintar dejamos claro que la diferencia se produce solo por la calidad del disolvente. Este dato solo nos proporciona como afecta en el espesor o el cuerpo de la pintura el disolvente.

Tablas #4 Lecturas comparativas en placas.

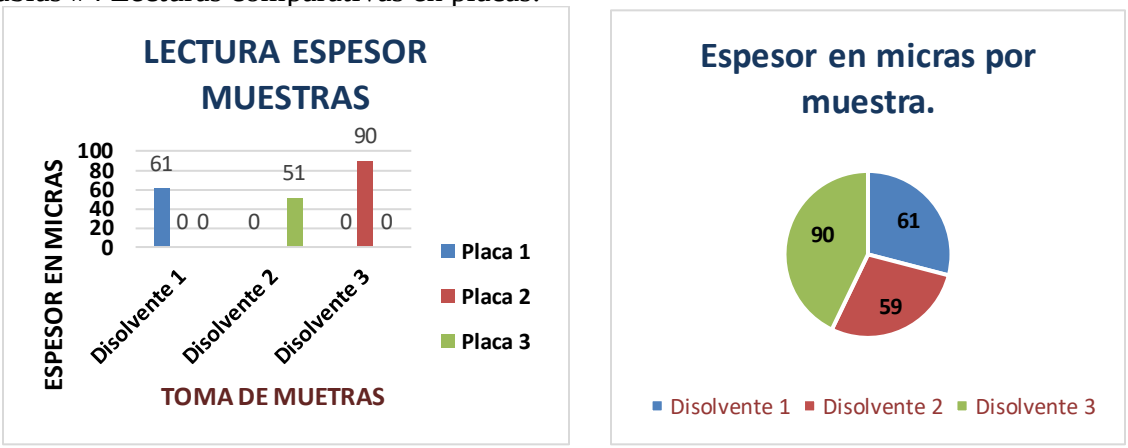

Fuente, Autores, 2023.

La segunda medición es el brillo de las placas, para ello la utilización de la herramienta electrónica que mide el espectro de luz (la reflectancia). “El brillo se mide en unidades de brillo (Gloss Units GU) con trazabilidad a patrones de referencia controlados en el BAM (Alemania), NRC (Canadá), NPL (Reino Unido) o ENAC (España)” **CEP, Centro Español**

del Plástico, 13 noviembre en Barcelona y en MCA, Madrid Cluster de Automoción el 15 de noviembre.

Figura #13 Medición de brillo de las placas.

Fuente autores, 2023.

Los datos obtenidos en las diferentes placas se contabilizan en la tabla de datos para su comparación y análisis.

Tabla #6 Medición de brillo en GU

TOMA DE LECTURA DATOS BASE DIESEL RALENTÍ ALTO							
Placas	MUESTRA 1	MAESTRA 2	MAESTRA 3	MUESTRA 4	MUESTRA 5	MUESTRA 6	MUESTRA 7
Placa Disolvente 1	81,2	81,2	81,2	81,2	81,2	81,2	81,2
Placa Disolvente 2	92,3	92,3	92,3	92,3	92,3	92,3	92,3
Placa Disolvente 3	97,9	97,9	97,9	97,9	97,9	97,9	97,9

Fuente autores, 2023

Tabla #7 Resultados

Grupos	*Cuenta*	*Suma*	*Promedio*	*Varianza*
Placa Disolvente 1	7	568,4	81,20	0,00
Placa Disolvente 2	7	646,1	92,30	0,00
Placa Disolvente 3	7	685,3	97,9	0,00

Fuente autores, 2023

Los datos son concluyentes en lo que a la medida de brillo se refiere, estos dan cuanta que el brillo final depende de la calidad de disolvente, es por ello que las marcas de alta desempeño tienen sus propios disolventes o sugieren uno en específico, el estudio demuestra

que la mejor calidad de disolvente nos solo que brinda un brillo intenso de alca calidad, adiciona un mejor cuerpo para que se aplique el pigmento, y un dato importante a mencionar es que mantiene el color del pigmento si variar, lo que no sucede con los otros disolvente de calidad inferior que no solo llegan al brillo deseado sino que tienden a cambiar el la tonalidad del color.

Para las pruebas de color no fue necesario de un instrumento por la claridad de reconocimiento visual, en este caso si podemos mencionar que hay un cambio significativo de color con el disolvente más básico porque se evidencia una pérdida de la pigmentación rojo intenso que pasa a ser un rojo tomate, en lo que respecta a la segunda placa con un disolvente de mediana calidad el cambio de color no es muy notorio a contra luz, pero ya en la luz es evidente que hay similitud pero se evidencia la pigmentación más tenue, adicional que el brillo visual en las tres placas de ensayo es súper notoria, si la calidad de los disolventes fueran muy similares por el estudio se estima que la diferencias serían mínimas pero de todos modos existirían, la investigación denota que se afecta al espesor de la capa aplicada, al tinte de la coloración y en especial al brillo de3 la pintura automotriz.

CONCLUSIONES

- Uno de los factores que inciden el en cambio de la intensidad de brillo y del cambio de la coloración es a causa del disolvente el estudio así lo demuestra. Si bien es cierto hay muchos factores que inciden en el cambio de color y la intensidad de brillo se podría asumir que la mayoría son por factores humanos, puesto que el operario puede cambiarlas en forma involuntaria, por desconocimiento, exceso de confianza en la combinación de cantidades de la formulación recomendada, o por creencias que si más o menos se pude secar de mejor menor manera, eliminadas estas condiciones humanas en el estudio por el control de cantidades por peso y la aplicación uniforme en cada placa de prueba, la siguiente parte que tienen que ver con el compuesto de las sustancias exclusivamente a la calidad del disolvente se determina por medio del estudio que este influye en forma directa en la calidad, el brillo e incluso del espesor de la pintura, el estudio determino tres clases de espesores diferentes en cada placa que no tienen un atendencia lineal con respecto a la calidad, el brillo que si tiene un tendencia lineal con respecto a la calidad, es decir cuando mejores propiedades tiene el disolvente mejor es el resultado del brillo.
- El estudio se ha caracterizado los solventes en tres formas de acedo a la información de sus prestaciones y características que permiten incorporarse a los diferentes procesos de pintando generando características de fluidez de la pintura, espesor de la misma y mantener las características de la pintura en lo que tiene que ver con el brillo y pigmentación de la misma. “Los solventes tienen dos características principales que afectan el uso de pinturas y recubrimientos: solubilidad, la capacidad de disolver otros químicos; y volatilidad, que mide qué tan rápido el solvente deja la pintura o el revestimiento”, **https://www.pinturasjet.com/novedades/disolventes-de**-pinturas basados en estos parámetros y en el caso de la volatilidad a todos los solventes se les coloco en el mismo marco para su secado, es decir entraron en un proceso de secado forzado por medio de lámparas de secado automotriz, siendo un parámetro cubierto por el estudio y estas cualidad también reflejan en un cambio en el terminado de la pintura.

- La mejor alternativa siempre va ser la que cumpla con la mayor parte de los parámetros necesarios para el repintado automotriz, el tipo de barniz adecuado para cada tipo la pintura y que la calidad sea la mejor con relación a la pintura base, no necesariamente el precio sino en rendimiento, cabe anotar que las mejores características de los solventes tienen componentes más costosos lo que si eleva su precio, los disolventes automotrices los hay de diferentes calidades y estos van de la mano del precio en muchos de ellos sin que por ello no se rompa la regla del costo beneficio, por ello los clientes por manejar costos más bajos u operarios de repintado automotriz por dejar un mejor margen de ganancia a su trabajo utilizan disolventes de baja calidad y empieza la discusión ya en el trabajo final cuando el trabajo está realizado.
- El estudio demuestra una que las variantes del espesor tienen una incidencia notoria, cabe destacar que las medidas realizadas son en micras y con un instrumento de alta precisión que no dejo dudas si hay una desviación estándar que se quiso medir para determinar si las medidas van 61, 59 y 90 micras respectivamente, una intensidad de brillo descrita por el instrumento de 81.2, 92.3, 97.9 respectivamente y por último que el color cambia por la calidad del disolvente. la placa número tres presenta el rojo con la intensidad de tinte que se adquirió y un brillo que cumple las expectativas del proceso de pintura, la placa numero dos ya presenta una ligera variación el pigmentación ya que la intensidad del rojo es más tenue y el brillo de igual forma tienen una reflectancia menor a la luz, y la tercera placa que consiste al disolvente de menor calidad de los tres presenta una coloración distinta en el color a tomar un tono tomate dejando de lado el rojo intenso de la pintura, un brillo muy bajo que da la sensación visual se haber utilizado un pigmento diferente al de la prueba.

BIBLIOGRAFIA

[1] J. DeGelder, P.Vandenabeele, F.Govaert y L.Moens, “Forensic analysis of automotive paints by Raman spectroscopy,” Journal of Raman Spectroscopy, vol. 36, nº 11, pp. 1059-1067, 2005. [Links]

[2] M.Skenderovska, B.Minceva-Sukarova y L.Andreeva, “Application of micro-Raman and FT-IR spectroscopy in forensic analysis of automotive topcoats in the Republic of Macedonia,” Macedonian Journal of Chemistry and Chemical Engineering, vol. 27, nº 1, pp. 9-17, 2008. [Links]

[3] J. M.Chalmers, H. G.Edwards y M. D.Hargreaves, Infrared and Raman spectroscopy in forensic science, John Wiley & Sons, 2012. [Links]

[4] A. C.Ferrari, “Raman spectroscopy of graphene and graphite: Disorder, electron-phonon coupling, doping and nonadiabatic effects,” Solid State Communications, vol. 143, nº 1, pp. 47-48, 2007. [Links]

[5] M. S.Dresselhaus, G.Dresselhaus, R.Saito y A.Jorio, “Raman spectroscopy of carbon nanotubes,” Physics Reports, vol. 409, nº 2, pp. 47-99, 2005. [Links]

[6] E.Smidt y K.Meissl, “The applicability of Fourier transform infrared (FT-IR) spectroscopy in waste management,” Waste Management, vol. 27, nº 2, pp. 268-276, 2007. [Links]

[7] C.Muehlethaler, G.Massonnet y P.Esseiva, “The application of chemometrics on Infrared and Raman spectra as a tool for the forensic analysis of paints,” Forensic science international, vol. 209, nº 1, pp. 173-182, 2011. [Links]

[8] E. JOURNAL OF RAMAN SPECTROSCOPY

JRS

J. Raman Spectrosc. 2005; **36**: 1059–1067
Published online 19 September 2005 in Wiley InterScience (www.interscience.wiley.com). DOI: 10.1002/jrs.1408

Forensic analysis of automotive paints by Raman spectroscopy

Joke De Gelder,[1]* Peter Vandenabeele,[1] Filip Govaert[2] and Luc Moens[1]

[1] Ghent University, Laboratory of Analytical Chemistry, Proeftuinstraat 86, B-9000 Ghent, Belgium
[2] National Institute of Forensic Science, Vilvoordse Steenweg 98/100, 1120 Brussels, Belgium

Received 21 April 2005; Accepted 25 July 2005

In this work, the possible contribution of Raman spectroscopy in forensic science is evaluated, more specifically for the analysis of automotive paint samples. Spectra from paint flakes as well as from cross sections were examined, in order to identify not only the pigments but also binders and extenders in all paint layers. Moreover, the possibility of distinguishing paint samples from different cars was evaluated to assess the use of vibrational spectroscopic techniques in the investigation of a hit-and-run accident.

The presence of rutile and extenders, such as calcite and barium sulphate, could be demonstrated by their characteristic Raman bands. However, the identification of the binder by Raman spectroscopy was hampered: only with additional information from IR analysis could most of the bands in the spectrum be assigned to molecular vibrations of the binders. In contrast, organic pigments, having very distinctive and well-resolved characteristic bands, could easily be identified by comparing the spectra from the basecoat of the sample with spectra from a reference database. Because of these characteristic bands, the basecoat seems to provide the best spectra to distinguish paint samples. Moreover, some paints can also be distinguished by the absence or presence of the bands from calcium carbonate and barium sulphate in the primer surfacer. When recording spectra from paint flakes, Raman bands from the spectra of the clearcoat as well as from the basecoat are obtained. Copyright 2005 John Wiley & Sons, Ltd.

KEYWORDS: automotive paints; forensic science; pigment; binders

INTRODUCTION

Besides its industrial importance,[1,2] the analysis of automotive coatings is of importance to forensic scientists, especially for the investigation of hit-and-run accidents.[3–5] Over the years, several protocols have been developed and optimised to analyse and to distinguish different paint samples. First, a microscopic examination is performed, revealing differences in colour, number and thickness of the different paint layers, the shape of particles (metal flakes, pigments, etc.) and their distribution in each layer.[6–8] Often, this first examination is followed by a chemical or spectroscopic analysis. Scanning electron microscopy (SEM), infrared spectroscopy (IR spectroscopy), X-ray fluorescence (XRF) and pyrolysis gas chromatography mass spectrometry (Py-GC-MS) are important and frequently used techniques.[9] While XRF reveals the elemental composition of the sample, Py-GC-MS identifies the organic compounds in the sample.[5,7,9,10] In principle, IR Ł

Correspondence to: Joke De Gelder, Ghent University, Laboratory of Analytical Chemistry, Proeftuinstraat 86, B-9000 Ghent, Belgium.
E-mail: joke.degelder@UGent.be

Contract/grant sponsor: Research Foundation-Flanders. Contract/grant sponsor: Research Council UGent.

spectroscopy, being a molecular spectroscopic technique, can be used to study both organic and inorganic compounds. However, as most IR spectrometers record spectra in the range between 600 and 4000 cm^{1}, the identification of some inorganic compounds is hampered. Moreover, as many inorganic and organic pigments are weak IR absorbers, their spectrum is often overwhelmed by the IR spectra of other compounds in the sample.[4,9,11–15]

In this work, Raman spectroscopy is evaluated as an analytical technique for the forensic analysis of automotive paint samples. Indeed, the non-destructive character of the technique, the (almost) absence of sample preparation and the good lateral resolution are advantageous features of Raman spectroscopy in this field of research. Moreover, the use of Raman spectroscopy is complementary to IR spectroscopy:[16] although both are vibrational spectroscopic techniques, their spectra supply different information because of the different nature of the interactions and the different selection rules.[17]

There are two important advantages of Raman spectroscopy over IR spectroscopy. Usually Raman bands do not overlap, while the bands in IR spectra do. Moreover, Raman spectra generally extend well below 600 cm^{1}, a region where

many inorganic pigments and extenders have important vibrational bands.[18] Because of the complementary nature of both techniques and because of the importance of IR spectroscopy in forensic science, it is worthwhile to examine the possible contribution of Raman spectroscopy to this research, although until now little work has been done on the Raman spectroscopic study of automotive paints.[16,17] These studies focussed on red organic pigments[16] and inorganic pigments[17] in the topcoat, while our explorative research gives an overview of the possibilities of Raman spectroscopy in car paint analysis by examining the pigments, binders and extenders in all paint layers.

The automotive paint samples in this study are effect paints (also known as metallics and pearlescent paints) consisting of four layers. The bottom layer (called the first primer or primer) provides good adhesion to the car body as well as to the subsequent layers. This layer consists of a binder, basic pigmentation, an anti-rust pigmentation and extenders. Above this layer, the primer surfacer is retrieved, giving mechanical strength to the coating and resistance against degradation by ultraviolet light and providing a good, even surface to maximise the appearance and performance of the basecoat. It contains the basic pigmentation, extenders and a binder. The third layer (the basecoat) gives colour to the paint through pigments, alumina platelets and mica particles that are embedded in the binder.

Finally, a binder layer (clearcoat) protects the basecoat from fast degradation that could occur to the alumina platelets or mica particles present at the surface of the basecoat.[9,19]

EXPERIMENTAL Sample preparation

Raman spectra were recorded from flakes as well as from cross sections. For IR analysis, only cross sections were used. The flakes were attached to microscope slides by doublesided tapes. Cross sections were made by embedding a flake in a methacrylate resin, Technovit 2000 LC (Heraeus Kulzer, Germany). Technovit 2000 LC was selected as embedding medium because of its easy usage and high transparency. It is a one-component light-curing acrylic resin, which cures in *ca* 30 min at low temperatures (peak temperature: 90 °C). Polymerisationoftheresiniscarriedoutinadeviceequip ped with blue light (Technotray CU, Heraeus Kulzer, Germany). Because of the resin's high transparency, small samples can be clearly observed and easily sectioned. When the resin had hardened, a microtome (Cut 4060 E, MicroTec, Germany) was used to produce cross sections, with a thickness of 5 μm. Cross sections were made parallel to the layer structure. By doing this, the highest possible surface area of a layer within a cross section is obtained. These cross sections were attached to a metal carrier by a procedure shown in Fig. 1(a). The metal carrier has the size of a microscope slide and contains three openings with a diameter of *ca* 8 mm. The carrier was covered with double-sided tape with three openings at the same place as those in the carrier. A cross section was then stretched out on a microscope slide with methanol, after which the carrier was pressed upon the cross section on the place of a hole in the tape. The cross section was then attached to the carrier as shown in Fig. 1(b). This sample preparation reduces the chance of spectral interference of the methacrylate resin and thecarrier.Giventhenon-destructivenatureofIRandRaman measurements, the same cross sections can be used for both the techniques. Raman and IR spectra of the embedding resin were measured to investigate possible physical overlap and spectral interference (Fig. 1(c)).

Fourier-transform infrared spectrometry (FTIR)

A Fourier-transform infrared (FTIR) spectrometer (Nicolet 510P, USA) equipped with a KBr beam splitter, an IR microscope (NIC-Plan, USA) with 32 ð objective (SpectraTech,USA)andamercurycadmiumtelluride(M CT)detector was used to analyse the chemical binders and extenders present in these coatings. With an aperture of 3.2 mm, a spot size of 100 μm is obtained. A hundred scans were collected with a resolution of 4 cm^{1} and the intensity (% transmittance) *versus* wavenumber (cm^{1}) was measured between 650 and 4000 cm^{1}. Spectra of each paint layer were recorded by transferring the metal carrier with a cross section to the sample stage and focussing on the layer of interest. The obtained spectra were interpreted and compared with commercial and our personal spectral libraries of paint materials. A spectrum of the embedding resin was measured to investigate possible physical overlap and spectral interference.

Raman spectrometry

The spectra were recorded with a Renishaw System 1000 spectrometer that was equipped with a 785-nm diode laser, with a power of 50 mW at the source, and between 1 and 2 mW on the sample by the use of 25 or 10% neutral density filters. The laser beam was focussed on the samples by a 50 ð objective lens, which produced a laser spot of approximately 2 μm. The spectrometer collects light in the

backscattering mode, which is dispersed on a 1200-lines mm^{1} grating and focussed on a Peltier-cooled CCD detector.

Because of the low sensitivity of the CCD detector above

$2000\ cm^{-1}$, no spectrawererecorded in the (C–H) stretching region (2700–3400 cm^{1}). Spectra from the clearcoats, primer surfacers and primers were recorded for up to 2 min and accumulated up to 60 times. In the basecoat, the presence of organic pigments, which are strong Raman scatterers, reduced the recording time to a maximum of 1 min and the accumulations to a maximum of 15. All spectra were baseline corrected.

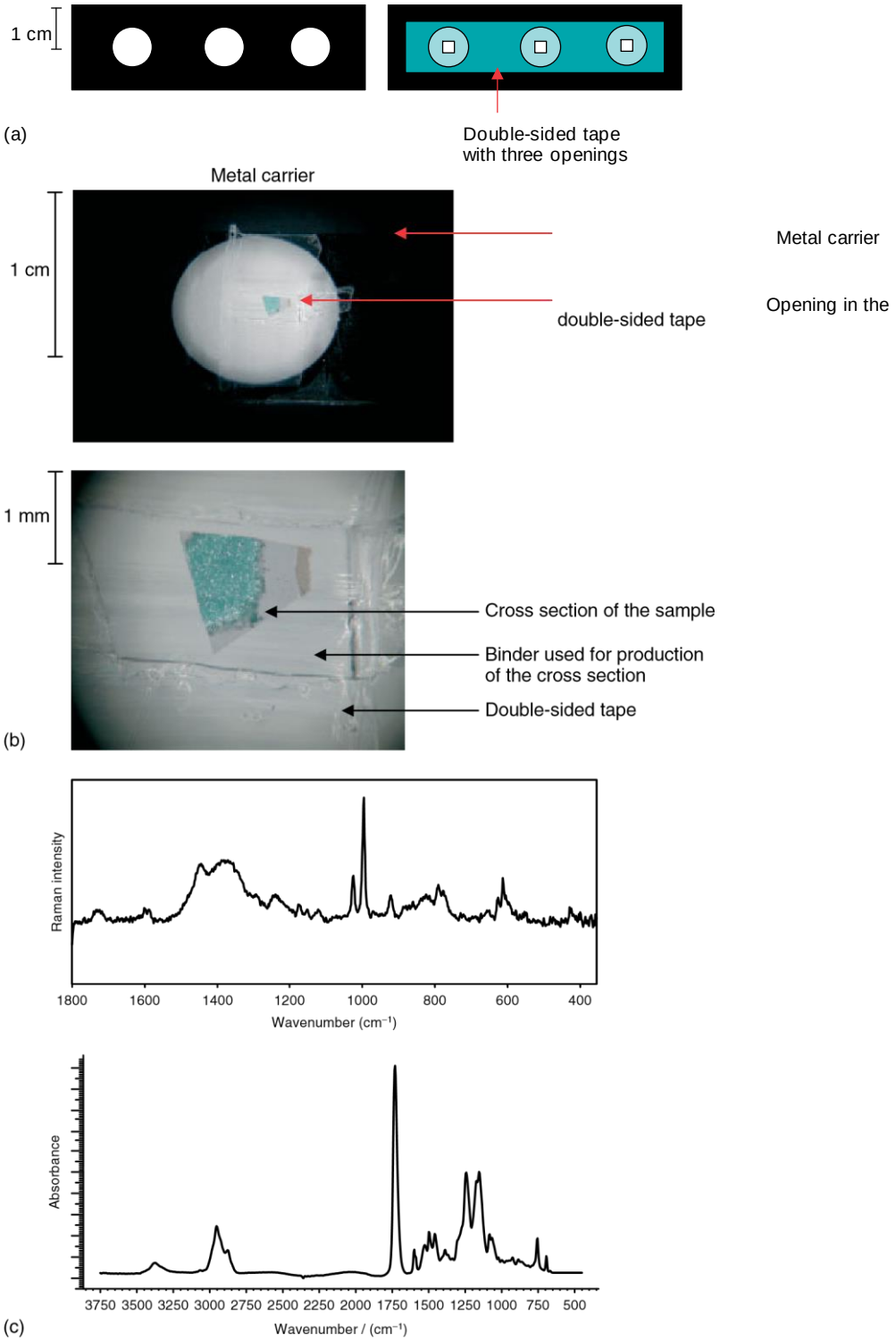

Figure 1. Sample preparation: attaching the cross section to a metal carrier (a, b) and Raman and IR spectra of the methacrylate resin used for cross sectioning (c).

RESULTS AND DISCUSSION Spectra

obtained from cross sections

In this study, the application of Raman spectroscopy in the forensic analysis of automotive paints was evaluated. The results were compared with the information obtained by IR spectrometry. Both techniques permit obtaining separate spectra from

each layer of different paint cross sections. Exact Raman wavenumbers are given in Table 1, while the

Table 1. Raman wavenumbers (in cm[1]) for each spectrum

Figure	Sample	Layer	Raman wavenumber (cm^{-1})
1(c)	Methacrylate (Technovit 2000 LC)		604 (sh), 613 (m), 626 (w), 653 (vw), 777 (w), 790 (m), 823 (w), 870 (vw), 922 (w), 996 (vs), 1025 (m), 1120 (vw), 1150 (vw), 1174 (vw), 1238 (w), 1293 (w), 1376 (s, br), 1444 (s), 1588 (vw), 1599 (vw), 1726 (vw)
2(a)	Dark blue metallic Citroen¨	P	444 (vs), 609 (s), 637 (vs), 820 (m), 1110 (m), 1182 (m, br), 1226 (w), 1250 (w), 1304 (m, br), 1453 (m, br), 1582 (sh), 1605 (s)
2(b)	Amazon green metallic Opel	P	447 (vs), 610 (vs), 633 (sh), 818 (m), 986 (w), 1109 (w), 1181 (m), 1250 (m, br), 1307 (m, br), 1453 (w), 1580 (sh), 1608 (m)
4(a)	Bordeaux metallic Alfa Romeo	PS	444 (vs), 608 (vs), 652 (sh), 984 (s), 1000 (s), 1302 (m, br), 1444 (w, br), 1584 (sh), 1600 (m), 1723 (w)
4(b)	Amazon green metallic Opel	PS	445 (vs), 609 (vs), 647 (sh), 711 (vw), 1038 (w), 1084 (m), 1302 (w, br), 1446 (vw, br), 1579 (sh), 1600 (w), 1720 (vw)
4(c)	Grey Ford Mondeo	PS	446 (s), 612 (m), 653 (sh), 984 (s), 1000 (m), 1301 (vs, br), 1583 (sh), 1602 (s, br), 1723 (w)
4(d)	Green Opel Astra	PS	446 (vs), 608 (vs), 646 (sh), 711 (vw), 1037 (w), 1084 (m), 1303 (m, br), 1382 (m, br), 1446 (m, br), 1580 (sh), 1598 (m), 1722 (w)
6(a)	Dark blue metallic Citroen¨	BC	686 (m), 702 (w), 748 (vs), 1157 (w), 1160 (w), 1182 (w), 1205 (w), 1257 (vw), 1327 (s), 1339 (s), 1390 (m), 1428 (m), 1443 (w), 1528 (vs)
6(b)	Dark blue metallic Renault	BC	377 (w), 406 (w), 477 (s), 494 (m), 582 (w), 620 (w), 639 (sh), 680 (m), 747 (m), 757 (w), 802 (m), 908 (vw), 952 (vw), 1001 (w), 1041 (w), 1142 (sh), 1154 (m), 1183 (m), 1283 (m), 1301 (m), 1328 (s), 1355 (vs), 1384 (vs), 1448 (vw), 1474 (w), 1526 (m), 1552 (w), 1597 (vw), 1618 (w)
6(c)	Green Opel Astra	BC	481 (vw), 593 (vw), 640 (vw), 682 (vs), 700 (sh), 738 (s), 744 (sh), 773 (m), 814 (w), 951 (vw), 976 (vw), 1078 (vw), 1140 (vw), 1186 (sh), 1209 (m), 1278 (m), 1285 (sh), 1298 (sh), 1314 (w), 1335 (m), 1355 (sh), 1384 (vw), 1445 (vw), 1503 (sh), 1533 (vs)
6(d)	Dioxazine violet pigment PV23		417 (w), 485 (w), 528 (m, w), 590 (w), 619 (w), 672 (w), 725 (vw), 749 (vw), 776 (vw), 808 (vw), 884 (vw), 920 (w), 933 (vw), 950 (vw), 993 (vw), 1108 (w), 1121 (vw), 1132 (vw), 1152 (vw), 1166 (m, w), 1206 (m), 1256 (m, w), 1280 (vw), 1333 (m, w), 1346 (m), 1391 (vs), 1431 (m), 1443 (w), 1477 (vw), 1590 (vw), 1610 (vw), 1643 (vw)
6(e)	Copper pthalocyanin pigment PB15		490 (vw), 593 (vw), 680 (w), 746 (s), 773 (vw), 837 (v), 951 (vw), 1005 (vw), 1105 (v), 1140 (w), 1181 (w), 1333 (m), 1446 (w), 1519 (vs)
6(f)	Indanthrone PB60		404 (vw), 476 (m), 493 (w), 582 (vw), 620 (v), 676 (vw), 757 (vw), 801 (w), 906 (vw), 999 (vw), 1040 (vw), 1155 (w, m), 1182 (w), 1283 (w, m), 1298 (w, m), 1325 (s), 1352 (vs), 1380 (vs), 1473 (vw), 1551 (w), 1616 (w)
6(g)	Chlorated copper pthalocyanin pigment PG7		686 (vs), 741 (s), 777 (m), 818 (w), 959 (vw), 981 (vw), 1083 (vw), 1214 (w-m), 1287 (m), 1339 (w), 1388 (vw), 1446 (vw), 1506 (vw), 1539 (vs)
9(a)	Dark blue metallic Citroen¨	CLC	598 (sh), 621 (w), 841 (w), 976 (m), 1002 (vs), 1032 (m), 1154 (vw), 1195 (vw), 1302 (vw), 1449 (m), 1587 (vw), 1602 (w), 1725 (vw)
9(b)	Green-grey metallic Toyota	CLC	617 (w), 745 (vw), 838 (vw), 973 (m), 998 (vs), 1028 (m), 1152 (vw), 1185 (vw), 1302 (w), 1372 (m, br), 1445 (m), 1596 (sh), 1601 (w), 1721 (vw)
9(c)	Amazon green metallic Opel	CLC	620 (w), 975 (m), 1001 (vs), 1030 (m), 1154 (vw), 1189 (vw), 1301 (w), 1371 (m, br), 1448 (m), 1585 (vw), 1602 (w), 1725 (vw)
9(d)	Green Opel Astra	CLC	618 (vw), 664 (vw), 775 (vw), 840 (w), 975 (m), 1000 (vs), 1030 (w), 1154 (vw), 1302 (sh), 1374 (s, br), 1447 (vs), 1596 (w), 1602 (vw), 1728 (vw), 1757 (vw)

10(a)	Dark blue metallic Citroen¨	F	590 (vw), 634 (vw), 683 (m), 697 (w), 746 (vs), 845 (vw), 956 (vw), 973 (w), 999 (m), 1030 (vw), 1117 (w), 1155 (m), 1181 (m), 1203 (m), 1254 (m), 1303 (sh), 1326 (s), 1337 (s), 1384 (sh), 1389 (m), 1422 (m), 1445 (m), 1527 (vs), 1584 (sh), 1600 (w)
10(b)	Dark blue metallic Citroen¨	CLC	598 (sh), 621 (w), 841 (w), 976 (m), 1002 (vs), 1032 (m), 1154 (vw), 1195 (vw), 1302 (vw), 1449 (m), 1587 (vw), 1602 (w), 1725 (vw)

(*Continued*)

Table 1. (*Continued*)

Figure	Sample	Layer	Raman wavenumber (cm^{-1})
10(c)	Dark blue metallic Citroen¨	BC	686 (m), 702 (w), 748 (vs), 1157 (w), 1160 (w), 1182 (w), 1205 (w), 1257 (vw), 1327 (s), 1339 (s), 1390 (m), 1428 (m), 1443 (w), 1528 (vs)
11(a)	Grey Ford Mondeo	F	653 (vw), 750 (vw), 840 (w), 974 (m), 1000 (vs), 1030 (w), 1189 (vw), 1302 (w), 1445 (m), 1600 (vw), 1724 (vw)
11(b)	Grey Ford Mondeo	CLC	618 (w), 746 (vw), 842 (w), 974 (m), 1000 (vs), 1029 (w), 1153 (vw), 1188 (vw), 1302 (w), 1371 (w, br), 144 (m), 1582 (vw), 1600 (w), 1727 (vw)
11(c)	Grey Ford Mondeo	BC	652 (m), 818 (vw), 974 (w), 1000 (vs), 1282 (sh), 1300 (m), 1370 (w), 1448 (w), 1586 (sh), 1603 (m), 1726 (m)

vw, very weak; w, weak; m, medium; s, strong; vs, very strong; sh, shoulder; br, broad; CLC, clearcoat; BC, basecoat; PS, primer surfacer; P, primer; F, flake.

Table 2. IR wavenumbers (in cm^{1}) for each spectrum

Figure	Sample	Layer	IR wavenumber (cm^{-1})
1(c)	Methacrylate (Technovit 2000 LC)		692 (m), 756 (m), 884 (vw), 924 (vw), 1084 (m), 1152 (s), 1244 (s), 1388 (w), 1456 (m), 1496 (m), 1524 (m), 1600 (m), 1732 (vs), 2879 (m), 2952 (s), 3378 (br)
3(a)	Dark blue metallic Citroen¨	P	669 (vw), 765 (vw), 802 (w), 829 (m), 916 (w), 1012 (sh), 1105 (s), 1182 (s), 1228 (s), 1302 (m), 1361 (w), 1382 (w), 1413 (m), 1458 (m), 1510 (vs), 1606 (m), 1732 (s), 2872 (m), 2931 (m), 2968 (m), 3037 (w), 3320 (br), 3619 (w), 3695 (w)
3(b)	Amazon green metallic Opel	P	657 (br), 829 (s), 914 (m), 1012 (sh), 1038 (s), 1076 (m), 1105 (s), 1184 (s), 1228 (vs), 1301 (m), 1361 (w), 1382 (w), 1414 (m), 1460 (m), 1510 (vs), 1606 (s), 1730 (s), 2872 (m), 2931 (m), 2966 (m), 3035 (w), 3329 (br), 3620 (w), 3695 (m)
5(a)	Bordeaux metallic Alfa Romeo	PS	671 (w), 731 (m), 830 (w), 984 (vw), 1018 (m), 1076 (s), 1134 (s), 1182 (m), 1238 (s), 1306 (m), 1375 (m), 1466 (s), 1510 (vw), 1537 (w), 1590 (vw), 1608 (vw), 1690 (m), 1728 (vs) 2874 (vw), 2936 (m), 2964 (m), 3389 (br), 3678 (w)
5(b)	Amazon green metallic Opel	PS	673 (w), 713 (w), 877 (s), 1022 (m), 1074 (m), 1122 (m), 1286 (s), 1448 (vs), 1550 (sh), 1580 (sh), 1600 (sh), 1690 (sh), 1724 (s), 1798 (w), 2512 (w), 2863 (m), 2935 (m), 3676 (vw)
5(c)	Grey Ford Mondeo	PS	730 (s), 814 (w), 983 (m), 1022 (w), 1076 (vs), 1124 (s), 1186 (s), 1238 (s), 1303 (m), 1375 (m), 1475 (m), 1512 (w), 1548 (m), 1727 (vs), 2868 (w), 2935 (m), 2957 (m), 3372 (br), 3676 (vw)
5(d)	Green Opel Astra	PS	669 (m), 713 (w), 875 (s), 1020 (s), 1074 (m), 1124 (m), 1286 (s), 1430 (vs), 1690 (m), 1724 (s), 1798 (w), 2513 (vw), 2860 (w), 2933 (m), 3676 (w)
7(a)	Dark blue metallic Citroen¨	BC	702 (m), 730 (m), 815 (m), 1078 (s), 1165 (s), 1236 (s), 1306 (w), 1363 (s), 1477 (s), 1552 (s), 1730 (vs), 2873 (m), 2931 (m), 2958 (m), 3026 (w), 3380 (br)
7(b)	Dark blue metallic Renault	BC	712 (w), 730 (m), 814 (m), 1018 (w), 1074 (s), 1165 (s), 1273 (s), 1284 (s), 1373 (s), 1477 (s), 1498 (s), 1550 (s), 1658 (m), 1727 (vs), 2850 (m), 2873 (mp), 2921 (m), 2962 (m), 3026 (w), 3380 (br)

7(c)	Green Opel Astra	BC	730 (m), 771 (w), 815 (m), 1003 (s), 1041 (w), 1072 (s), 1095 (w), 1122 (w), 1153 (w), 1160 (w), 1240 (s), 1286 (s), 1305 (s), 1367 (m), 1388 (m), 1388 (s), 1548 (s), 1727 (vs), 2856 (m), 2927 (s), 3367 (br)
8(a)	Amazon green metallic Opel	CLC	701 (s), 730 (w), 760 (m), 815 (m), 1022 (m), 1093 (m), 1166 (s), 1228 (m), 1307 (w), 1378 (m), 1454 (m), 1492 (m), 1552 (s), 1730 (vs), 2873 (m), 2931 (s), 2956 (s), 3027 (w), 3390 (br)
8(b)	Green Opel Astra	CLC	702 (m), 765 (m), 815 (w), 1041 (w), 1076 (w), 1168 (s), 1286 (s), 1367 (m), 1386 (m), 1456 (s), 1550 (s), 1691 (s), 1730 vs), 2873 (m), 2931 (s), 2958 (s), 3028 (vw), 3372 (br)

vw, very weak; w, weak; m, medium; s, strong; vs, very strong; sh, shoulder; br, broad; CLC, clearcoat; BC, basecoat; PS, primer surfacer; P, primer; F, flake.

text contains estimated Raman wavenumbers for bands that occur in spectra of the same layer. Assignments of specific Raman bands to the binder are based on Ref. 20. Pigments and extenders were identified by the use of a personal database with reference Raman spectra.[21] Table 2 gives a list of IR absorption bands of each spectrum shown in this paper.

Spectral interference of the adjacent embedding resin was avoided by measuring at the centre of the layer of interest. Spot sizes of 100 μm for IR analysis and 2 μm for Raman analysis are small enough to focus on only one layer. Although the embedding resin has similar absorption characteristics as some automotive paints, the binders of the paint samples could clearly be identified.

The primers of all paints examined in this study, give rise to spectra with a similar profile as shown in Fig. 2. This similarity was expected as all primers contained epoxy binders and aluminium silicate according to IR analyses. Figure 3shows IR spectra of these two similar primers. Epoxy binder bands at 830, 1180, 1240, 1410, 1510 and 1610 cm^{1} and absorption bands of aluminium silicate at 1010, 1035, 3340, 3620, 3654 and 3695 cm^{1} can clearly be observed. Aluminium silicate caused a shoulder in the Raman spectrum (Fig. 2) at *ca* $635\ cm^{-1}$, but unlike IR spectroscopy, Raman spectroscopy showed the presence of rutile (TiO_2: *ca* 446 and $609\ cm^{-1}$). The doublet at *ca* 1580 and 1606 cm^{1} caused by a quadrant stretch suggests the use of benzene derivatives (e.g. bisphenol A) in the production of the epoxy binder. This supposition is supported by the presence of a band at *ca* $820\ cm^{-1}$ that could be assigned to ring vibrations of *para* substituted benzenes. Nevertheless, this band could also (partly) have resulted from the skeletal stretches of secondary alcohols. The epoxy binder is responsible for the bands at *ca* $1110\ cm^{-1}$ as well as at *ca* $1182\ cm^{-1}$, which could be assigned to C–C backbone and C–C out-of-plane vibrations, respectively. Furthermore, the CH_2 twisting and rocking vibrations, CH_2 in-phase twisting vibrations, and the CH_3 and CH_2 deformations cause bands in the regions 1175–1310, 1295–1310 and 1446–1473 cm^{1}. Only one of the primers that were examined contained, next to the epoxy binder, a polyurethane binder also. In the latter spectrum, an extra band at *ca* $1725\ cm^{-1}$ was detected, which could be attributed to a C═O stretching vibration. Although not confirmed by IR analysis, the band at 986 cm^{1} in spectrum 2(c) could be caused by the SO_4^{2-} symmetric stretching of barium sulphate.

The Raman spectra of the primer surfacer (the four spectra shown in Fig. 4) all show bands at *ca* 446 and 609 cm^{1}, which point to the presence of rutile. A closer look at these bands revealed the existence of a shoulder at *ca* $650\ cm^{-1}$, which could be assigned to magnesium silicate. Spectra (a) and (c) (Alfa Romeo bordeaux metallic and Ford Mondeo grey) show a band at 984 cm^{1}, which was assigned to the SO_4^{2-} symmetric stretching vibration of barium sulphate, while spectra (b) and (d) (Opel Amazon green metallic and Opel Astra green) show bands at 711 and 1084 cm^{1} due to

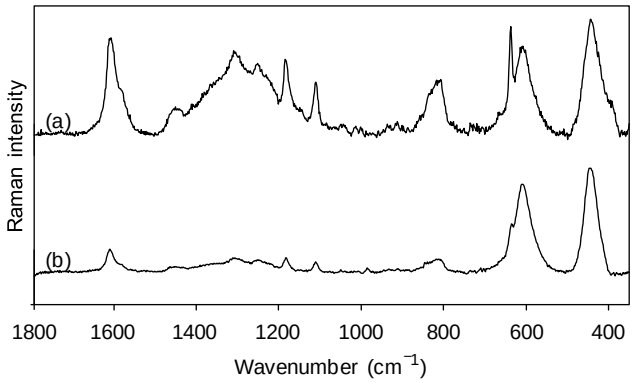

Figure 2. Raman spectra recorded from the primer of cross sections of a dark blue metallic Citroen (a) and an Amazon¨ green metallic Opel (b) (spectrum (b) was Fourier-smoothed by GRAMS 5.2).

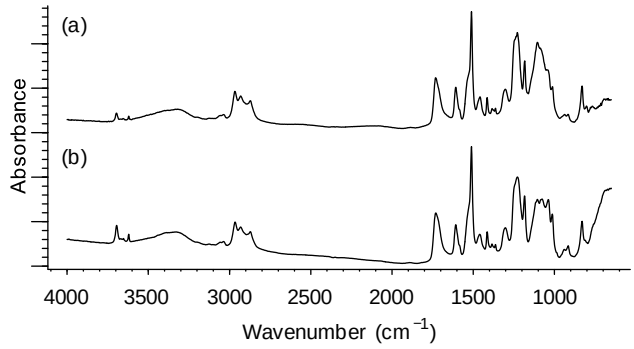

Figure 3. IR spectra recorded from the primer of cross sections of a dark blue metallic Citroen (a) and an Amazon¨ green metallic Opel (b).

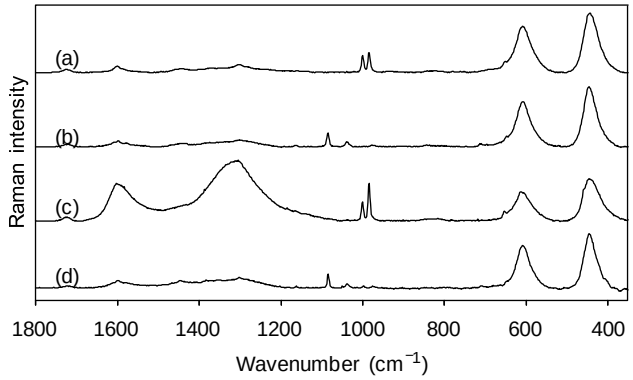

Figure 4. Raman spectra recorded from the primer surfacer of cross sections of a Bordeaux metallic Alfa Romeo (a), an Amazon green metallic Opel (b), a grey Ford Mondeo (c) and a green Opel Astra (d).

the presence of calcite ($CaCO_3$). The broadbands at about 1301 and 1602 cm^1 in spectrum (c) reveal the presence of carbon black. The band at *ca* 1722 cm^{-1} present in all spectra can be assigned to the C═O stretching vibration of polyurethane, polyester or alkyd binders, from which their presence was confirmed by IR analyses. Other bands resulting from the binder include those in the region of 1175–1310 and 1446–1473 cm^1 due to CH_2 twisting, rocking and in-phase twisting vibrations, and CH_3 and CH_2 deformations, respectively. At *ca* 1580 and 1600 cm^1 in spectra (a), (b) and (d), a doublet could be assigned to the quadrant stretching of benzene derivates that are

frequently used in the production of the polyester, polyurethane and alkyd binders. The presence of aromatics also gives rise to bands at 1000 (spectra (a), (c)) and *ca*1038 cm^{-1} (spectra (b), (d)), which can be attributed to trigonal ring breathing and aromatic ring vibrations respectively. Indeed, for a primer surfacer, many characteristics were confirmed by IR analysis as shown in Fig. 5. All IR spectra contain absorption bands of aluminium silicate (670, 1020 and 3676 cm^{1}). Spectra (a) and (c) contain a sulphate band at 980 cm^{1} and spectra (b) and (d) bands of calcite (875, 1445 and 1795 cm^{-1}).

Figure 6 shows the Raman spectra of the basecoat as recorded from some cross sections (spectra (a)–(c)) along with reference spectra of some organic pigments (spectra (d)–(g)). Spectrum (a) was recorded from a dark blue metallic Citroenand exhibits bands from bothspectra(d) and¨ (e) corresponding to a violet dioxazine pigment (PV23) and a copper pthalocyanin pigment (PB15), respectively. In the spectrum of a dark blue metallic Renault (spectrum (b)) there are, next to an indanthrone pigment (PB60, spectrum (f)), also small bands visible from copper pthalocyanin (PB15, spectrum (e)). The basecoat of a green Opel Astra (spectrum (c)) clearly contains a chlorated copper pthalocyanin pigment (spectrum (g)). The bands of the organic pigments totally mask bands of binders. From these examples, it is clear that the organic pigments are very easy to identify by comparing their spectra to a database of reference spectra.[21] This is a great advantage over IR spectroscopy, where nearly no bands of organic pigments can be observed in the spectra of the basecoat. IR spectra permit, on the other hand, to

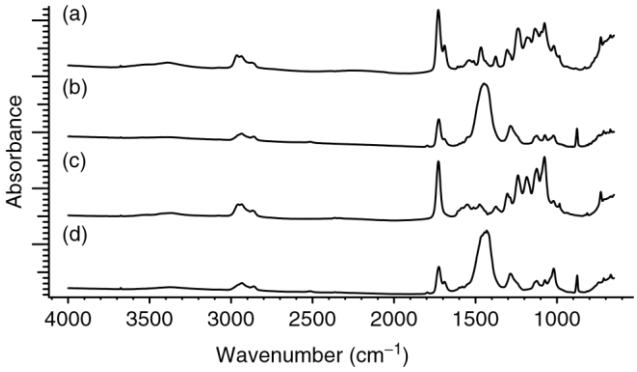

Figure 5. IR spectra recorded from the primer surfacer of cross sections of a Bordeaux metallic Alfa Romeo (a), an Amazon green metallic Opel (b), a grey Ford Mondeo (c) and a green Opel Astra (d).

identify the binders used in these basecoats. Figure 7 shows IR spectra of three different basecoats. All basecoats contain melamine used to cross link the primary binder such as acrylic, polyester and alkyd.

From IR studies, it seems that the clearcoats of all paints that were examined consisted of melamine styrene binders, possibly with an acrylic, alkyd or polyurethane binder. Figure 8 depicts clearly the melamine (815 and

1550 cm^{-1} and styrene (700, 760, 1450 and 1490 cm^{-1})absorption bands in both IR spectra. IR spectrum (b) can be differentiated by its polyurethane band at 1690 cm^{1}. As shown in Fig. 9, the Raman spectra of the clearcoats are very similar as well. The Raman bands at approximately 975,

1001 and 1031 cm[1], present in all spectra, were assigned to the triazine ring breathing of the melamine resin, trigonal ring breathing and in-plane CH deformation of the styrene binder, respectively. Other bands that can be attributed to the styrene binder are those at 620 and 1190 cm[1] (last one probably masked in spectrum (d) by a broader band) due to

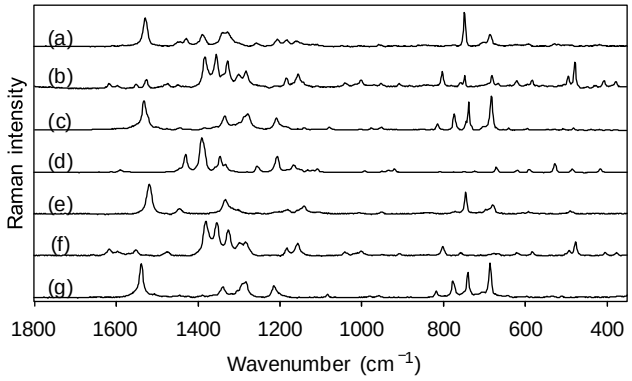

Figure 6. Raman spectra recorded from the basecoat of cross sections of a dark blue metallic Citroen (a), a dark blue metallic¨ Renault (b) and a green Opel Astra (c), along with reference spectra from a dioxazine violet pigment PV23 (d), a copper pthalocyanin pigment PB15 (e), indanthrone PB60 (f) and a chlorated copper pthalocyanin pigment PG7 (g).

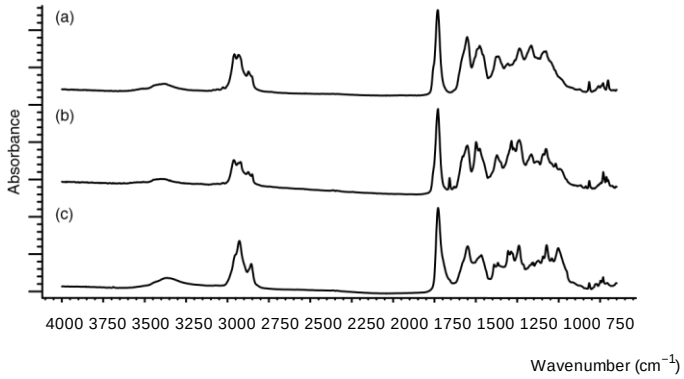

Figure 7. IR spectra recorded from the basecoat of cross sections of a dark blue metallic Citroen (a), a dark blue metallic¨ Renault (b) and a green Opel Astra (c).

a ring deformation and a C_6H_5–C stretching, respectively, and the doublet at *ca* $1590/1602\ \mathrm{cm}^{-1}$ from a ring stretching.

Furthermore, the bands in the regions 1175–1310, 1295–1310 and 1446–1473 cm[1] can be assigned to CH_2 twisting and rocking vibrations, CH_2 in-phase twisting vibrations, and CH_3 in-phase bending and CH_2 wagging, respectively. The band at *ca* $1725\ \mathrm{cm}^{-1}$ in spectra (b), (c) and (d) and the band at 1757 cm[1] in spectrum (d), could be attributed to C═O stretches from the acrylic, alkyd or polyurethane binders. The bands due to ring vibration of *para* substituted benzenes and symmetric C–N–C stretches from secondary amines are visible in the regions 720–830 and 850–900 cm[1].

Evaluation of the capability to distinguish automotive paint samples by spectra from cross sections and from flakes

The Raman and IR spectra of the different clearcoats (Figs 9 and 8, respectively) are very similar, which makes it difficult to distinguish the paints by studying this layer. The same remark can be made for the spectra of the primers (Figs 2 and 3). Further research on reproducibility of the spectra of samples from different cars of the same brand and evaluation of the variation of spectra of samples of cars from different

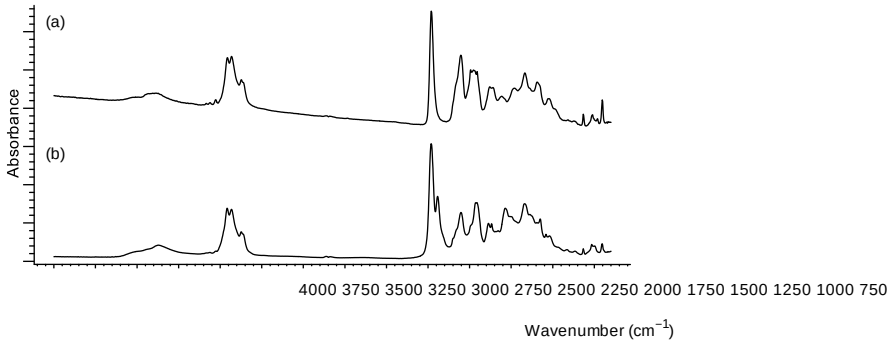

Figure 8. IR spectra recorded from the clearcoat of cross sections of an Amazon green metallic Opel (a) and a green Opel Astra (b).

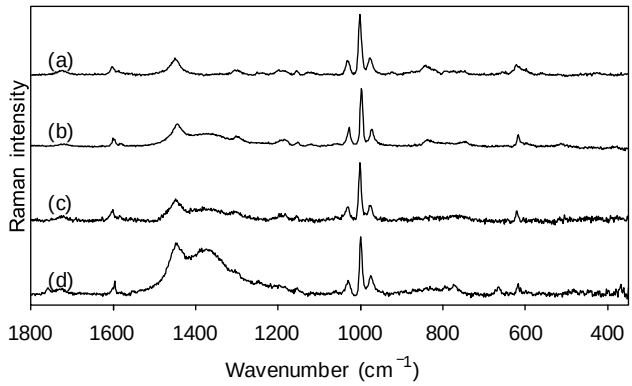

Figure 9. Raman spectra recorded from the clearcoat of cross sections of a dark blue metallic Citroen (a), a green–grey¨ metallic Toyota (b), an Amazon green metallic Opel (c) and a green Opel Astra (d).

brands that use similar binders would reveal if these spectra could be used to distinguish automotive paints. On the contrary, the Raman spectra of the primer surfacer can be used to distinguish certain coatings by the absence or the presence of the bands caused by calcium carbonate or barium sulphate, as shown in Fig. 4. The same characteristics of the primer surfacer can be observed by IR spectrometry as well, whereas the identification of rutile is done by Raman spectrometry. However, the most promising candidate for distinguishing automotive paint samples is the basecoat, as Raman spectra of these contain the characteristic bands from organic pigments. Even in paints of the same colour (Fig. 6, spectra (a), (b)), different pigments may be present, allowing the distinction between the paint samples. The ability to distinguish two paints with the same colour (e.g. dark blue metallic) through the Raman spectra of the basecoat is a very promising tool in forensic analysis. IR analysis of this layer reveals only the binder characteristics.

Next to the measurements on cross sections, Raman spectra were also recorded from paint flakes. These spectra contained bands from both the clearcoat and the basecoat as shown in Fig. 10. Only when the paint did not contain any organic pigments in the basecoat, the bands in the

spectrum of the clearcoat dominated over those from the basecoat (Fig. 11). The observation of bands from organic pigments from the basecoat in these spectra suggests that the paints could also be distinguished by measurements on flakes. This reduces the sample preparation even further, as it is no longer necessary to make cross sections.

CONCLUSIONS

In this explorative study, we have demonstrated that Raman spectra can be obtained from the different layers of automotive paint from their cross sections. Assigning bands to vibrations of the binders has proved to be difficult, and identification of the binder is possible only by a full vibrational approach, including IR spectroscopy. In

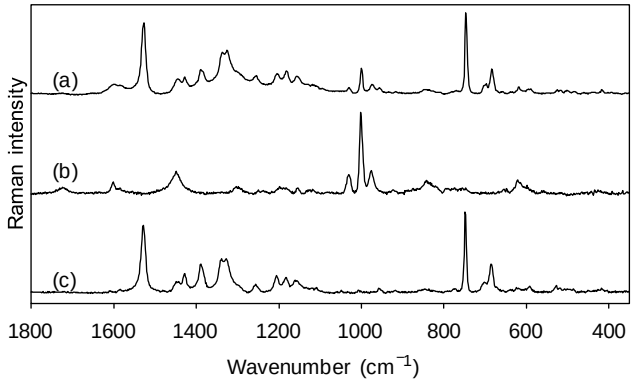

Figure 10. Raman spectra of a dark blue metallic Citroen¨ recorded from a flake (a), from the clearcoat of a cross section (b) and from the basecoat of a cross section (c).

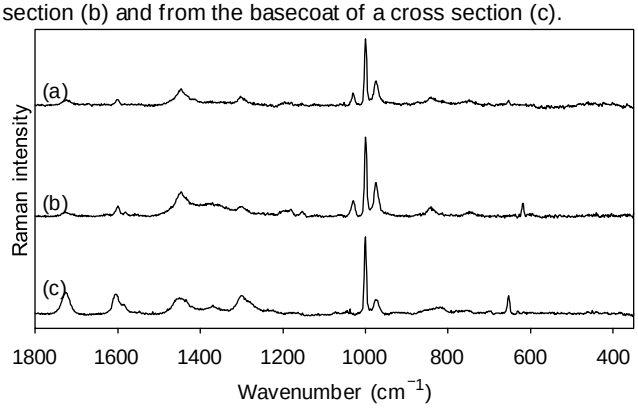

Figure 11. Raman spectra of a grey Ford Mondeo recorded from a flake (a), from the clearcoat of a cross section (b) and from the basecoat of a cross section (c).

contrast, it was demonstrated that Raman spectroscopy as such is suitable for the identification of pigments and extenders present in automotive paints, where especially the identification of organic pigments and rutile provides an advantage over IR spectroscopy. Moreover, the paints can easily be distinguished from each other by comparing the spectra of the basecoat. Discrimination of different paint samples is also possible by the presence or absence of bands from calcium carbonate or barium sulphate in the primer surfacers, while the primers provide little to no possibility to distinguish the paints. Because the spectra obtained from measurements on flakes

show bands from the clearcoat as well as from the basecoat, they can also be used to differentiate paint samples. These measurements have the advantage of no sample preparation. However, mention should be made that the discriminating power of the spectra of the basecoat could be lost partly by the use of the same organic pigments by paint manufacturers of different brands. Although research on a large scale would give an answer to this question, we feel that Raman spectroscopy can make a significant contribution to the forensic analysis of automotive paints. In this explorative study, a limited number of samples were used. Further research requires an increase in sample material, in order to give a more viable evaluation of the possibility of Raman spectroscopy to identify pigments and to discriminate paint samples.

Acknowledgements

J. De Gelder and P. Vandenabeele wish to thank the Research Foundation-Flanders (F.W.O.-Vlaanderen) for their grants as Research Assistant and Postdoctoral Fellow respectively. The authors also wish to thank the Research Foundation-Flanders (F.W.O.-Vlaanderen) and the Research Council UGent (B.O.F.) for their financial support.

REFERENCES

1. Adamson K. *Prog. Polym. Sci*. 2000; **25**: 1363.
2. Stevani CV, de farcia DLA, Porto JS, Trindade DJ, Bechara EJH.*Polym. Degrad. Stab*. 2000; **68**: 61.
3. Deakan D. *J. Forensic Sci*. 1975; **20**: 283.
4. Suzuki EM. *J. Forensic Sci*. 1996; **41**: 376.
5. Wampler TP, Bishea GA, Simonsick WJ. *J.Anal.Appl.Pyrol*. 1997; **40**: 79.
6. Gothard JA. *J. Forensic Sci*. 1976; **21**: 636.
7. Hobbs AL, Almirall JR. *Anal. Bioanal. Chem*. 2003; **376**: 1265.
8. Ryland SG, Kopec RJ. *J. Forensic Sci*. 1979; **24**: 140.
9. Govaert F, National Institute of Forensic Science, VilvoordseSteenweg 98/100, 1120 Brussels, Belgium, Personal Communication.
10. Stewart WD. *J. Forensic Sci*. 1975; **19**: 121.
11. Suzuki EM. *J. Forensic Sci*. 1996; **41**: 393. 12. Suzuki EM. *J. Forensic Sci*. 1997; **42**: 619.
13. Suzuki EM. *J. Forensic Sci*. 1998; **43**: 514.
14. Suzuki EM. *J. Forensic Sci*. 1999; **44**: 1151.
15. Suzuki EM. *J. Forensic Sci*. 1999; **44**: 297.
16. Massonet G, Stoecklein W. *Sci. Justice* 1999; **39**: 181.
17. Suzuki EM, Carrabba M. *J. Forensic Sci*. 2001; **46**: 1053.
18. Kuptsov AH. *J. Forensic Sci*. 1994; **39**: 305.
19. Biethan U, Funke W. *Ullman's Encyclopedia of Industrial Chemistry* (3rd ed.). VCH veslagsgeselschaft: Weinheim, 1990; 359.
20. Lin-Vien D, Colthup NB, Fateley WG, Grasselli JG. *The Handbook of Infrared and Raman Characteristic Frequencies of Organic Molecules*. Academic Press: San Diego, 1991.
21. Vandenabeele P, Hardy A, Edwards HGM, Moens L. *Appl. Spectrosc*. 2001; **55**: 525.

Spectroscopy, vol. 31, nº 4, pp. 253-271, 1977. [Links]

[11] Y.Roggo, P.Chalus, L.Maurer, C.Lema-Martinez, A.Edmond y N.Jent, “A review of near infrared spectroscopy and chemometrics in pharmaceutical technologies,” Journal of Pharmaceutical and Biomedical Analysis, vol. 44, nº 3, pp. 683-700, 2007. [Links]

[12] J. C.Carter, W. E.Brewer y S. M.Angel, “Raman spectroscopy for the in situ identification of cocaine and selected adulterants,” Applied Spectroscopy, vol. 54, nº 12, pp. 1876-1881, 2000. [Links]

[13] Ž.Šmit, K.Janssens, K.Proost y I.Langus, “Confocal μ-XRF depth analysis of paint layers,” Nuclear Instruments and Methods in Physics Research Section B: Beam Interactions with Materials and Atoms, vol. 219, pp. 35-40, 2004. [Links]

[14] P. L.Stiles, J. A.Dieringer, N. C.Shah y R. P. VanDuyne, “Surface-Enhanced Raman Spectroscopy,” Annual Review of Analytical Chemistry, vol. 1, p. 601-626, 2008. [Links]

[15] K. A.Willets y R. P. VanDuyne, “Localized Surface Plasmon Resonance Spectroscopy and Sensing,” Annual Review of Physical Chemistry, vol. 58, pp. 267-297, 2007. [Links]

[16] P.Lee y D.Meisel, “Adsorption and surface-enhanced Raman of dyes on silver and gold sols,” The Journal of Physical Chemistry, vol. 86, nº 17, pp. 3391-3395, 1982. [Links]

[17] M.Monge, “Nanopartículas de plata: métodos de síntesis en disolución y propiedades bactericidas,” Anales de Química, vol. 105, nº 1, pp. 33-41, 2009. [Links]

[18] G.Duan, C.Zhang, A.Li, X.Yang, L.Lu y X.Wang, “Preparation and characterization of mesoporous zirconia made by using a poly (methyl methacrylate) template.,” Nanoscale research letters, vol. 3, nº 3, p. 118, 2008. [Links]

ANEXOS.

JOURNAL OF RAMAN SPECTROSCOPY

JRS

J. Raman Spectrosc. 2005; **36**: 1059–1067
Published online 19 September 2005 in Wiley InterScience (www.interscience.wiley.com). DOI: 10.1002/jrs.1408

Forensic analysis of automotive paints by Raman spectroscopy

Joke De Gelder,[1]* Peter Vandenabeele,[1] Filip Govaert[2] and Luc Moens[1]

[1] Ghent University, Laboratory of Analytical Chemistry, Proeftuinstraat 86, B-9000 Ghent, Belgium
[2] National Institute of Forensic Science, Vilvoordse Steenweg 98/100, 1120 Brussels, Belgium

Received 21 April 2005; Accepted 25 July 2005

In this work, the possible contribution of Raman spectroscopy in forensic science is evaluated, more specifically for the analysis of automotive paint samples. Spectra from paint flakes as well as from cross sections were examined, in order to identify not only the pigments but also binders and extenders in all paint layers. Moreover, the possibility of distinguishing paint samples from different cars was evaluated to assess the use of vibrational spectroscopic techniques in the investigation of a hit-and-run accident.

The presence of rutile and extenders, such as calcite and barium sulphate, could be demonstrated by their characteristic Raman bands. However, the identification of the binder by Raman spectroscopy was hampered: only with additional information from IR analysis could most of the bands in the spectrum be assigned to molecular vibrations of the binders. In contrast, organic pigments, having very distinctive and well-resolved characteristic bands, could easily be identified by comparing the spectra from the basecoat of the sample with spectra from a reference database. Because of these characteristic bands, the basecoat seems to provide the best spectra to distinguish paint samples. Moreover, some paints can also be distinguished by the absence or presence of the bands from calcium carbonate and barium sulphate in the primer surfacer. When recording spectra from paint flakes, Raman bands from the spectra of the clearcoat as well as from the basecoat are obtained. Copyright © 2005 John Wiley & Sons, Ltd.

KEYWORDS: automotive paints; forensic science; pigment; binders

INTRODUCTION

Besides its industrial importance,[1,2] the analysis of automotive coatings is of importance to forensic scientists, especially for the investigation of hit-and-run accidents.[3–5] Over the years, several protocols have been developed and optimised to analyse and to distinguish different paint samples. First, a microscopic examination is performed, revealing differences in colour, number and thickness of the different paint layers, the shape of particles (metal flakes, pigments, etc.) and their distribution in each layer.[6–8] Often, this first examination is followed by a chemical or spectroscopic analysis. Scanning electron microscopy (SEM), infrared spectroscopy (IR spectroscopy), X-ray fluorescence (XRF) and pyrolysis gas chromatography mass spectrometry (Py-GC-MS) are important and frequently used techniques.[9] While XRF reveals the elemental composition of the sample, Py-GC-MS identifies the organic compounds in the sample.[5,7,9,10] In principle, IR Ł

Correspondence to: Joke De Gelder, Ghent University, Laboratory of Analytical Chemistry, Proeftuinstraat 86, B-9000 Ghent, Belgium.
E-mail: joke.degelder@UGent.be

Contract/grant sponsor: Research Foundation-Flanders. Contract/grant sponsor: Research Council UGent.

spectroscopy, being a molecular spectroscopic technique, can be used to study both organic and inorganic compounds. However, as most IR spectrometers record spectra in the range between 600 and 4000 cm^{1}, the identification of some inorganic compounds is hampered. Moreover, as many inorganic and organic pigments are weak IR absorbers, their spectrum is often overwhelmed by the IR spectra of other compounds in the sample.[4,9,11–15]

In this work, Raman spectroscopy is evaluated as an analytical technique for the forensic analysis of automotive paint samples. Indeed, the non-destructive character of the technique, the (almost) absence of sample preparation and the good lateral resolution are advantageous features of Raman spectroscopy in this field of research. Moreover, the use of Raman spectroscopy is complementary to IR spectroscopy:[16] although both are vibrational spectroscopic techniques, their spectra supply different information because of the different nature of the interactions and the different selection rules.[17]

There are two important advantages of Raman spectroscopy over IR spectroscopy. Usually Raman bands do not overlap, while the bands in IR spectra do. Moreover, Raman spectra generally extend well below 600 cm^{1}, a region where

many inorganic pigments and extenders have important vibrational bands.[18] Because of the complementary nature of both techniques and because of the importance of IR spectroscopy in forensic science, it is worthwhile to examine the possible contribution of Raman spectroscopy to this research, although until now little work has been done on the Raman spectroscopic study of automotive paints.[16,17] These studies focussed on red organic pigments[16] and inorganic pigments[17] in the topcoat, while our explorative research gives an overview of the possibilities of Raman spectroscopy in car paint analysis by examining the pigments, binders and extenders in all paint layers.

The automotive paint samples in this study are effect paints (also known as metallics and pearlescent paints) consisting of four layers. The bottom layer (called the first primer or primer) provides good adhesion to the car body as well as to the subsequent layers. This layer consists of a binder, basic pigmentation, an anti-rust pigmentation and extenders. Above this layer, the primer surfacer is retrieved, giving mechanical strength to the coating and resistance against degradation by ultraviolet light and providing a good, even surface to maximise the appearance and performance of the basecoat. It contains the basic pigmentation, extenders and a binder. The third layer (the basecoat) gives colour to the paint through pigments, alumina platelets and mica particles that are embedded in the binder.

Finally, a binder layer (clearcoat) protects the basecoat from fast degradation that could occur to the alumina platelets or mica particles present at the surface of the basecoat.[9,19]

EXPERIMENTAL Sample preparation

Raman spectra were recorded from flakes as well as from cross sections. For IR analysis, only cross sections were used. The flakes were attached to microscope slides by doublesided tapes. Cross sections were made by embedding a flake in a methacrylate resin, Technovit 2000 LC (Heraeus Kulzer, Germany). Technovit 2000 LC was selected as embedding medium because of its easy usage and high transparency. It is a one-component light-curing acrylic resin, which cures in *ca* 30 min at low temperatures (peak temperature: 90 °C). Polymerisationoftheresiniscarriedoutinadeviceequip ped with blue light (Technotray CU, Heraeus Kulzer, Germany). Because of the resin's high transparency, small samples can be clearly observed and easily sectioned. When the resin had hardened, a microtome (Cut 4060 E, MicroTec, Germany) was used to produce cross sections, with a thickness of 5 μm. Cross sections were made parallel to the layer structure. By doing this, the highest possible surface area of a layer within a cross section is obtained. These cross sections were attached to a metal carrier by a procedure shown in Fig. 1(a). The metal carrier has the size of a microscope slide and contains three openings with a diameter of *ca* 8 mm. The carrier was covered with double-sided tape with three openings at the same place as those in the carrier. A cross section was then stretched out on a microscope slide with methanol, after which the carrier was pressed upon the cross section on the place of a hole in the tape. The cross section was then attached to the carrier as shown in Fig. 1(b). This sample preparation reduces the chance of spectral interference of the methacrylate resin and thecarrier.Giventhenon-destructivenatureofIRandRaman measurements, the same cross sections can be used for both the techniques. Raman and IR spectra of the embedding resin were measured to investigate possible physical overlap and spectral interference (Fig. 1(c)).

Fourier-transform infrared spectrometry (FTIR)

A Fourier-transform infrared (FTIR) spectrometer (Nicolet 510P, USA) equipped with a KBr beam splitter, an IR microscope (NIC-Plan, USA) with 32 ð objective (SpectraTech,USA)andamercurycadmiumtelluride(M CT)detector was used to analyse the chemical binders and extenders present in these coatings. With an aperture of 3.2 mm, a spot size of 100 μm is obtained. A hundred scans were collected with a resolution of 4 cm^{1} and the intensity (% transmittance) *versus* wavenumber (cm^{1}) was measured between 650 and 4000 cm^{1}. Spectra of each paint layer were recorded by transferring the metal carrier with a cross section to the sample stage and focussing on the layer of interest. The obtained spectra were interpreted and compared with commercial and our personal spectral libraries of paint materials. A spectrum of the embedding resin was measured to investigate possible physical overlap and spectral interference.

Raman spectrometry

The spectra were recorded with a Renishaw System 1000 spectrometer that was equipped with a 785-nm diode laser, with a power of 50 mW at the source, and between 1 and 2 mW on the sample by the use of 25 or 10% neutral density filters. The laser beam was focussed on the samples by a 50 ð objective lens, which produced a laser spot of approximately 2 μm. The spectrometer collects light in the

backscattering mode, which is dispersed on a 1200-lines mm^{1} grating and focussed on a Peltier-cooled CCD detector.

Because of the low sensitivity of the CCD detector above

$2000\ cm^{-1}$, no spectrawererecorded in the (C–H) stretching region (2700–3400 cm^{1}). Spectra from the clearcoats, primer surfacers and primers were recorded for up to 2 min and accumulated up to 60 times. In the basecoat, the presence of organic pigments, which are strong Raman scatterers, reduced the recording time to a maximum of 1 min and the accumulations to a maximum of 15. All spectra were baseline corrected.

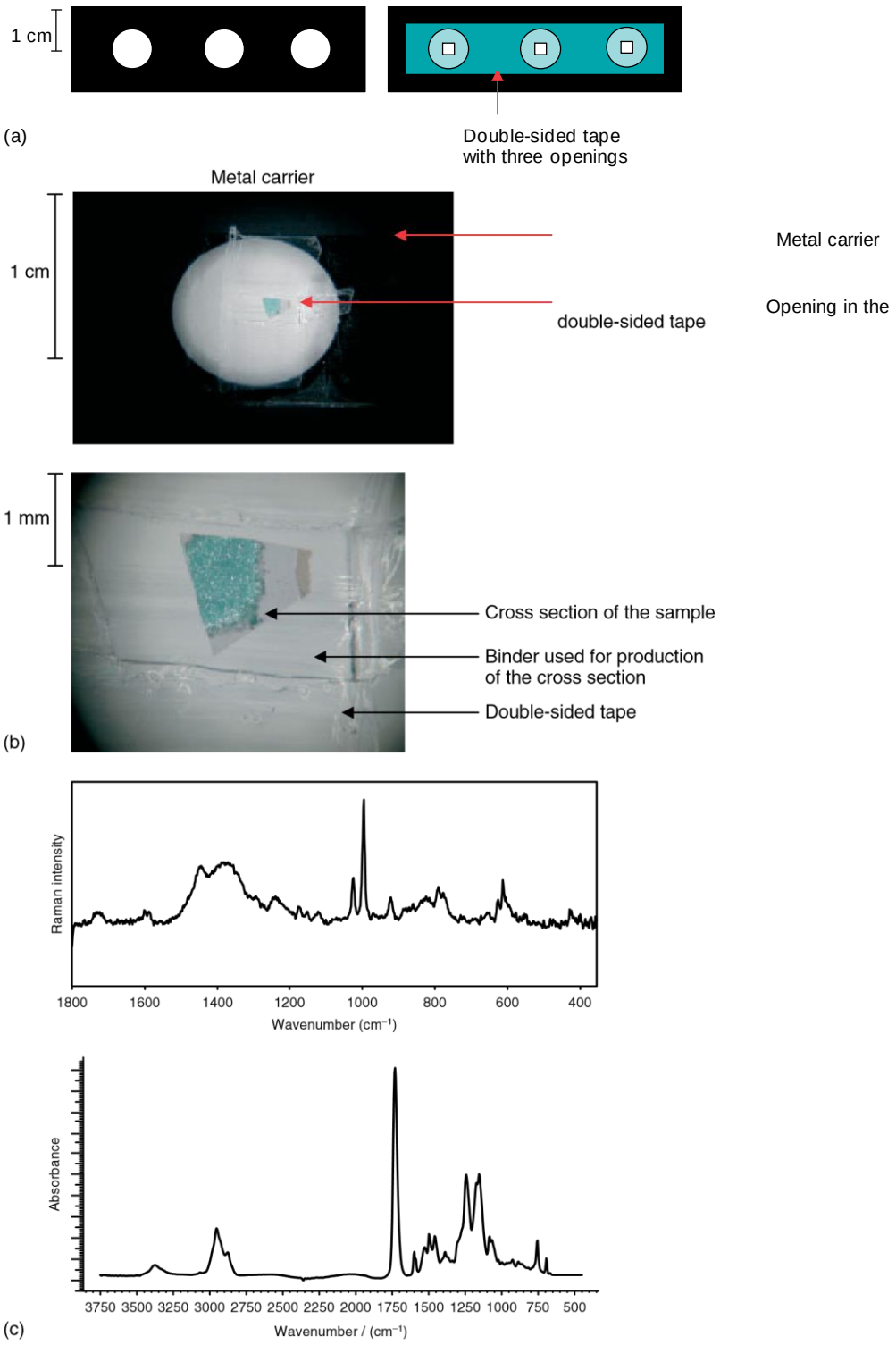

Figure 1. Sample preparation: attaching the cross section to a metal carrier (a, b) and Raman and IR spectra of the methacrylate resin used for cross sectioning (c).

RESULTS AND DISCUSSION Spectra

obtained from cross sections

In this study, the application of Raman spectroscopy in the forensic analysis of automotive paints was evaluated. The results were compared with the information obtained by IR spectrometry. Both techniques permit obtaining separate spectra from

each layer of different paint cross sections. Exact Raman wavenumbers are given in Table 1, while the

Table 1. Raman wavenumbers (in cm[1]) for each spectrum

Figure	Sample	Layer	Raman wavenumber (cm^{-1})
1(c)	Methacrylate (Technovit 2000 LC)		604 (sh), 613 (m), 626 (w), 653 (vw), 777 (w), 790 (m), 823 (w), 870 (vw), 922 (w), 996 (vs), 1025 (m), 1120 (vw), 1150 (vw), 1174 (vw), 1238 (w), 1293 (w), 1376 (s, br), 1444 (s), 1588 (vw), 1599 (vw), 1726 (vw)
2(a)	Dark blue metallic Citroen¨	P	444 (vs), 609 (s), 637 (vs), 820 (m), 1110 (m), 1182 (m, br), 1226 (w), 1250 (w), 1304 (m, br), 1453 (m, br), 1582 (sh), 1605 (s)
2(b)	Amazon green metallic Opel	P	447 (vs), 610 (vs), 633 (sh), 818 (m), 986 (w), 1109 (w), 1181 (m), 1250 (m, br), 1307 (m, br), 1453 (w), 1580 (sh), 1608 (m)
4(a)	Bordeaux metallic Alfa Romeo	PS	444 (vs), 608 (vs), 652 (sh), 984 (s), 1000 (s), 1302 (m, br), 1444 (w, br), 1584 (sh), 1600 (m), 1723 (w)
4(b)	Amazon green metallic Opel	PS	445 (vs), 609 (vs), 647 (sh), 711 (vw), 1038 (w), 1084 (m), 1302 (w, br), 1446 (vw, br), 1579 (sh), 1600 (w), 1720 (vw)
4(c)	Grey Ford Mondeo	PS	446 (s), 612 (m), 653 (sh), 984 (s), 1000 (m), 1301 (vs, br), 1583 (sh), 1602 (s, br), 1723 (w)
4(d)	Green Opel Astra	PS	446 (vs), 608 (vs), 646 (sh), 711 (vw), 1037 (w), 1084 (m), 1303 (m, br), 1382 (m, br), 1446 (m, br), 1580 (sh), 1598 (m), 1722 (w)
6(a)	Dark blue metallic Citroen¨	BC	686 (m), 702 (w), 748 (vs), 1157 (w), 1160 (w), 1182 (w), 1205 (w), 1257 (vw), 1327 (s), 1339 (s), 1390 (m), 1428 (m), 1443 (w), 1528 (vs)
6(b)	Dark blue metallic Renault	BC	377 (w), 406 (w), 477 (s), 494 (m), 582 (w), 620 (w), 639 (sh), 680 (m), 747 (m), 757 (w), 802 (m), 908 (vw), 952 (vw), 1001 (w), 1041 (w), 1142 (sh), 1154 (m), 1183 (m), 1283 (m), 1301 (m), 1328 (s), 1355 (vs), 1384 (vs), 1448 (vw), 1474 (w), 1526 (m), 1552 (w), 1597 (vw), 1618 (w)
6(c)	Green Opel Astra	BC	481 (vw), 593 (vw), 640 (vw), 682 (vs), 700 (sh), 738 (s), 744 (sh), 773 (m), 814 (w), 951 (vw), 976 (vw), 1078 (vw), 1140 (vw), 1186 (sh), 1209 (m), 1278 (m), 1285 (sh), 1298 (sh), 1314 (w), 1335 (m), 1355 (sh), 1384 (vw), 1445 (vw), 1503 (sh), 1533 (vs)
6(d)	Dioxazine violet pigment PV23		417 (w), 485 (w), 528 (m, w), 590 (w), 619 (w), 672 (w), 725 (vw), 749 (vw), 776 (vw), 808 (vw), 884 (vw), 920 (w), 933 (vw), 950 (vw), 993 (vw), 1108 (w), 1121 (vw), 1132 (vw), 1152 (vw), 1166 (m, w), 1206 (m), 1256 (m, w), 1280 (vw), 1333 (m, w), 1346 (m), 1391 (vs), 1431 (m), 1443 (w), 1477 (vw), 1590 (vw), 1610 (vw), 1643 (vw)
6(e)	Copper pthalocyanin pigment PB15		490 (vw), 593 (vw), 680 (w), 746 (s), 773 (vw), 837 (v), 951 (vw), 1005 (vw), 1105 (v), 1140 (w), 1181 (w), 1333 (m), 1446 (w), 1519 (vs)
6(f)	Indanthrone PB60		404 (vw), 476 (m), 493 (w), 582 (vw), 620 (v), 676 (vw), 757 (vw), 801 (w), 906 (vw), 999 (vw), 1040 (vw), 1155 (w, m), 1182 (w), 1283 (w, m), 1298 (w, m), 1325 (s), 1352 (vs), 1380 (vs), 1473 (vw), 1551 (w), 1616 (w)
6(g)	Chlorated copper pthalocyanin pigment PG7		686 (vs), 741 (s), 777 (m), 818 (w), 959 (vw), 981 (vw), 1083 (vw), 1214 (w-m), 1287 (m), 1339 (w), 1388 (vw), 1446 (vw), 1506 (vw), 1539 (vs)
9(a)	Dark blue metallic Citroen¨	CLC	598 (sh), 621 (w), 841 (w), 976 (m), 1002 (vs), 1032 (m), 1154 (vw), 1195 (vw), 1302 (vw), 1449 (m), 1587 (vw), 1602 (w), 1725 (vw)
9(b)	Green-grey metallic Toyota	CLC	617 (w), 745 (vw), 838 (vw), 973 (m), 998 (vs), 1028 (m), 1152 (vw), 1185 (vw), 1302 (w), 1372 (m, br), 1445 (m), 1596 (sh), 1601 (w), 1721 (vw)
9(c)	Amazon green metallic Opel	CLC	620 (w), 975 (m), 1001 (vs), 1030 (m), 1154 (vw), 1189 (vw), 1301 (w), 1371 (m, br), 1448 (m), 1585 (vw), 1602 (w), 1725 (vw)
9(d)	Green Opel Astra	CLC	618 (vw), 664 (vw), 775 (vw), 840 (w), 975 (m), 1000 (vs), 1030 (w), 1154 (vw), 1302 (sh), 1374 (s, br), 1447 (vs), 1596 (w), 1602 (vw), 1728 (vw), 1757 (vw)

10(a)	Dark blue metallic Citroen¨	F	590 (vw), 634 (vw), 683 (m), 697 (w), 746 (vs), 845 (vw), 956 (vw), 973 (w), 999 (m), 1030 (vw), 1117 (w), 1155 (m), 1181 (m), 1203 (m), 1254 (m), 1303 (sh), 1326 (s), 1337 (s), 1384 (sh), 1389 (m), 1422 (m), 1445 (m), 1527 (vs), 1584 (sh), 1600 (w)
10(b)	Dark blue metallic Citroen¨	CLC	598 (sh), 621 (w), 841 (w), 976 (m), 1002 (vs), 1032 (m), 1154 (vw), 1195 (vw), 1302 (vw), 1449 (m), 1587 (vw), 1602 (w), 1725 (vw)

(*Continued*)

Table 1. (*Continued*)

Figure	Sample	Layer	Raman wavenumber (cm^{-1})
10(c)	Dark blue metallic Citroen¨	BC	686 (m), 702 (w), 748 (vs), 1157 (w), 1160 (w), 1182 (w), 1205 (w), 1257 (vw), 1327 (s), 1339 (s), 1390 (m), 1428 (m), 1443 (w), 1528 (vs)
11(a)	Grey Ford Mondeo	F	653 (vw), 750 (vw), 840 (w), 974 (m), 1000 (vs), 1030 (w), 1189 (vw), 1302 (w), 1445 (m), 1600 (vw), 1724 (vw)
11(b)	Grey Ford Mondeo	CLC	618 (w), 746 (vw), 842 (w), 974 (m), 1000 (vs), 1029 (w), 1153 (vw), 1188 (vw), 1302 (w), 1371 (w, br), 144 (m), 1582 (vw), 1600 (w), 1727 (vw)
11(c)	Grey Ford Mondeo	BC	652 (m), 818 (vw), 974 (w), 1000 (vs), 1282 (sh), 1300 (m), 1370 (w), 1448 (w), 1586 (sh), 1603 (m), 1726 (m)

vw, very weak; w, weak; m, medium; s, strong; vs, very strong; sh, shoulder; br, broad; CLC, clearcoat; BC, basecoat; PS, primer surfacer; P, primer; F, flake.

Table 2. IR wavenumbers (in cm^{1}) for each spectrum

Figure	Sample	Layer	IR wavenumber (cm^{-1})
1(c)	Methacrylate (Technovit 2000 LC)		692 (m), 756 (m), 884 (vw), 924 (vw), 1084 (m), 1152 (s), 1244 (s), 1388 (w), 1456 (m), 1496 (m), 1524 (m), 1600 (m), 1732 (vs), 2879 (m), 2952 (s), 3378 (br)
3(a)	Dark blue metallic Citroen¨	P	669 (vw), 765 (vw), 802 (w), 829 (m), 916 (w), 1012 (sh), 1105 (s), 1182 (s), 1228 (s), 1302 (m), 1361 (w), 1382 (w), 1413 (m), 1458 (m), 1510 (vs), 1606 (m), 1732 (s), 2872 (m), 2931 (m), 2968 (m), 3037 (w), 3320 (br), 3619 (w), 3695 (w)
3(b)	Amazon green metallic Opel	P	657 (br), 829 (s), 914 (m), 1012 (sh), 1038 (s), 1076 (m), 1105 (s), 1184 (s), 1228 (vs), 1301 (m), 1361 (w), 1382 (w), 1414 (m), 1460 (m), 1510 (vs), 1606 (s), 1730 (s), 2872 (m), 2931 (m), 2966 (m), 3035 (w), 3329 (br), 3620 (w), 3695 (m)
5(a)	Bordeaux metallic Alfa Romeo	PS	671 (w), 731 (m), 830 (w), 984 (vw), 1018 (m), 1076 (s), 1134 (s), 1182 (m), 1238 (s), 1306 (m), 1375 (m), 1466 (s), 1510 (vw), 1537 (w), 1590 (vw), 1608 (vw), 1690 (m), 1728 (vs) 2874 (vw), 2936 (m), 2964 (m), 3389 (br), 3678 (w)
5(b)	Amazon green metallic Opel	PS	673 (w), 713 (w), 877 (s), 1022 (m), 1074 (m), 1122 (m), 1286 (s), 1448 (vs), 1550 (sh), 1580 (sh), 1600 (sh), 1690 (sh), 1724 (s), 1798 (w), 2512 (w), 2863 (m), 2935 (m), 3676 (vw)
5(c)	Grey Ford Mondeo	PS	730 (s), 814 (w), 983 (m), 1022 (w), 1076 (vs), 1124 (s), 1186 (s), 1238 (s), 1303 (m), 1375 (m), 1475 (m), 1512 (w), 1548 (m), 1727 (vs), 2868 (w), 2935 (m), 2957 (m), 3372 (br), 3676 (vw)
5(d)	Green Opel Astra	PS	669 (m), 713 (w), 875 (s), 1020 (s), 1074 (m), 1124 (m), 1286 (s), 1430 (vs), 1690 (m), 1724 (s), 1798 (w), 2513 (vw), 2860 (w), 2933 (m), 3676 (w)
7(a)	Dark blue metallic Citroen¨	BC	702 (m), 730 (m), 815 (m), 1078 (s), 1165 (s), 1236 (s), 1306 (w), 1363 (s), 1477 (s), 1552 (s), 1730 (vs), 2873 (m), 2931 (m), 2958 (m), 3026 (w), 3380 (br)
7(b)	Dark blue metallic Renault	BC	712 (w), 730 (m), 814 (m), 1018 (w), 1074 (s), 1165 (s), 1273 (s), 1284 (s), 1373 (s), 1477 (s), 1498 (s), 1550 (s), 1658 (m), 1727 (vs), 2850 (m), 2873 (mp), 2921 (m), 2962 (m), 3026 (w), 3380 (br)

7(c)	Green Opel Astra	BC	730 (m), 771 (w), 815 (m), 1003 (s), 1041 (w), 1072 (s), 1095 (w), 1122 (w), 1153 (w), 1160 (w), 1240 (s), 1286 (s), 1305 (s), 1367 (m), 1388 (m), 1388 (s), 1548 (s), 1727 (vs), 2856 (m), 2927 (s), 3367 (br)
8(a)	Amazon green metallic Opel	CLC	701 (s), 730 (w), 760 (m), 815 (m), 1022 (m), 1093 (m), 1166 (s), 1228 (m), 1307 (w), 1378 (m), 1454 (m), 1492 (m), 1552 (s), 1730 (vs), 2873 (m), 2931 (s), 2956 (s), 3027 (w), 3390 (br)
8(b)	Green Opel Astra	CLC	702 (m), 765 (m), 815 (w), 1041 (w), 1076 (w), 1168 (s), 1286 (s), 1367 (m), 1386 (m), 1456 (s), 1550 (s), 1691 (s), 1730 vs), 2873 (m), 2931 (s), 2958 (s), 3028 (vw), 3372 (br)

vw, very weak; w, weak; m, medium; s, strong; vs, very strong; sh, shoulder; br, broad; CLC, clearcoat; BC, basecoat; PS, primer surfacer; P, primer; F, flake.

text contains estimated Raman wavenumbers for bands that occur in spectra of the same layer. Assignments of specific Raman bands to the binder are based on Ref. 20. Pigments and extenders were identified by the use of a personal database with reference Raman spectra.[21] Table 2 gives a list of IR absorption bands of each spectrum shown in this paper.

Spectral interference of the adjacent embedding resin was avoided by measuring at the centre of the layer of interest. Spot sizes of 100 μm for IR analysis and 2 μm for Raman analysis are small enough to focus on only one layer. Although the embedding resin has similar absorption characteristics as some automotive paints, the binders of the paint samples could clearly be identified.

The primers of all paints examined in this study, give rise to spectra with a similar profile as shown in Fig. 2. This similarity was expected as all primers contained epoxy binders and aluminium silicate according to IR analyses. Figure 3 shows IR spectra of these two similar primers. Epoxy binder bands at 830, 1180, 1240, 1410, 1510 and 1610 cm^{1} and absorption bands of aluminium silicate at 1010, 1035, 3340, 3620, 3654 and 3695 cm^{1} can clearly be observed. Aluminium silicate caused a shoulder in the Raman spectrum (Fig. 2) at *ca* $635\ cm^{-1}$, but unlike IR spectroscopy, Raman spectroscopy showed the presence of rutile (TiO_2: *ca* 446 and $609\ cm^{-1}$). The doublet at *ca* 1580 and 1606 cm^{1} caused by a quadrant stretch suggests the use of benzene derivatives (e.g. bisphenol A) in the production of the epoxy binder. This supposition is supported by the presence of a band at *ca* $820\ cm^{-1}$ that could be assigned to ring vibrations of *para* substituted benzenes. Nevertheless, this band could also (partly) have resulted from the skeletal stretches of secondary alcohols. The epoxy binder is responsible for the bands at *ca* $1110\ cm^{-1}$ as well as at *ca* $1182\ cm^{-1}$, which could be assigned to C–C backbone and C–C out-of-plane vibrations, respectively. Furthermore, the CH_2 twisting and rocking vibrations, CH_2 in-phase twisting vibrations, and the CH_3 and CH_2 deformations cause bands in the regions 1175–1310, 1295–1310 and 1446–1473 cm^{1}. Only one of the primers that were examined contained, next to the epoxy binder, a polyurethane binder also. In the latter spectrum, an extra band at *ca* $1725\ cm^{-1}$ was detected, which could be attributed to a C═O stretching vibration. Although not confirmed by IR analysis, the band at 986 cm^{1} in spectrum 2(c) could be caused by the SO_4^{2-} symmetric stretching of barium sulphate.

The Raman spectra of the primer surfacer (the four spectra shown in Fig. 4) all show bands at *ca* 446 and 609 cm^{1}, which point to the presence of rutile. A closer look at these bands revealed the existence of a shoulder at *ca* $650\ cm^{-1}$, which could be assigned to magnesium silicate. Spectra (a) and (c) (Alfa Romeo bordeaux metallic and Ford Mondeo grey) show a band at 984 cm^{1}, which was assigned to the SO_4^{2-} symmetric stretching vibration of barium sulphate, while spectra (b) and (d) (Opel Amazon green metallic and Opel Astra green) show bands at 711 and 1084 cm^{1} due to

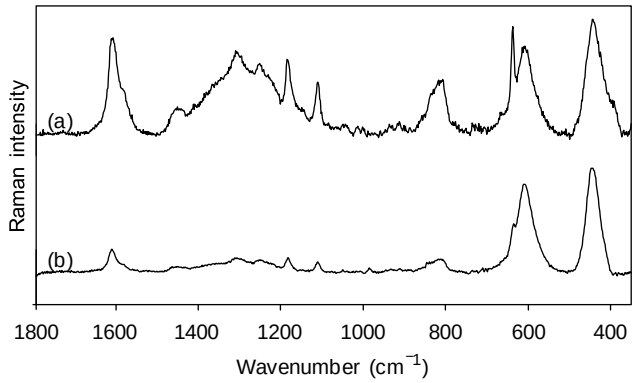

Figure 2. Raman spectra recorded from the primer of cross sections of a dark blue metallic Citroen (a) and an Amazon¨ green metallic Opel (b) (spectrum (b) was Fourier-smoothed by GRAMS 5.2).

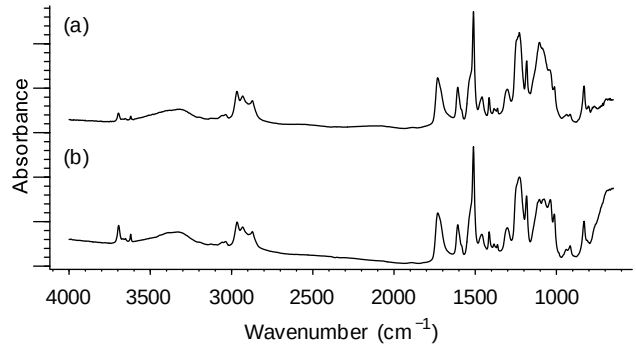

Figure 3. IR spectra recorded from the primer of cross sections of a dark blue metallic Citroen (a) and an Amazon¨ green metallic Opel (b).

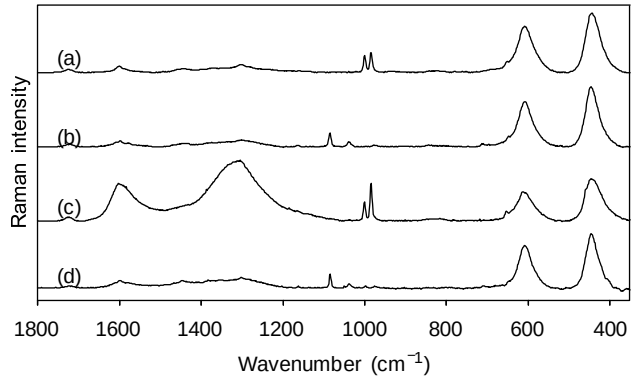

Figure 4. Raman spectra recorded from the primer surfacer of cross sections of a Bordeaux metallic Alfa Romeo (a), an Amazon green metallic Opel (b), a grey Ford Mondeo (c) and a green Opel Astra (d).

the presence of calcite ($CaCO_3$). The broadbands at about 1301 and 1602 cm^1 in spectrum (c) reveal the presence of carbon black. The band at *ca* 1722 cm^{-1} present in all spectra can be assigned to the C═O stretching vibration of polyurethane, polyester or alkyd binders, from which their presence was confirmed by IR analyses. Other bands resulting from the binder include those in the region of 1175–1310 and 1446–1473 cm^1 due to CH_2 twisting, rocking and in-phase twisting vibrations, and CH_3 and CH_2 deformations, respectively. At *ca* 1580 and 1600 cm^1 in spectra (a), (b) and (d), a doublet could be assigned to the quadrant stretching of benzene derivates that are

frequently used in the production of the polyester, polyurethane and alkyd binders. The presence of aromatics also gives rise to bands at 1000 (spectra (a), (c)) and *ca*1038 cm^{-1} (spectra (b), (d)), which can be attributed to trigonal ring breathing and aromatic ring vibrations respectively. Indeed, for a primer surfacer, many characteristics were confirmed by IR analysis as shown in Fig. 5. All IR spectra contain absorption bands of aluminium silicate (670, 1020 and 3676 cm^{1}). Spectra (a) and (c) contain a sulphate band at 980 cm^{1} and spectra (b) and (d) bands of calcite (875, 1445 and 1795 cm^{-1}).

Figure 6 shows the Raman spectra of the basecoat as recorded from some cross sections (spectra (a)–(c)) along with reference spectra of some organic pigments (spectra (d)–(g)). Spectrum (a) was recorded from a dark blue metallic Citroenand exhibits bands from bothspectra(d) and¨ (e) corresponding to a violet dioxazine pigment (PV23) and a copper pthalocyanin pigment (PB15), respectively. In the spectrum of a dark blue metallic Renault (spectrum (b)) there are, next to an indanthrone pigment (PB60, spectrum (f)), also small bands visible from copper pthalocyanin (PB15, spectrum (e)). The basecoat of a green Opel Astra (spectrum (c)) clearly contains a chlorated copper pthalocyanin pigment (spectrum (g)). The bands of the organic pigments totally mask bands of binders. From these examples, it is clear that the organic pigments are very easy to identify by comparing their spectra to a database of reference spectra.[21] This is a great advantage over IR spectroscopy, where nearly no bands of organic pigments can be observed in the spectra of the basecoat. IR spectra permit, on the other hand, to

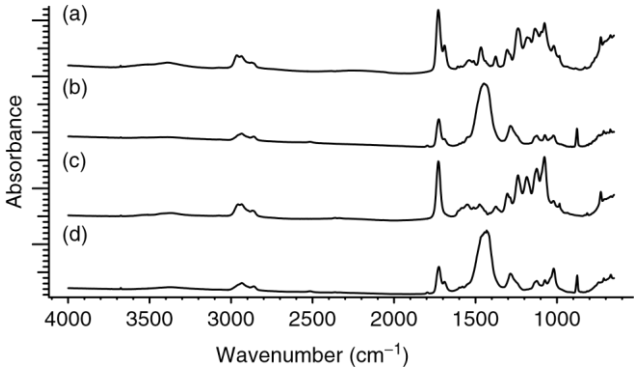

Figure 5. IR spectra recorded from the primer surfacer of cross sections of a Bordeaux metallic Alfa Romeo (a), an Amazon green metallic Opel (b), a grey Ford Mondeo (c) and a green Opel Astra (d).

identify the binders used in these basecoats. Figure 7 shows IR spectra of three different basecoats. All basecoats contain melamine used to cross link the primary binder such as acrylic, polyester and alkyd.

From IR studies, it seems that the clearcoats of all paints that were examined consisted of melamine styrene binders, possibly with an acrylic, alkyd or polyurethane binder. Figure 8 depicts clearly the melamine (815 and

1550 cm^{-1} and styrene (700, 760, 1450 and 1490 cm^{-1})absorption bands in both IR spectra. IR spectrum (b) can be differentiated by its polyurethane band at 1690 cm^{1}. As shown in Fig. 9, the Raman spectra of the clearcoats are very similar as well. The Raman bands at approximately 975,

1001 and 1031 cm^{1}, present in all spectra, were assigned to the triazine ring breathing of the melamine resin, trigonal ring breathing and in-plane CH deformation of the styrene binder, respectively. Other bands that can be attributed to the styrene binder are those at 620 and 1190 cm^{1} (last one probably masked in spectrum (d) by a broader band) due to

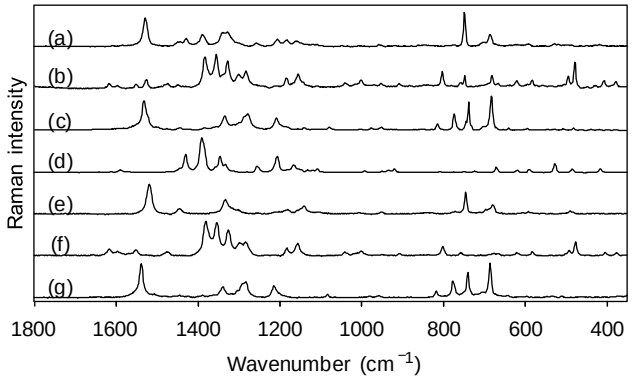

Figure 6. Raman spectra recorded from the basecoat of cross sections of a dark blue metallic Citroen (a), a dark blue metallic¨ Renault (b) and a green Opel Astra (c), along with reference spectra from a dioxazine violet pigment PV23 (d), a copper pthalocyanin pigment PB15 (e), indanthrone PB60 (f) and a chlorated copper pthalocyanin pigment PG7 (g).

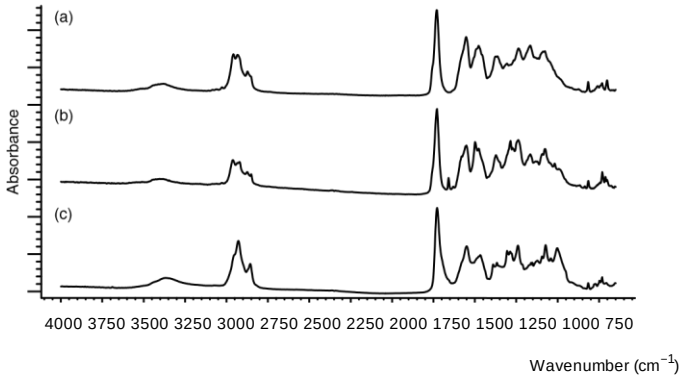

Figure 7. IR spectra recorded from the basecoat of cross sections of a dark blue metallic Citroen (a), a dark blue metallic¨ Renault (b) and a green Opel Astra (c).

a ring deformation and a C_6H_5–C stretching, respectively, and the doublet at *ca* $1590/1602\ \mathrm{cm}^{-1}$ from a ring stretching.

Furthermore, the bands in the regions 1175–1310, 1295–1310 and 1446–1473 cm^{1} can be assigned to CH_2 twisting and rocking vibrations, CH_2 in-phase twisting vibrations, and CH_3 in-phase bending and CH_2 wagging, respectively. The band at *ca* $1725\ \mathrm{cm}^{-1}$ in spectra (b), (c) and (d) and the band at 1757 cm^{1} in spectrum (d), could be attributed to C═O stretches from the acrylic, alkyd or polyurethane binders. The bands due to ring vibration of *para* substituted benzenes and symmetric C–N–C stretches from secondary amines are visible in the regions 720–830 and 850–900 cm^{1}.

Evaluation of the capability to distinguish automotive paint samples by spectra from cross sections and from flakes

The Raman and IR spectra of the different clearcoats (Figs 9 and 8, respectively) are very similar, which makes it difficult to distinguish the paints by studying this layer. The same remark can be made for the spectra of the primers (Figs 2 and 3). Further research on reproducibility of the spectra of samples from different cars of the same brand and evaluation of the variation of spectra of samples of cars from different

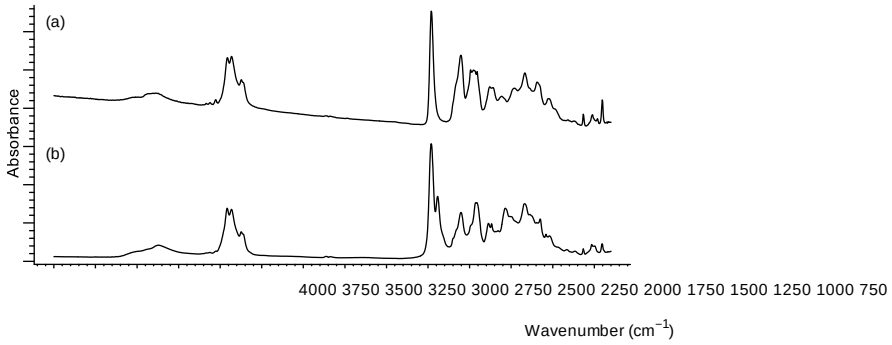

Figure 8. IR spectra recorded from the clearcoat of cross sections of an Amazon green metallic Opel (a) and a green Opel Astra (b).

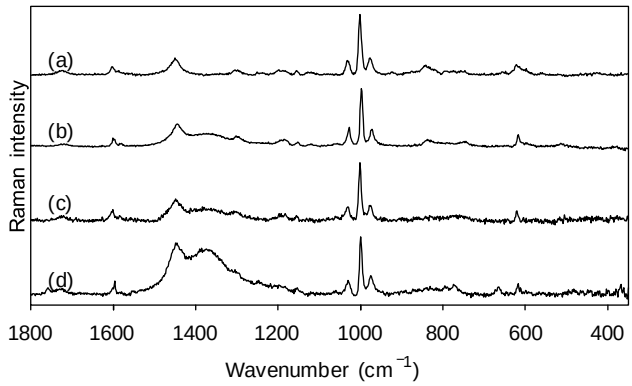

Figure 9. Raman spectra recorded from the clearcoat of cross sections of a dark blue metallic Citroen (a), a green–grey¨ metallic Toyota (b), an Amazon green metallic Opel (c) and a green Opel Astra (d).

brands that use similar binders would reveal if these spectra could be used to distinguish automotive paints. On the contrary, the Raman spectra of the primer surfacer can be used to distinguish certain coatings by the absence or the presence of the bands caused by calcium carbonate or barium sulphate, as shown in Fig. 4. The same characteristics of the primer surfacer can be observed by IR spectrometry as well, whereas the identification of rutile is done by Raman spectrometry. However, the most promising candidate for distinguishing automotive paint samples is the basecoat, as Raman spectra of these contain the characteristic bands from organic pigments. Even in paints of the same colour (Fig. 6, spectra (a), (b)), different pigments may be present, allowing the distinction between the paint samples. The ability to distinguish two paints with the same colour (e.g. dark blue metallic) through the Raman spectra of the basecoat is a very promising tool in forensic analysis. IR analysis of this layer reveals only the binder characteristics.

Next to the measurements on cross sections, Raman spectra were also recorded from paint flakes. These spectra contained bands from both the clearcoat and the basecoat as shown in Fig. 10. Only when the paint did not contain any organic pigments in the basecoat, the bands in the

spectrum of the clearcoat dominated over those from the basecoat (Fig. 11). The observation of bands from organic pigments from the basecoat in these spectra suggests that the paints could also be distinguished by measurements on flakes. This reduces the sample preparation even further, as it is no longer necessary to make cross sections.

CONCLUSIONS

In this explorative study, we have demonstrated that Raman spectra can be obtained from the different layers of automotive paint from their cross sections. Assigning bands to vibrations of the binders has proved to be difficult, and identification of the binder is possible only by a full vibrational approach, including IR spectroscopy. In

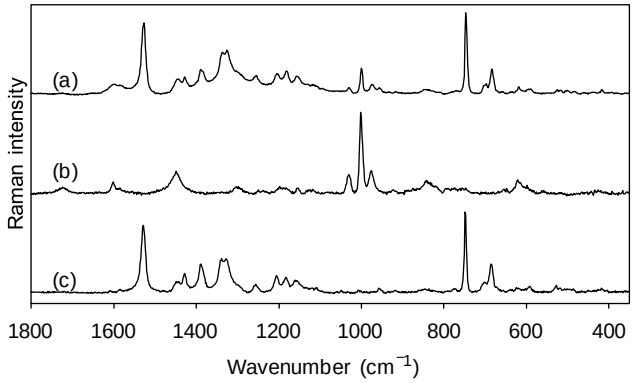

Figure 10. Raman spectra of a dark blue metallic Citroen¨ recorded from a flake (a), from the clearcoat of a cross section (b) and from the basecoat of a cross section (c).

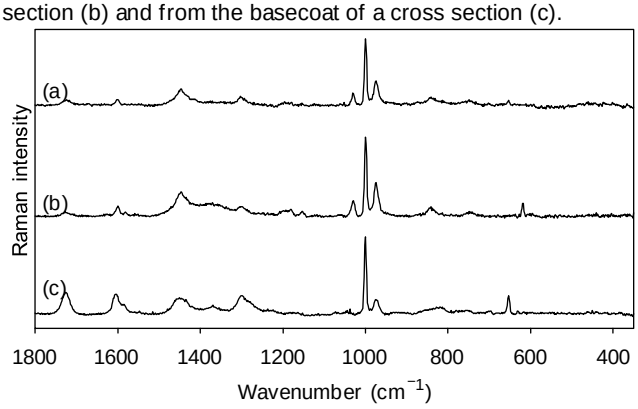

Figure 11. Raman spectra of a grey Ford Mondeo recorded from a flake (a), from the clearcoat of a cross section (b) and from the basecoat of a cross section (c).

contrast, it was demonstrated that Raman spectroscopy as such is suitable for the identification of pigments and extenders present in automotive paints, where especially the identification of organic pigments and rutile provides an advantage over IR spectroscopy. Moreover, the paints can easily be distinguished from each other by comparing the spectra of the basecoat. Discrimination of different paint samples is also possible by the presence or absence of bands from calcium carbonate or barium sulphate in the primer surfacers, while the primers provide little to no possibility to distinguish the paints. Because the spectra obtained from measurements on flakes

show bands from the clearcoat as well as from the basecoat, they can also be used to differentiate paint samples. These measurements have the advantage of no sample preparation. However, mention should be made that the discriminating power of the spectra of the basecoat could be lost partly by the use of the same organic pigments by paint manufacturers of different brands. Although research on a large scale would give an answer to this question, we feel that Raman spectroscopy can make a significant contribution to the forensic analysis of automotive paints. In this explorative study, a limited number of samples were used. Further research requires an increase in sample material, in order to give a more viable evaluation of the possibility of Raman spectroscopy to identify pigments and to discriminate paint samples.

Acknowledgements

J. De Gelder and P. Vandenabeele wish to thank the Research Foundation-Flanders (F.W.O.-Vlaanderen) for their grants as Research Assistant and Postdoctoral Fellow respectively. The authors also wish to thank the Research Foundation-Flanders (F.W.O.-Vlaanderen) and the Research Council UGent (B.O.F.) for their financial support.

REFERENCES

1. Adamson K. *Prog. Polym. Sci*. 2000; **25**: 1363.
2. Stevani CV, de farcia DLA, Porto JS, Trindade DJ, Bechara EJH.*Polym. Degrad. Stab*. 2000; **68**: 61.
3. Deakan D. *J. Forensic Sci*. 1975; **20**: 283.
4. Suzuki EM. *J. Forensic Sci*. 1996; **41**: 376.
5. Wampler TP, Bishea GA, Simonsick WJ. *J.Anal.Appl.Pyrol*. 1997; **40**: 79.
6. Gothard JA. *J. Forensic Sci*. 1976; **21**: 636.
7. Hobbs AL, Almirall JR. *Anal. Bioanal. Chem*. 2003; **376**: 1265.
8. Ryland SG, Kopec RJ. *J. Forensic Sci*. 1979; **24**: 140.
9. Govaert F, National Institute of Forensic Science, VilvoordseSteenweg 98/100, 1120 Brussels, Belgium, Personal Communication.
10. Stewart WD. *J. Forensic Sci*. 1975; **19**: 121.
11. Suzuki EM. *J. Forensic Sci*. 1996; **41**: 393. 12. Suzuki EM. *J. Forensic Sci*. 1997; **42**: 619.
13. Suzuki EM. *J. Forensic Sci*. 1998; **43**: 514.
14. Suzuki EM. *J. Forensic Sci*. 1999; **44**: 1151.
15. Suzuki EM. *J. Forensic Sci*. 1999; **44**: 297.
16. Massonet G, Stoecklein W. *Sci. Justice* 1999; **39**: 181.
17. Suzuki EM, Carrabba M. *J. Forensic Sci*. 2001; **46**: 1053.
18. Kuptsov AH. *J. Forensic Sci*. 1994; **39**: 305.
19. Biethan U, Funke W. *Ullman's Encyclopedia of Industrial Chemistry* (3rd ed.). VCH veslagsgeselschaft: Weinheim, 1990; 359.
20. Lin-Vien D, Colthup NB, Fateley WG, Grasselli JG. *The Handbook of Infrared and Raman Characteristic Frequencies of Organic Molecules*. Academic Press: San Diego, 1991.
21. Vandenabeele P, Hardy A, Edwards HGM, Moens L. *Appl. Spectrosc*. 2001; **55**: 525.

RESUMEN

[18]

La aplicación de las técnicas espectroscópicas en el análisis de la evidencia forense es cada vez más frecuente debido la sensibilidad y confiabilidad de éstas. Se ha encontrado que cuando la evidencia consiste en fragmentos de pintura automotriz, las técnicas microscópicas de análisis visual en conjunto con las técnicas espectroscópicas, como la técnica Raman y el infrarrojo, pueden ayudar a identificar el vehículo del que proviene el fragmento. En este trabajo se demuestra que la técnica Raman resulta muy conveniente en el análisis de pequeños fragmentos de pintura, pues permite establecer su procedencia por comparación del perfil de los espectros, además, permite identificar algunos de los constituyentes de la pintura: matriz polimérica, pigmentos y otros componentes secundarios. En Costa Rica, el uso de la técnica de espectroscopía Raman, como parte de los análisis rutinarios en el Departamento de Ciencias Forenses del OIJ, está en proceso de desarrollo y por ello consideramos que los resultados de esta investigación pueden contribuir a su implementación.

Palabras clave: Pintura automotriz; evidencia forense; espectroscopia Raman

ABSTRACT

[22]

Nowadays, the application of spectroscopic techniques in the analysis of forensic evidence is increasingly common due to its sensitivity and reliability. When evidence consists of fragments of automotive paint, microscopic and visual analysis techniques, in conjunction with other techniques, such as Raman and infrared spectroscopy, can help to identify the vehicle from which the fragment comes from. This paper shows that using Raman spectroscopy is very favorable in the analysis of small fragments of paint, because it allows establishing its origin by comparing profiles of different spectra. In addition, by this technique the identification of some of the constituents of the automotive paint such as: the polymeric matrix, the pigments and, other minor components can be performed. In Costa Rica, the use of Raman spectroscopy technique as part of a routine analysis in the Department of Forensic Sciences of the Organismo de Investigación Judicial (OIJ) is under development; therefore, the results of this research could contribute to its implementation.

Keywords: Automotive paint; forensic evidence; Raman spectroscopy

INTRODUCCIÓN

Los estudios periciales que se realizan en los laboratorios de Ciencias Forenses requieren, cada vez más, el uso de técnicas analíticas modernas que apoyen los resultados obtenidos. Solo con una evidencia rigurosamente sustentada en pruebas estandarizadas y validadas, es posible que las conclusiones de los estudios sean de utilidad en los procesos judiciales. Algunas de las técnicas habituales en los análisis forenses son la microscopía óptica, la cromatografía, la microscopía electrónica, la espectroscopía infrarroja y la espectroscopía Raman [1][2][3]. En los laboratorios forenses de nuestro país se utiliza de forma habitual la espectroscopia infrarroja, mientras que la técnica Raman es relativamente reciente y todavía está en proceso de implementación en el análisis de evidencia forense.

La espectroscopia infrarroja (IR) por reflectancia total atenuada y la microespectroscopia Raman son dos técnicas de análisis con alta sensibilidad y especificidad, las cuales se pueden utilizar en el análisis e identificación de un gran número de sustancias líquidas y sólidas [4][5][6] . Aunque para ambas técnicas la preparación de las muestras es relativamente simple, para la técnica Raman es más sencilla porque se requiere menos tiempo y menor cantidad de muestra. Las características de estas dos técnicas analíticas han hecho que la mayoría de las pruebas estandarizadas que se aplican en el análisis de evidencias de casos forenses, las utilicen como pruebas de referencia primaria [7][3].

La sensibilidad de la espectroscopia IR y Raman se debe a que con poca cantidad de muestra es posible obtener suficiente señal para generar espectros bien definidos. En cuanto a su resolución, esta se debe a que los espectros IR y Raman están relacionados con las energías de vibración de los enlaces moleculares, es decir, con los enlaces presentes en las sustancias analizadas, los cuales suelen ser característicos, por lo tanto, permitiría diferenciar o identificar los componentes presentes en la muestra utilizando bases de datos de referencia [8][9].

En el caso de la espectroscopia IR el material tiene que presentar enlaces con momento dipolar. Cuando un enlace con momento dipolar interactúa con la radiación infrarroja, induce vibraciones que reducen la reflectancia o la transmitancia y es posible obtener el espectro IR. Por su parte, para que una sustancia genere señal Raman, debe inducirse una polarización momentánea del enlace con una radicación monocromática. Cuando un enlace no presenta momento dipolar, es más sencillo inducirlo con la radiación de excitación, esta propiedad se denomina polarizabilidad. En otras palabras, los enlaces que presentan mayor polarizabilidad son aquellos con menor carácter polar. Dicha interacción produce unos pocos fotones con diferente energía de la radiación incidente, la diferencia de energía de estos fotones está asociada con los estados vibracionales de la sustancia. Esta situación hace que ambas técnicas sean complementarias, pues una técnica funciona mejor con enlaces polares (IR) y la otra con enlaces no polares (Raman) [10][11]. En la mayor parte de los casos, una misma sustancia puede ser identificada con las dos técnicas, aunque es posible que con una de las dos se generen mejores resultados.

En los casos forenses donde participan vehículos automotores, es frecuente que una parte de las evidencias recolectadas correspondan a fragmentos de pintura multicapa. Habitualmente, estos fragmentos contienen varias capas de pintura de aspecto diferente, lo que permite caracterizar los mismos mediante el estudio del número, el grosor, el orden y el color de las capas. Si en el transcurso de una investigación se encuentra el vehículo del que se sospecha que proviene el fragmento, es posible realizar comparaciones con muestras obtenidas del vehículo sospechoso con estas propiedades físicas.

Pero también ocurre que cada capa puede tener una composición química particular, lo cual brinda otra posibilidad para establecer correspondencias o diferencias. Cuando se desea establecer la coincidencia de estas muestras con la pintura del vehículo sospechoso mediante la técnica de espectroscopia Raman e IR, se puede realizar un análisis de diferencias y similitudes de los espectros. En otros casos, por la naturaleza del análisis o por el tamaño del fragmento, lo que interesa es la caracterización o la identificación de algunas de las sustancias presentes en los fragmentos.

Las técnicas IR y Raman tienen la ventaja de que garantizan la integridad de la muestra lo que, en el caso de los análisis forenses, es un factor importante. Además, la técnica Raman que se utiliza en los análisis forenses, suele acoplarse con un microscopio confocal, lo cual hace posible el análisis de muestras muy pequeñas en diferentes planos focales. El microscopio permite analizar muestras con dimensiones de micrómetros y la confocalidad permite el análisis de la muestra en diferentes planos focales. Esta facilidad también brinda la posibilidad, en algunos casos, de obtener espectros a través de coberturas transparentes, tales como bolsas plásticas o botellas de vidrio, lo cual incrementa la utilidad de la técnica en el estudio de evidencia forense [12]. A diferencia de la espectroscopia IR, mediante la espectroscopia Raman se puede obtener el espectro de capas individuales de pintura automotriz, siendo que sus espesores típicos son de pocos micrómetros [13].

La técnica IR presenta algunos inconvenientes como lo es la presencia de humedad. El fenómeno más importante que afecta a la técnica Raman es la fluorescencia del material al ser iluminado con la luz del láser. No obstante, mediante el efecto SERS (Surface Enhanced Raman Spectroscopy) se puede incrementar en varios órdenes de magnitud la señal Raman que proviene de las moléculas, reduciendo la importancia relativa de la fluorescencia [14]. Este aumento de la intensidad se explica, principalmente, por la interacción electromagnética de la luz con los electrones de las nanopartículas metálicas y por el contacto cercano de las moléculas del material analizado con el metal. Estas condiciones resultan en un aumento del campo electromagnético que actúa sobre las moléculas a través de excitaciones conocidas como resonancias de plasmones [15] . Precisamente, las pinturas suelen presentar efecto de fluorescencia importante, por lo que con el uso de la metodología SERS es posible evitar algunas de estas dificultades y analizar muestras de pintura que en ciertas circunstancias y con otras técnicas, serían de difícil análisis.

En este artículo se presentan los resultados de los análisis de fragmentos de pintura automotriz multicapa realizados principalmente con espectroscopía Raman.

MATERIALES Y MÉTODOS

Muestras de pintura. Las muestras se obtienen a partir de pequeños fragmentos desprendidos del vehículo o extraídas mediante una hoja metálica afilada con la que se obtiene un segmento de pintura que se extiende desde la capa base, la cual se encuentra adherida al metal. Posteriormente, las muestras son seleccionadas para asegurar la integridad de las capas, pues algunos de los fragmentos presentan deformaciones importantes en el espesor de las capas o inclusive, el desprendimiento de alguna de ellas.

Microscopía Raman. Los espectros fueron obtenidos utilizando un microscopio Raman confocal, modelo DXR de la marca Thermo Scientific, equipado con láseres de diodos de 532 nm (Potencia máxima de 10 mW), 633 nm (Potencia máxima de 8 mW) y 780 nm (Potencia máxima de 24 mW); cada uno con potencias que pueden variar en pasos desde 0.1 mW hasta su valor máximo. El instrumento está equipado con un detector del tipo CCD. La resolución espectral del instrumento varía de 2 cm^{-1} a 5 cm^{-1}.

Microscopía Infrarroja. Los espectros de la muestra fueron obtenidos utilizando un espectrómetro infrarrojo FT-IR Nicolet 380 de la marca Thermo Scientific, equipado con ATR y cristal de diamante, con una resolución < 0.9 cm^{-1}. El rango espectral utilizado fue de 3500 cm^{-1} a 400 cm^{-1}; además, los espectros fueron utilizados sin ningún procesamiento posterior de los datos.

Preparación de muestras para la espectroscopía Raman. Los fragmentos de pintura fueron lavados con agua jabonosa y posteriormente enjuagados varias veces con agua destilada en baño ultrasónico. De estos fragmentos se extraen pequeñas virutas, obtenidas mediante cortes longitudinales realizados con una hoja quirúrgica afilada. Las pequeñas virutas se colocan sobre un vidrio portaobjetos, lo que permite realizar mediciones transversales de cada una de las capas.

Preparación de los coloides de plata. Una solución coloidal consiste en una dispersión de pequeñas partículas en un medio. En este caso, las partículas dispersadas consisten de nanopartículas de plata (AgNP) o agregados de ellas, dispersas en agua.

Los coloides fueron preparados de acuerdo al método de Lee y Meisel [16][17]a partir de una disolución de nitrato de plata ($AgNO_3$) y citrato de sodio ($Na_3C_6H_5O_7$) como agente reductor. Se disolvieron 45 mg de $AgNO_3$ en 250 ml de agua, llevándose, bajo agitación constante, hasta el punto de ebullición. Luego se añadió 5 ml de una disolución de $Na_3C_6H_5O_7$ al 1 %. La disolución se mantuvo en el punto de ebullición por un periodo de 45 min, obteniéndose una solución amarillo-verdosa. De esta solución se toman 10 ml, a los que se elimina el sobrenadante previa centrifugación y se completa nuevamente con agua ultrapura al volumen inicial.

También se prepara una disolución en agua desionizada de 18,223 µg/ml de 1,2-Di(4Piridil) Etileno. Se mezclan en volúmenes iguales 1 µl de solución de nanopartículas y 1 µl de la disolución de Di-Etileno para determinar la actividad de las nanopartículas antes de la realización de los ensayos.

RESULTADOS Y DISCUSIÓN

En esta sección se detallan los resultados obtenidos al utilizar las técnicas de espectroscopía Raman convencional, metodología SERS y espectroscopía infrarroja.

Para obtener los espectros de las capas que componen la pintura se procura que el haz del láser incida dentro de los límites de cada capa, obteniendo así el espectro individual de cada una. La figura 1 muestra el espectro de dos capas internas de una pintura automotriz, cada capa tendrá un espectro Raman característico. En la Figura 1 se señalan algunas frecuencias que únicamente están presentes en una de las dos capas, también se observa que muchas de las frecuencias coinciden, esto se debe a que dentro de la composición general de las capas se encuentra la matriz, los solventes y diluyentes que generan los mismos picos Raman en los espectros de diferentes capas.

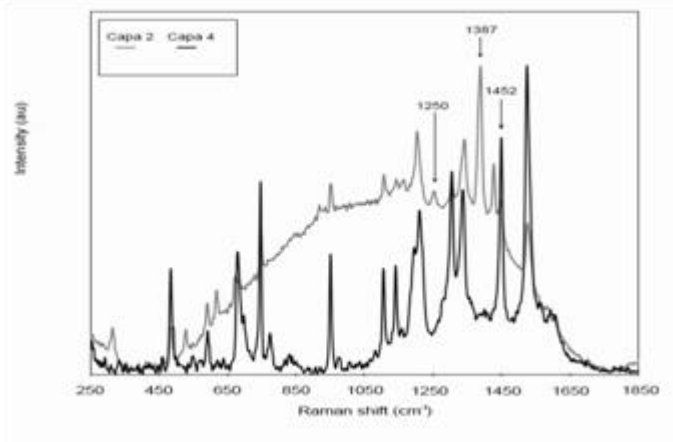

Figura 1 Espectro Raman de dos capas de una misma muestra de pintura automotriz cuyo color externo es negro. Los espectros se encuentran normalizados. La capa 2 presenta fluorescencia. *Laboratorio de Espectroscopía Raman, Tecnológico de Costa Rica*.

Para investigar los compuestos presentes en las muestras de pintura, los espectros obtenidos se comparan directamente con las líneas espectrales de los componentes que comúnmente se utilizan para fabricar pinturas automotrices. En la Figura 2 se identifican los picos característicos del violeta de dioxacina dentro del espectro de una de las capas de la muestra; aquí es posible ver que los picos de la dioxacina coinciden en posición y proporción con los picos del espectro de la capa 2, por lo que es posible asegurar que hay violeta de dioxacina en su composición, además se aprecia que la capa 4 no contiene este pigmento.

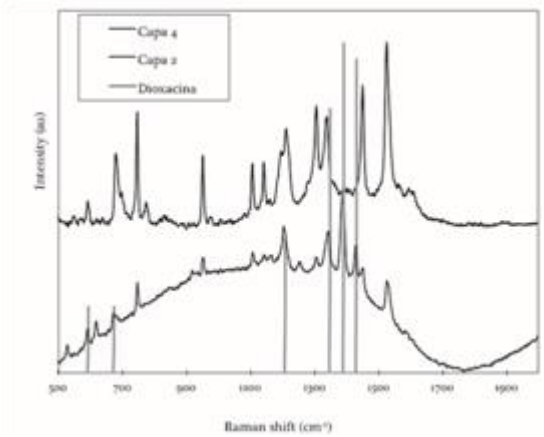

Figura 2 Espectro Raman de una muestra de color exterior negro comparada con las frecuencias características de la dioxacina. *Laboratorio de Espectroscopía Raman, Tecnológico de Costa Rica.*

Sin embargo, la pintura automotriz está formada de muchos otros componentes. En la Figura 3 se analiza la presencia del metacrilato en una muestra de pintura, en este caso es posible observar una buena coincidencia

de los picos. Para confirmar esta inferencia, puede usarse el espectro infrarrojo de la muestra como fuente de información complementaria. En la Figura 4 se puede ver que para la muestra estudiada, el perfil del espectro es coincidente con el espectro del metacrilato [18], además varios de los picos corresponden a los grupos funcionales que están presentes en el metacrilato. Con la información de ambos espectros (infrarrojo y Raman) es posible comprobar que la muestra de pintura estudiada contiene metacrilato.

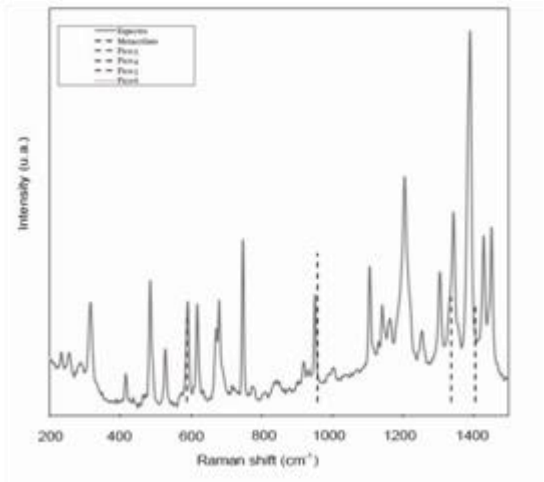

Figura 3 Espectro Raman de una muestra automotriz (color exterior azul). Se muestran los picos característicos del metacrilato. *Laboratorio de Espectroscopía Raman, TEC.*

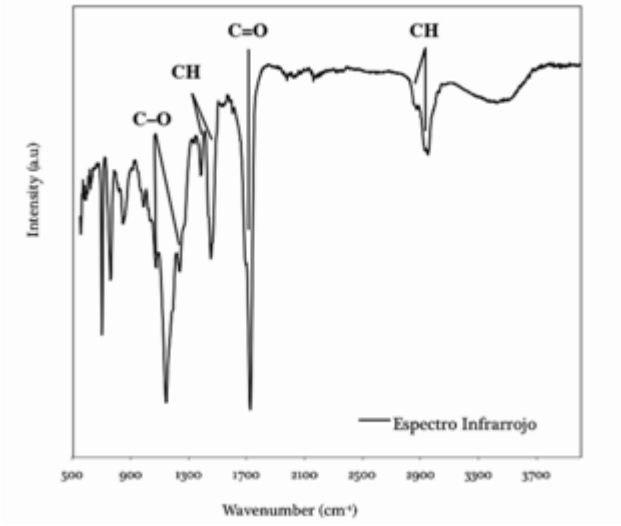

Figura 4 Espectro infrarrojo de una muestra de pintura color azul. También se señalan los grupos funcionales del metacrilato. *Laboratorio CEQUIATEC, TEC.*

La frecuencia Raman dispersada es independiente del láser utilizado, ésta característica se debe a que la frecuencia emitida corresponde a un estado vibracional específico de la molécula. Sin embargo, la intensidad de la dispersión Raman sí se verá afectada por el láser elegido. La Figura 5 muestra una pintura automotriz analizada con dos láseres de diferente longitud de onda, aquí se observa que la forma del espectro no cambia, es decir, la posición de los picos principales se mantiene, sin embargo, la intensidad sí varía, es decir, la altura de cada pico es diferente.

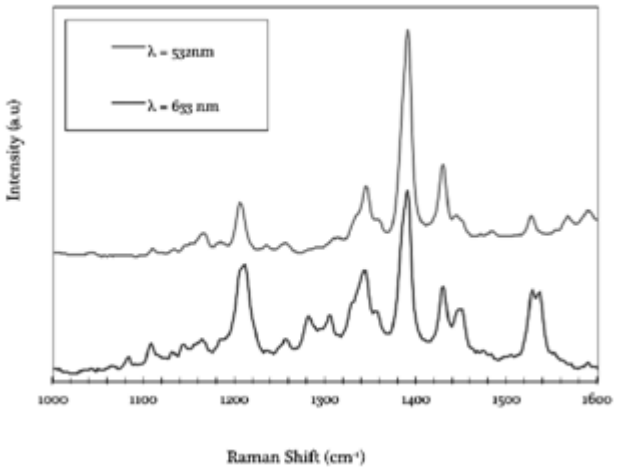

Figura 5 Espectro Raman de una pintura automotriz de color exterior gris. *Laboratorio de Espectroscopía Raman, Tecnológico de Costa Rica*.

Al utilizar diferentes láseres, el espectro obtenido podría presentar fluorescencia, por este motivo la posibilidad de utilizar más de un láser para caracterizar una muestra puede representar una ventaja. Podría ser que la emisión Raman con uno de los láseres sea muy débil o que la fluorescencia sea muy intensa para recolectar información, pero al cambiar de láser, estos problemas podrían disminuir. También puede ocurrir que aunque se utilicen distintos láseres con distintas potencias no se logre adquirir un espectro del que se pueda obtener información, en estos casos se puede acudir a la técnica SERS, la cual permite incrementar en varios órdenes de magnitud la señal Raman. Para lograr este efecto se debe contar con una solución de nanopartículas de plata. La solución de nanopartículas de plata se analizó mediante un microscopio electrónico de transmisión (Figura 6).

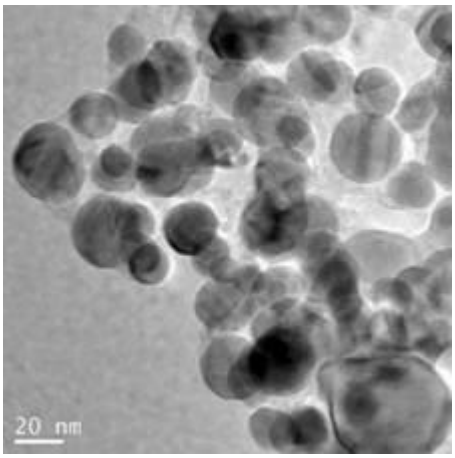

Figura 6 Micrografía TEM de las nanopartículas de plata obtenidas por el método Lee - Meisel.

Laboratorio de nanotecnología, TEC.

Se pueden observar nanopartículas con geometría esférica, mayoritariamente con diámetros entre 20 nm y 35 nm. La distribución de tamaños se puede variar mediante el tiempo del tratamiento térmico, produciendo un aumento del diámetro de las nanopartículas con el incremento del tiempo de tratamiento. En la Figura 7 se observa el espectro Raman de la disolución 1,2-Di(4-Piridil) Etileno sin nanopartículas y con nanopartículas, lo cual indica que ocurre el efecto SERS.

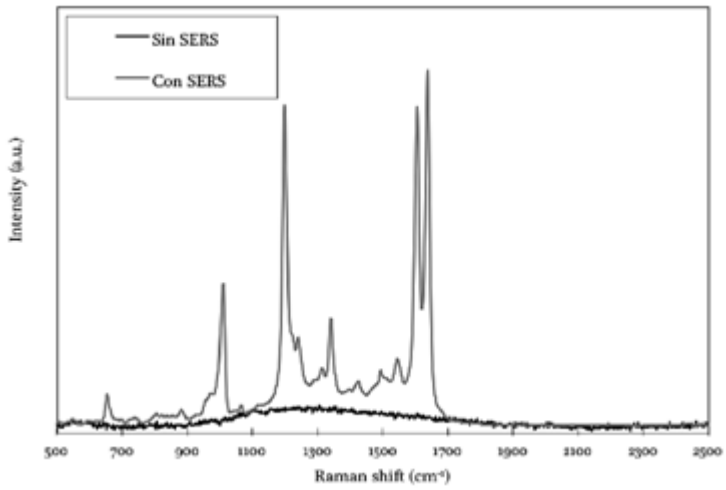

Figura 7 Espectro Raman de la disolución 1,2-Di(4-Piridil) Etileno con nanopartículas y sin nanopartículas de plata. *Laboratorio de Espectroscopía Raman, TEC*.

En la espectroscopía Raman se pueden utilizar las nanopartículas en diversas aplicaciones, en este caso, se deposita una gota de 2 µl de la solución de nanopartículas directamente sobre la superficie de una capa de pintura automotriz. Una vez seca se realiza el ensayo en las regiones cercanas al borde de la gota, pues ahí es donde se encuentra la mayor concentración de nanopartículas. La Figura 8 presenta el espectro Raman de una muestra de pintura automotriz, la cual no ha sido posible observar mediante la espectroscopía Raman convencional, pero sí mediante la metodología SERS.

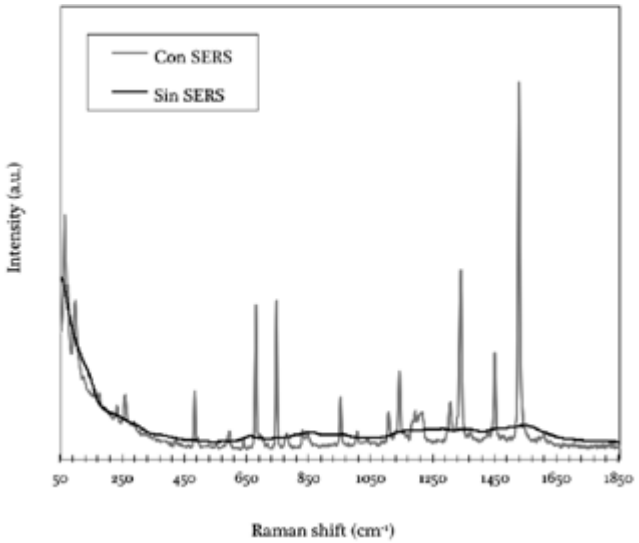

Figura 8 Espectro Raman de una muestra de pintura automotriz obtenido a) sin nanopartículas y b) mediante SERS. *Laboratorio de Espectroscopía Raman, TEC*.

CONCLUSIONES

En este trabajo se comprueba que es posible caracterizar pequeños fragmentos de pintura automotriz utilizando técnicas espectroscópicas. Además, es posible generar espectros de las capas individuales del

fragmento, lo cual permite identificar distintos componentes en cada capa y por lo tanto, caracterizar el fragmento de manera precisa por las diferentes propiedades de sus capas.

El microscopio del equipo Raman permite enfocar adecuadamente el haz en un área pequeña, de este modo es posible generar el espectro Raman de cada capa, con lo que se puede analizar las diferencias de los espectros e identificar los componentes de éstas. El equipo permite utilizar distintos láseres lo que mejora la obtención de información referente a una muestra.

Las muestras de pintura automotriz fueron analizadas con técnicas de espectroscopía Raman e infrarroja. Estos análisis permitieron distinguir y comprobar la presencia de algunos de los componentes que comúnmente se encuentran en las pinturas. Ambas técnicas son complementarias porque permiten distinguir componentes diferentes en una muestra y también confirmar la presencia de los mismos.

Cuando el espectro de una muestra Raman presenta fluorescencia, puede ser tratado con la metodología SERS para incrementar la señal Raman, lo que permite caracterizar la muestra. En el Laboratorio de Espectroscopía Raman de la Escuela de Física del Tecnológico de Costa Rica se desarrolló la destreza para implementar la metodología SERS (incluida la preparación de las nanopartículas de Ag) que es un análisis de gran valor, porque aumenta la variedad de muestras que pueden ser estudiadas.

La rigurosidad de los resultados generados en nuestro laboratorio, pueden contribuir al desarrollo de la espectroscopía Raman en el ámbito de las Ciencias Forenses en Costa Rica.

AGRADECIMIENTOS

Agradecemos el apoyo del Consejo de la Escuela de Física y el respaldo y financiamiento de la Vicerrectoría de Investigación y Extensión (VIE) del Instituto Tecnológico de Costa Rica. También agradecemos la colaboración del Lic. Max Méndez de la Sección de Pericias Físicas del Departamento de Ciencias Forenses del OIJ, por su ayuda en el suministro de las muestras de pintura y en la explicación de las técnicas de caracterización visual de los fragmentos de pintura automotriz. Agradecemos además, la colaboración del Laboratorio de Nanotecnología del TEC por las imágenes del microscopio electrónico de transmisión, del CEQUIATEC por los espectros infrarrojos realizados por el investigador M.Sc. Allen Puente Urbina y del químico Lic. Oscar Lacy Mora. Finalmente, agradecemos a todos los estudiantes asistentes del TEC que participaron en este proyecto, por su valiosa colaboración.

Applications of Vibrational Spectroscopy in Criminal Forensic Analysis

Edward G. Bartick

Reproduced from:

Handbook of Vibrational Spectroscopy

John M. Chalmers and Peter R. Griffiths (Editors)

Applications of Vibrational Spectroscopy in Criminal Forensic Analysis

Edward G. Bartick
FBI Academy, Quantico, VA, USA

This is publication number 01-06 of the Laboratory Division of the Federal Bureau of Investigation. Names of commercial manufacturers are provided for identification only and inclusion does not imply endorsement by the Federal Bureau of

Investigation.

1 INTRODUCTION TO FORENSIC ANALYSIS

Sir Arthur Conan Doyle is believed by many to have first popularized the application of forensic analysis through his fictional character Sherlock Holmes, originally published in 1887. This work is thought to have inspired many of the early forensic scientists. One of these was Frenchman Edmond Locard, who proposed that when two objects come into contact with one another, a cross-transfer of evidence occurs.[1,2] This statement is known as Locard's Exchange Principle and is the foundation for use of physical evidence to link or at least associate a suspect to a crime scene or a victim. Depending on the nature of the evidence, a wide range of analytical methods are used in forensic casework. This article illustrates how vibrational spectroscopy is used to identify or compare physical evidence in criminal forensic analysis.

A broad definition of the term "forensic", according to 'Webster's New World Dictionary,' is "suitable for a law court or public debate". With the application of forensic science, one must demonstrate in court that the evidence analyzed has relevance to the case in question. The significance of evidence related to a case is often determined by whether the physical evidence has individual or class characteristic properties.

Individual characteristics are properties of evidence that can be attributed to a common source with an extremely high degree of certainty. Class characteristics are properties of evidence that can only be associated with a group and never with a single source.[3]

Fingerprint and DNA evidence are accepted as having individual characteristics. However, fibers or copy toners are identified by their class characteristics and, because of the large production of these materials, they cannot be individualized. The strength of fiber evidence depends on the likelihood of those same type of fibers being randomly located on the suspect. Common fibers such as blue or white cotton from jeans or shirts, respectively, have little evidential value. But blue nylon-6,6 fibers with an unusual crosssection would have more significant value, because there are fewer in existence. Forensic scientists have thoroughly developed statistical values for DNA and fingerprint data to demonstrate individual characteristics. Statistics are more difficult to apply to class evidence, but approaches to apply them are being investigated. The information obtained by vibrational spectroscopy is usually characteristic of classes of materials, but in some instances the identification of specific components demonstrates an uncommon characteristic. If a contaminant on an evidential material is identified as a rare substance specific to the crime scene, the evidence would demonstrate a high likelihood of originating from the crime scene. Therefore, vibrational spectroscopy is used to identify chemical properties that contribute in varying degrees to the evidential value in criminal forensic analysis.

2 GENERAL USE OF VIBRATIONAL SPECTROSCOPY IN FORENSIC ANALYSIS

2.1 Infrared spectroscopy

Several authors have provided general overviews for the use of infrared (IR) spectroscopy in forensic analysis.[4–6] The applications vary to cover a wide range of physical evidence in the form of bulk materials and micro-sized particles. Historically, dispersive IR spectrometers were generally found useful for bulk samples such as drugs. Micro-sized samples were analyzed with skilled patience in beam

condenser accessories. For example, the Royal Canadian Mounted Police (RCMP) Forensic Service Laboratories (FSL) used high-pressure diamond-anvil cells in beam condensers for the analysis of automotive paint chips transferred from hitand-run vehicles.[7–9]

With the development of Fourier transform infrared (FT-IR) spectroscopy, the application of IR to forensic analysis became more prevalent because of the increased speed and sensitivity of FT-IR. The development of diffuse reflection (DR) accessories provided ease of sample introduction for several forensic applications. Samples with matte-finished surfaces could be analyzed with no sample preparation. Samples such as illicit drugs that previously required extensive grinding to make KBr pellets required less preparation. Suzuki was the first to apply the DR method to forensics with the analysis of drugs, polymers, wood and solvents.[10] He continued with additional work on drugs,[11] polymer foams[12] and paints.[13,14] Document analysis by DR has been reported for copy toners[15,16] and inks.[17] It was not until the 1990s that the use of FT-IR became more regularly applied in forensic laboratories. The introduction of lower cost spectrometers and microscopes paved the way for FT-IR use in forensic analysis. FT-IR microscope development is considered a milestone achievement for forensic analysis and is considered the most significant recent advancement for microsample analysis.[5] Sample preparation to introduce specimens into microscopes is frequently easier, because only a small portion of the sample is required for placement in the IR beam for transmission spectroscopy. For example, to analyze paint from a surface, all that is required is a sliver sliced from the surface with a scalpel. Therefore, standard sized samples are often reduced in size and analyzed in microscopes because of convenient sample preparation.[18] The reflection techniques, reflection-absorption (R-A), specular reflection, diffuse reflection (DR), and internal reflection spectroscopy (IRS), frequently referred to as attenuated total reflection (ATR),[19] provide additional ease of sampling in IR microscopes. Because reflection methods require little or no sample preparation, they are used at least as frequently as traditional transmission methods.

Gas chromatography (GC) with IR detection (GC/IR) for analysis of mixtures has not found much application in forensic analysis. GC combined with mass spectrometry (MS), or GC/MS, superseded GC/IR, and the ultimate sensitivity benefits of MS for trace components have overshadowed the use of GC/IR in forensic analysis. However, GC/IR used as a separation and identification tool for large samples has proven successful in drug analysis. Because IR analysis can be used to identify isomers, it can sometimes be used to identify isomeric forms that render a drug active and subsequently controlled.

The recent developments of single or multiple reflection, horizontal ATR accessories for use in sample compartments have been very useful for forensic analysis. Small liquid or solid samples, less than a millimeter in diameter, can be measured. Typically, diamond internal reflection elements (IREs) are used for durability. Some IREs consist of thin diamonds backed with other materials to reduce cost. These ATR accessories offer the option of extended frequency ranges to near 200cm^{1} in spectrometers with cesium iodide optics. The extended range can be used to nondestructively acquire information regarding paint pigments and inorganic fillers in polymeric materials.

2.2 Raman spectroscopy

Recent technological advancement in Raman spectrometers has provided a reason for exploring this method in forensic applications. While the applications have been slow to find their way into forensic laboratories, the advantages are being recognized and Raman spectrometers are starting to find use in forensic analysis.[20] Fourier transform (FT) Raman received early attention in the redevelopment of

Raman technology. The 1064nm near-infrared (NIR) excitation laser that is used with FT systems causes fewer samples to fluoresce than the visible wavelength lasers previously used. However, with the lower energy, longer wavelength laser, signal averaging and rapid scans provided by FT systems are required to attain the quality of spectra desired. Unfortunately, the lower scattering power of the longer wavelength excitation impedes application to microsamples that are commonly required with forensic analysis, thus limiting the use of microscopes with FT Raman. Dispersive Raman systems that use NIR lasers ranging from 780 to 840nm have greater scattering efficiency. Combined with sensitive charge coupled device (CCD) detectors and improved monochromators, these systems have more general use compared to FT Raman systems and have thus taken the forefront for a wide range of sample analysis. Additionally, fiber optic probes are used

on dispersive systems to sample through glass bottles and plastic bags, making noninvasive sampling possible. These probes contribute to the application of small, rugged Raman spectrometers designed specifically for field use. Portability and ease of sampling are attractive features that are included in these Raman systems that can be used along with an array of other analytical instruments to be carried to crime scenes where the analysis of potentially hazardous materials is conducted without risk of transporting them back to the laboratory.

3 POLYMER ANALYSIS

3.1 General polymers

Vibrational spectroscopy is applicable to a wide range of physical evidence. Because polymers are so common, they frequently play an evidentiary role in criminal cases. Polymeric materials such as fibers, paints and adhesive tapes are frequently analyzed to identify characteristic information regarding their composition. Physical and chemical information on these materials is stored in computer databases to help determine the manufacturer or, supplier, or simply to discriminate between many similar samples of material. Some of the available databases will be described as part of the analyses mentioned in the forthcoming pages. Other general polymeric materials found as evidence do not fall into a particular category and must be studied on a caseby-case basis without the aid of comparison with similar material in a database.

The following is a case example where a polymeric material became important evidence. Early one morning, on a luxury cruise ship off the coast of California, a man reported to the captain that his wife had been blown overboard. Considering the minimal wind conditions, the captain became suspicious and alerted the law enforcement authorities. Several hours after the overboard report, the woman's body was recovered by the US Coast Guard. The clothing that both the man and woman were wearing at the time of the incident was forwarded to the FBI Laboratory. The woman's running pants appeared soiled with an orange substance on both legs. Careful examination of her pants with a stereo microscope revealed orange-colored, rubbery particles. Examination of the man's running pants also revealed rubbery particles that appeared identical. On the ship's deck, at the location of the overboard incident, there was an orange-colored, rubberized running track. A portion of the track material was removed from the ship and forwarded to the laboratory for analysis. The particles were removed from both pairs of running pants and flattened in a compression cell to make them sufficiently thin to perform transmission analysis using an FT-IR microscope system.

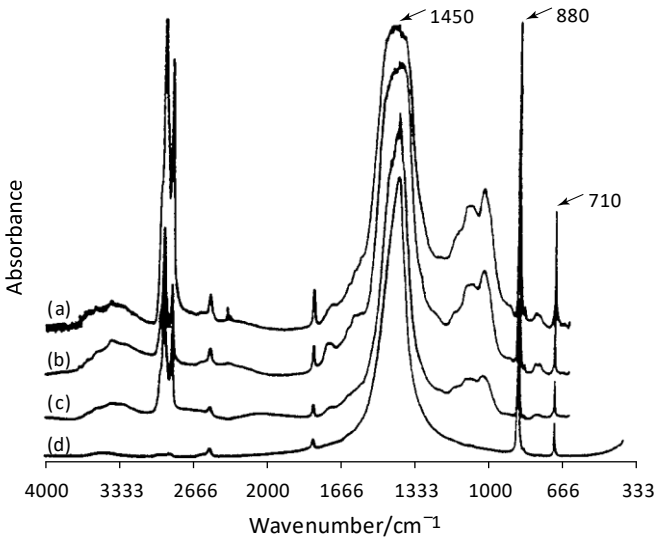

Figure 1. Cruise ship homicide case. Spectra of rubber particle evidence from sweat pants from both (a) the victim and (b) the suspect, (c) running track and (d) calcite reference.

Particles from the track material were prepared in the same way, and the spectra of all three samples were compared as shown in Figure 1. The three spectra of the rubberized material matched closely. The material was heavily filled with calcite ($CaCO_3$), identified by the intense, broad C–O antisymmetric stretch near 1450cm[1], and narrow out-of-plane and in-plane bends near 880 and 710cm[1], respectively.[21] To determine the force required to embed the particles in the pants, a fabric similar to that of the

pants was rubbed across the removed track piece at different degrees of pressure. The investigators found that it was necessary to rub the fabric with significant pressure, such as in the case of dragging a person, to cause the transfer and embed the material in the fabric. They determined that the transfer of particles suggested an altercation between the individuals, and, therefore, this evidence weighed heavily and resulted in a homicide conviction. The combined comparison of evidential materials by microscopic examination, IR analysis, and physical testing played a significant role in this case without witnesses.

3.2 Copy toners

Questioned documents involving fraud and threatening letters are often produced on printers, copy machines and facsimile machines. The machine model identification of this common office equipment has been achieved through comparison of the resins of the toners used as ink. These "copy toners" have been studied for forensic analysis as a class of polymeric material. An example where copy toner analysis was used to produce an investigative lead was in a case involving a copied address label. A packaged bomb, mailed to a corporate executive, had an address label that appeared to be an enlarged copy of the company's return address logo typically used on company envelopes. Investigators suspected that the bomb had been mailed by an employee with access to internal supplies and that the person had copied an envelope using equipment within the company. There were over 200 copy machines, involving 62 different copier models, located throughout the facility. It was important for the investigators to know the copier model used to narrow the area of the investigation to employees with convenient access to a copier model of the type used to print the label. Sample pages were prepared from each of the 62 models and forwarded to the FBI Laboratory for analysis. In the laboratory, the samples were prepared for IR analysis using a heat transfer technique to remove the toner from the documents. The preparation technique involves heating the back of the paper with a soldering iron at a specified temperature and smearing the toner onto aluminum foil attached to a glass microscope slide. Spectra were obtained with an FT-IR microscope by R-A. With this method, the IR beam passes through the sample and is reflected from the aluminum foil to the detector via the microscope optics.[22] Figure 2(a) shows the original spectrum of the toner from the

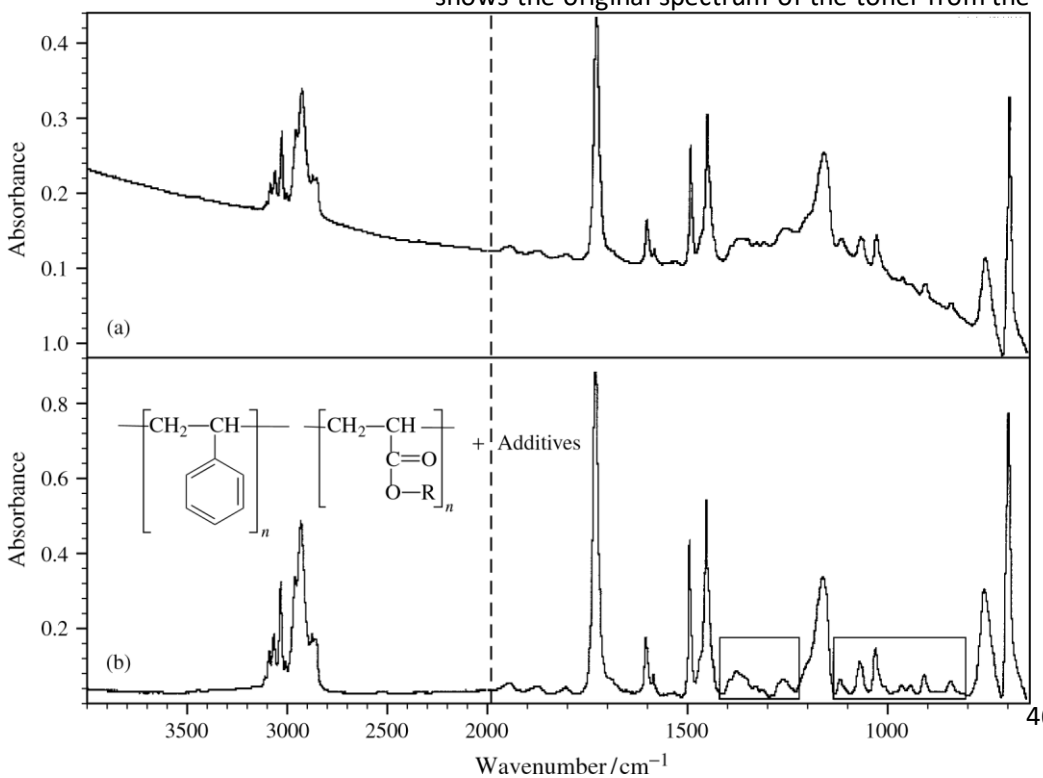

Figure 2. Poly(styrene:acrylate) resin copy toner spectrum from an address label on a bomb package: (a) original uncorrected spectrur (b) flattened spectrum showing boxed regions where additive absorptions can be observe

bomb package label. This spectrum is sloped due to scattering from the carbon black particles used for the copy image. The baseline flattened spectrum in Figure 2(b) is typical of a styrene/acrylate copolymer. Significant variations in the IR spectra are produced by the polymeric resins which contain numerous additives that vary in type and quantity. A visual comparison of the case sample spectrum was made with the 62 spectra of the model types in the building. One Kodak model type matched closely with the case sample spectrum. The spectrum was also searched in an IR database of copy toner resins categorized based on over 800 copier and printer models.[23] The search software narrowed the toner type to a group containing 24 models of machines. By careful scrutiny of the peaks, it was possible to narrow the spectra to six Kodak models in the database. The Kodak copier model from the corporate building was included in the computer search. Therefore, the results of the visual inspection and the computer search of the spectra corroborated. Two-thirds of the binders contained in the spectral database consist of the styrene resins plus additives to provide desired properties in particular copy machines. Other types of binders used are phenolic and polyethylene resins. The regions boxed off in Figure 2(b) contain small bands from the additives that provide the differentiating spectral features of this toner resin. Because the building contained only eight examples of that particular Kodak model, the results of this analysis permitted the investigators to narrow their search to personnel working in limited locations of the

building. Thus, a suspect was determined in considerably less time than if the company's entire personnel required investigation.

3.3 Fibers

Textile fibers are often transferred between clothing during personal contact in violent crimes such as rape and homicide. The foremost method of analysis for this type of evidence is visual light microscopy, though IR is very useful to further specify fiber type. Fibers from the clothing of the victim and suspect are screened microscopically for similarity, closely comparing physical and optical properties of the fibers. These properties may vary significantly due to the color, shape, texture, and chemistry of textiles. Polarized light microscopy is used to determine the generic classification of the polymer type, and IR microscopic analysis plays an important role by identifying subclasses of synthetic fibers.[24,25] A spectral library of 83 polymeric fiber types, obtained by transmission spectroscopy on flattened single fibers, was developed to aid forensic examiners in the identification of fiber composition.[26–29] IR is particularly useful for subclassifying acrylic fibers that are seen frequently as a wool alternative in sweaters and readily transfer between individuals during contact. These fibers consist of at least 85% polyacrylonitrile[28] plus copolymers and ionic end-groups to enhance dyeing properties. Figure 3 shows spectra of the three most common acrylic copolymers. The band shape of the C–O stretch in the region between 1300 and 1000cm^{1} varies depending on its position or environment within the comonomer structure as a methacrylate, methyl methacrylate or vinyl acetate. Over 20 variations of acrylics can be identified by IR.[30] Thus, IR is a very useful tool in providing information that further discriminates fiber types to enhance the evidential value of a sample.

Raman spectrometry promises to complement IR analysis of textile fibers due to the ease of sampling and the additional information it provides. Light microscopy analysis requires fiber samples to be mounted in a liquid medium, under coverslips, on a glass slide. Because glass absorbs strongly in the IR, the fibers must be removed and cleaned prior to IR analysis. Raman analysis, on the other hand, has been successfully performed on single fibers mounted on glass microscope slides,[31,32] thus avoiding the need to remove the fibers from the slide mount. The additional sample preparation time is not required and, once mounted, the chance of fiber loss is minimal. Figure 4 illustrates the process of obtaining a nylon-6 fiber spectrum using microscopic Raman analysis. Figure 4(a) includes spectral contributions from the fiber, Permount mounting medium and glass from the coverslip. Figure 4(b) shows the result of Permount subtracted from the original spectrum. The nylon-6 spectrum remains in Figure 4(c) after the glass contributions are subtracted. The baseline is flattened for the final spectrum shown in Figure 4(d). The signal-tonoise ratio is less than obtaining a spectrum without being mounted under a coverslip, but it is sufficient to identify the fiber by the prominent characteristic bands as labeled. The band assignments of the major peaks are labeled in

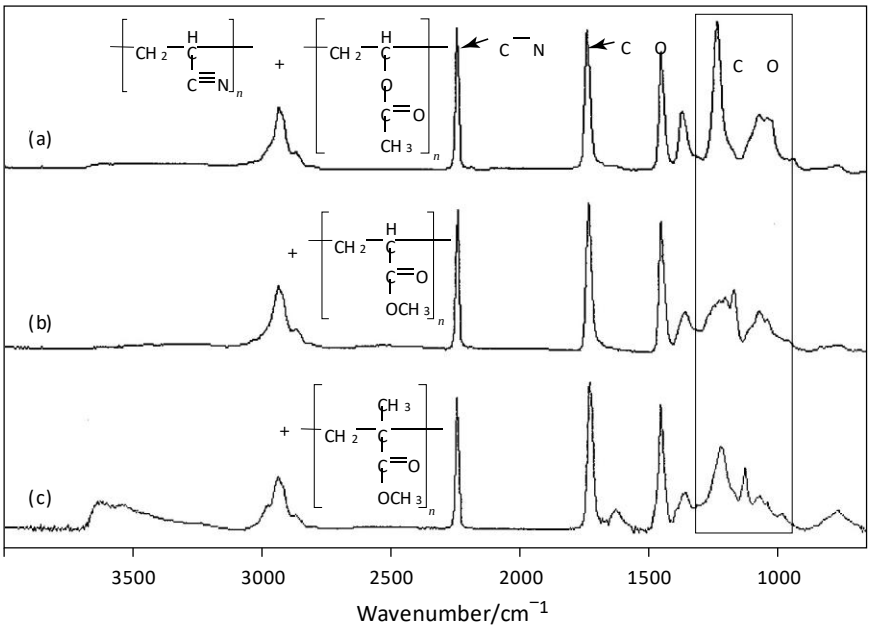

Figure 3. IR spectra of acrylic copolymer fibers: (a) poly(acrylonitrile:vinyl acetate); (b) poly(acrylonitrile:methyl acrylate); (c) poly(acrylonitrile:methyl methacrylate).

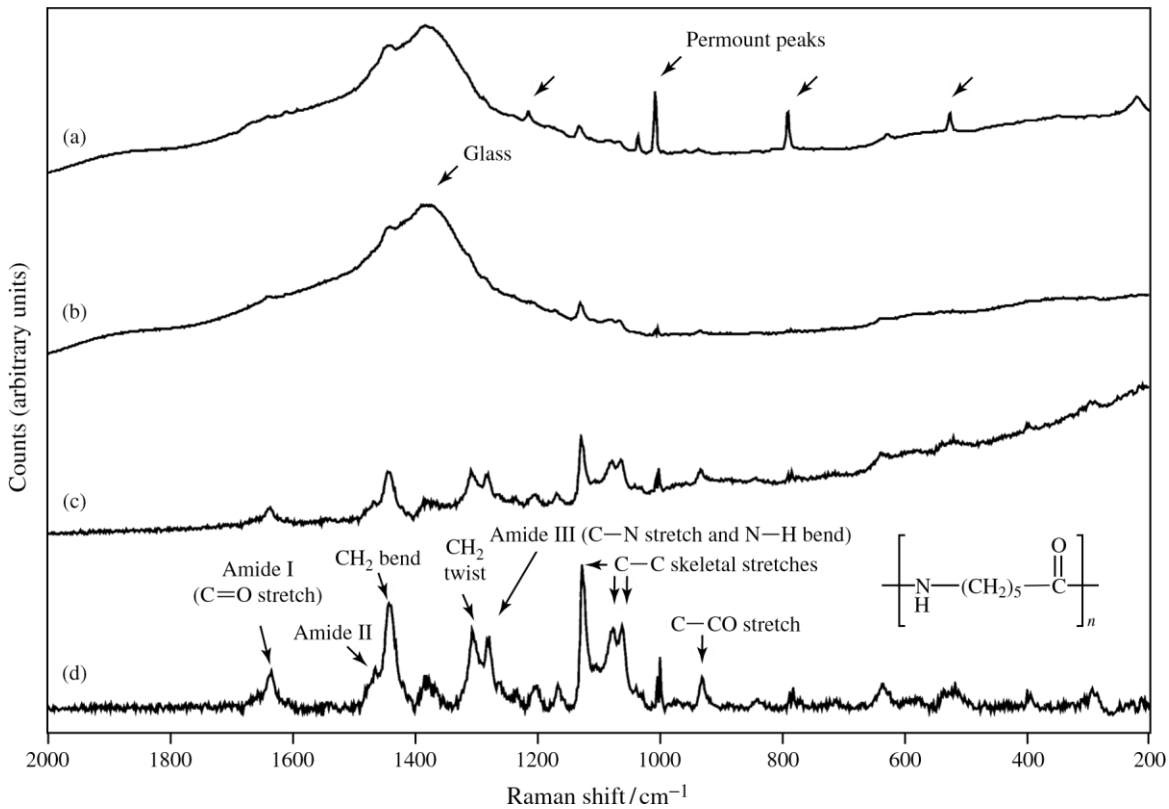

Figure 4. Raman spectra of a nylon-6 fiber mounted under a coverslip on a glass microscope slide: (a) original spectrum, (b) Permount mounting medium subtracted; (c) glass subtracted; (d) baseline flattened with the major characteristic bands labeled.

accordance with Hendra *et al.*[33] Raman spectra differ from IR spectra because the selection rules for Raman vary from IR, thereby producing complementary information. The information obtained by Raman is at times more definitive in determining the polymeric structure. Since Raman

spectroscopy demonstrates spectral response from dyes, the dye information can be useful. However, the dye spectral features can interfere with identification of the polymeric composition of fibers. A protocol to determine whether to use Raman or IR when analyzing dyed and undyed fibers, grouped by generic class, is currently being established in the FBI Laboratory. To further characterize the fibers, dye spectral features could provide information regarding the dye type. Studies have been conducted using surface enhanced Raman spectroscopy (SERS) to study dye composition using silver colloid substrates.[34,35] While the spectral features are significantly enhanced by SERS, this method requires that the fibers are removed from the glass slides, resulting in an additional step and a chance of fiber loss. Raman analysis has demonstrated certain advantages over IR, but the strengths and limitations of both are still under study to determine where each of the methods can be used to obtain the greatest information with the most convenient analysis procedure.

3.4 Paints

IR spectroscopy of paints has been useful in forensic analysis since the 1960s. Automotive, architectural, art, marine, aircraft, tool, and other types of paints may become evidence in a variety of crime scene scenarios.[36] After visual light microscopy, IR analysis offers the most information in forensic paint examination. The organic binders are frequently identified with IR, and both organic and inorganic pigments can often be identified. Scientists from the RCMP have been classifying automotive paints based on chemical composition since the 1970s.[7–9] The original analysis was performed with the use of high-pressure diamond-anvil cells in beam condensers on dispersive IR spectrometers. Since then, the RCMP and other analysts have changed to using the less cumbersome low-pressure compression diamond cells with beam condensers in FT-IR systems. Inorganic pigment components in paints have revealing spectral features at the lower wavenumbers. Beam condensers are used rather than FT-IR microscopes to overcome the limited frequency range of mercury cadmium telluride (MCT) detectors used in IR microscopes. For paint analysis, the extended range to near 200cm^{1} is obtained with CsI optics and a standard deuterated triglycine sulfate (DTGS) detector in the spectrometer bench.

Physical and chemical information obtained by light microscopy and IR analysis on automotive paint, used to potentially identify make, model and year of vehicles, is readily searched in a database. The computerized library, developed by the RCMP, is widely used by forensic laboratories throughout North America.[37] Necessitated by the international nature of the automotive industry, European, Japanese and Australian forensic laboratories will soon be contributing to this database in order to provide a more comprehensive collection. Scientists from forensic working groups of the listed countries are contributing automotive paint samples and data from their respective nations and plan to continue collaboration.

Paint types other than automotive do not usually display as much diversity in chemistry, color and layer structure. Therefore, a wider variety of analytical instruments are often used to characterize these paints. Along with microscopy and IR spectroscopy, other methods frequently used are pyrolysis GC/MS and inorganic analysis by scanning electron microscopy with energy dispersive Xray spectroscopy (SEM/EDX) or X-ray diffraction (XRD) analysis.

Researchers are beginning to demonstrate the usefulness of Raman analysis for organic and inorganic pigment identification in paint.[38,39] Figure 5 compares IR and Raman paint spectra of a yellow acrylic melamine enamel automotive paint. The IR spectrum in Figure 5(a) clearly shows the resin binder features. The N–H stretch near

$3350\,\mathrm{cm}^{-1}$, the C–H stretches near 3000cm[1], the CDO stretch near 1730cm[1], the C–N stretch near 1540cm[1], and the typical C–O envelope from 1300 to 1000cm[1] are observed in the IR. Of particular interest to paint analysis are any contributions by pigments. The weak, broad band at $868\,\mathrm{cm}^{-1}$ appears to be contributed by chrome yellow, as shown in the reference spectrum (Figure 5(b)). However, because of the band's comparatively low intensity and lack of detail in the paint spectrum, it would be difficult to positively identify chrome yellow by this method alone. The peaks labeled at 659, 425 and 357cm[1] are rutile, a crystal form of titanium dioxide. Figure 5(d) is the Raman spectrum of the yellow auto paint. The major peaks at 843 and 365cm[1] match up with the Raman spectrum of chrome yellow shown in Figure 5(c). Peaks at 611 and 446cm[1] are contributed by rutile, as shown in

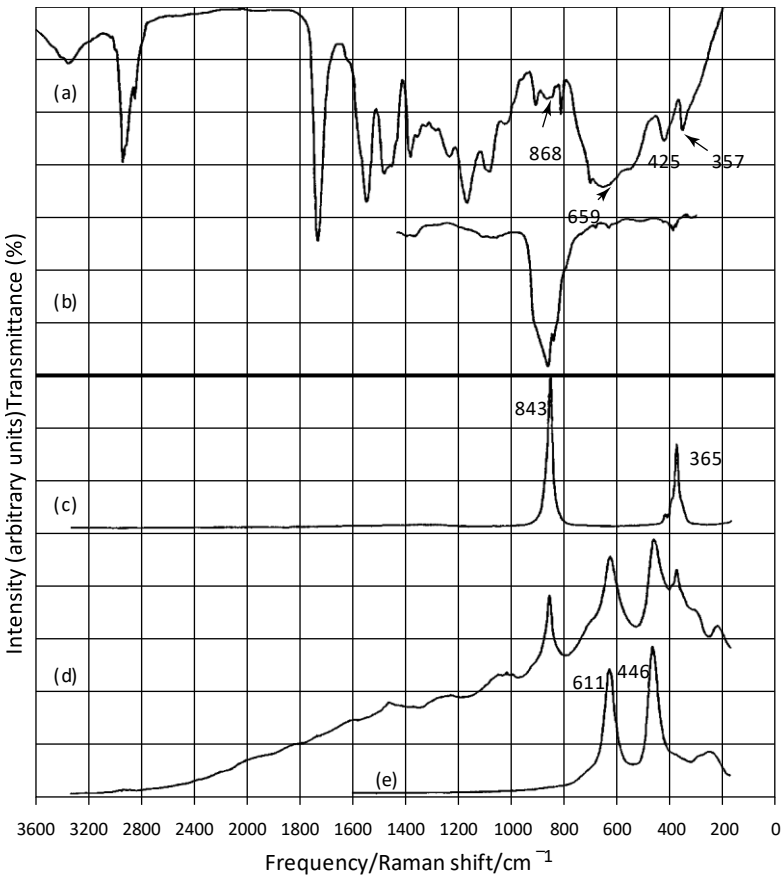

Figure 5. IR and Raman spectra of yellow acrylic melamine enamel auto paint with pigments: (a) IR spectrum of the auto paint; (b) IR spectrum of chrome yellow pigment; (c) Raman spectrum of chrome yellow pigment; (d) Raman spectrum of the yellow auto paint; (e) Raman spectrum of rutile. (Spectra provided by E. Suzuki, Washington State Patrol, Forensic Laboratory, Seattle, WA.)

Figure 5(e). With Raman, the high scattering efficiency of some pigments, relative to those of binders, helps to easily determine the pigment components, as interfering binder peaks are not a problem.

3.5 Tapes

Pressure-sensitive adhesive tapes play an important role in forensic analysis as evidenced by their diverse uses. Electrical tapes can be used in wiring electronic devices to bombs, duct tapes in binding victims of violent crimes, and other tapes in wrapping packages containing drugs, bombs or other threatening material. By carefully characterizing tapes submitted as evidence, they can be compared with known tapes in a suspect's possession or they can be studied to develop investigative leads when the brand can be established. IR spectroscopy can be useful with ATR accessories in determining the major organic components of both the adhesives and backings. In the past multiple reflection accessories were used, but more recently single reflection ATR accessories for the IR microscopes have been used to acquire spectra of small, uncontaminated areas on the tapes. While this is convenient, the frequency range is limited by the MCT detectors used on the microscopes which cut off near 700–650 cm^{-1}. A study has demonstrated the usefulness of a single-reflection, horizontal sample compartment accessory using a diamond interface backed with KRS-5.[40] This accessory provides a spectral range from 4000 to 260$cm^{1}$when used with cesium iodide optics in the spectrometer. The extended range below 400cm^{1} permits acquisition of spectral features of the inorganic fillers commonly found in duct tape adhesives and less frequently found in the film backing. Figure 6(a) shows an atypical duct tape backing spectrum containing calcium carbonate (calcite). The calcite filler has a lattice band[21] near 315cm^{1} that would not have been observed without the extended frequency range capabilities. The C–O asymmetric stretching band[21] near 1450cm^{1} underlies the C–H bending band near 1460cm^{1}. The C–O out-of-plane bend can be observed near 880cm^{1}. The spectrum in Figure 6(b) is more typical of polyethylene backing showing only the C–H bands without the filler features. Because fillers are not typically used in the backings, analysis of this unusual duct tape evidence could provide increased discriminating value.

To more fully characterize tapes, other analytical methods are used. The physical characteristics are observed and measured with the unaided eye and microscopically, and inorganic composition is determined by SEM/EDX and XRD analysis. Physical characteristics, such as the yarn counts and weave type on the fabric reinforcement within duct tapes, may

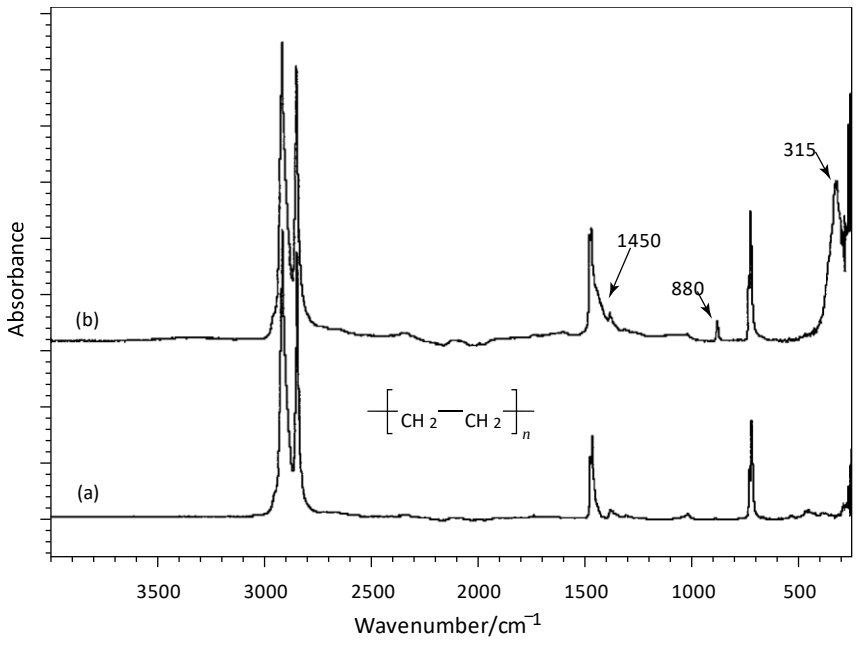

Figure 6. IR spectra of duct tape backing film by ATR: (a) typical polyethylene backing; (b) backing containing calcite.

quickly narrow down the brand possibilities. XRD can provide further information about the inorganic components like distinguishing between anatase and rutile crystalline forms of titanium dioxide extenders. TiO_2 is frequently used in duct tape adhesives and some manufacturers prefer a specific crystalline structure, thus identification of the mineral type can assist with identifying the manufacturer. All of the information obtained by the various analyses has recently been placed in a searchable database for quick comparison of tape properties.[41]

4 DRUGS

IR has been used for the analysis of both licit and illicit drugs for many years.[4,42] The computerized drug library produced at the Georgia State Crime Laboratory (GSCL) is a standard in forensic analysis. Currently, it contains over 2000 spectra of drugs and related chemicals. Samples prepared in standard 13-mm KBr pellets have been used for inclusion of drug spectra in the library. However, recently the GSCL successfully applied ATR to drug analysis.[43] Horizontal ATR sample compartment accessories with three reflections provide sufficient sensitivity to acquire spectra of approximately 400ng of lysergic acid diethylamide (LSD) as a film cast from chloroform (Figure 7). The region between 2400 and 1800cm^1 was blanked to remove the uncompensated diamond absorption produced by the IRE. The ATR spectra of drugs can be successfully searched in the original transmission spectral library in spite of the intensity differences in the peaks. This method is beginning to gain acceptance in laboratories around the USA. The FBI Laboratory has started an ATR database of drugs for computer spectral searching. Recently, a drug library of 455 spectra by ATR was produced at the Illinois State Police Laboratory.[44]

GC combined with IR (GC/IR) simplifies the analysis of drug mixture samples typical of those associated with clandestine laboratories and is a standard procedure of the Drug Enforcement Administration (DEA) laboratories. For the analysis of methamphetamine and related compounds, the DEA is required to identify the optical

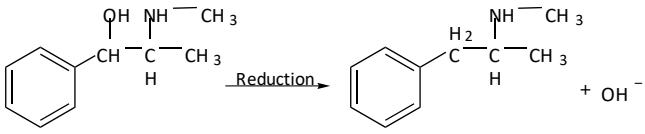

Ephedrine Methamphetamine

Figure 8. Reduction reaction of ephedrine to methamphetamine.

stereoisomers (d and l forms). IR is more effective than MS in differentiating diastereoisomers. Thus, the diastereoisomers ephedrine and pseudoephedrine, which are precursors for methamphetamine, are identifiable compounds by this method. Figure 8 shows the reduction reaction of the ephedrine to methamphetamine. Figure 9 illustrates the comparison of the gas phase spectra of these compounds. In Figure 9(a) and (b), the region between 1300 and 1000cm^1 shows subtle but consistently different spectral features of the diastereoisomers ephedrine and pseudoephedrine. The spectra of amphetamine and methamphetamine, shown in Figure 9(c) and (d), respectively, do not have the OH stretching band near 3600cm^1, because the reduction reaction removes the OH attached to the carbon next to the phenyl group. The spectra of amphetamine and methamphetamine differ in the entire region below 1700cm^1. The most pronounced difference lies with the NH deformation band near 1600cm^1, which is significantly greater in intensity for the primary amine, amphetamine. Once these components are identified, capillary electrophoresis (CE) is required to determine the optical stereoisomer (d or l enantiomer) present. Since the

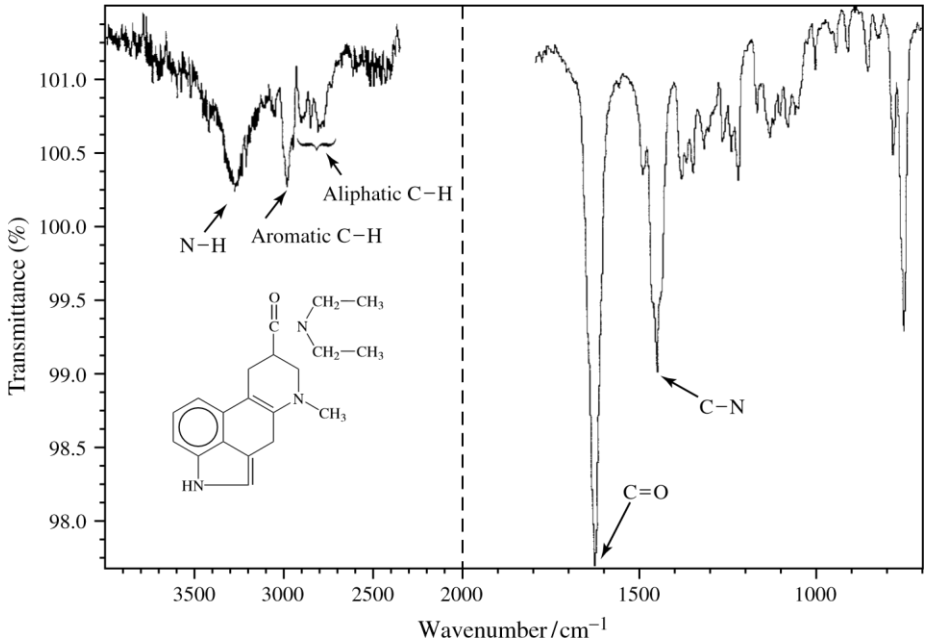

Figure 7. Spectrum of 400ng of LSD by ATR. (Spectrum provided by Robert Ollis, Georgia Bureau of Investigation Crime Laboratory, Decator, GA.)

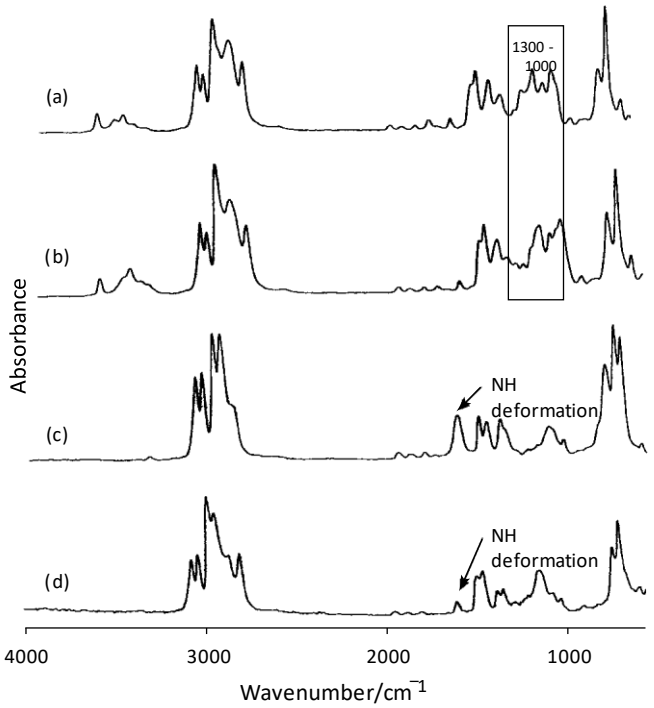

Figure 9. Clandestine laboratory mix separated by GC/IR. Spectra of: (a) ephedrine; (b) pseudoephedrine; (c) amphetamine; (d) methamphetamine. (Spectra provided by Henry Blum, DEA Laboratory, Washington, DC.)

most potent and sought-after methamphetamine is the d enantiomer, the DEA analyzes the mixtures to confirm the presence of d-methamphetamine. Either the l-ephedrine or the d-pseudoephedrine enantiomer may be used to produce d-methamphetamine. CE separates all eight structures of ephedrine, pseudoephedrine and methamphetamine for the final identification of the existing d or l enantiomer versions.

Raman spectroscopy is beginning to attract interest both in the laboratory and for field drug analysis. Many drugs are excellent Raman scatterers, and therefore lend themselves to rapid analysis with direct laser beams, fiber optic probes and microscopes. The application of fiber optic probes provides the ability to obtain spectra for drug samples contained in plastic bags or bottles, thereby making field analysis simple. Several field portable Raman spectrographs have become available on the market. These instruments have been compared for such features as frequency range, resolution, laser excitation and portability in terms of power requirements, size and weight.[45] While still in an early stage, this field approach appears to have great promise.

5 EXPLOSIVES

As with many types of forensic evidence, explosives produce unique IR spectra, thus making IR useful for identification of the major components in bulk explosives.[46] Separation methods are often required with mixtures of components, prior to spectroscopic methods to identify the components. Due to the sensitivity often required, particularly for postblast residues, GC/MS is

frequently applied to explosives analysis. Liquid chromatographic methods, ion chromatography and CE are also frequently applied because of the separation capabilities of these methods.

ATR has been successfully applied to plastic explosives in bulk form and after extraction. Keto[47] demonstrated an extraction method for the determination of C-4 military explosive. In his method, the explosive hexahydro-1,3,5trinitro-1,3,5-triazine (RDX), the plasticizer and the rubber binder from C-4 are separated selectively by solvent extraction and filtration. The extracts are cast as a film on an ATR crystal for IR analysis. Bartick and Merrill[48] have shown how the development of a database of bulk plastic explosives can be used to successfully identify the general plastic explosive type and even the manufacturer. A library of pure explosives components can be searched to potentially identify the explosive material. Figure 10 shows the explosive component RDX, identified from a questioned plastic explosive mixture. A library search of the plastic explosive library identified the questioned explosive as C-4.

Often, unknown materials are found at crime scenes and, for safety considerations, it is important to determine the chemical composition prior to handling and bringing the material to the laboratory for analysis. Early studies with Raman spectroscopy of trace explosives were done by Lewis *et al*.[49–52] to determine the basic requirements of a field portable system. Successful results were obtained for all samples with a 1064-nm laser FT system, and most samples were successfully analyzed on a dispersive system using 632.8nm excitation. Lewis *et al*. considered the best potential for field systems to be a compromise that would

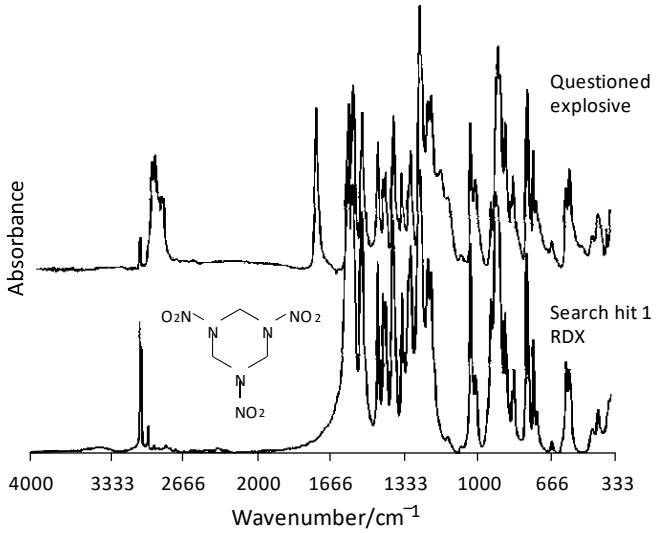

Figure 10. ATR spectrum of a C-4 plastic explosive mix and RDX library pick for the explosive component.

use a NIR 785-nm laser on a dispersive spectrometer. Cheng *et al*.[53] have done additional studies that include imaging Semtex plastic explosive deposited in fingerprints on aluminum foil. RDX and pentaethythritol tetranitrate, the explosive Semtex components, were isolated in the prints, and spectra were obtained with a microscope system. Currently, the FBI Laboratory uses an echelle dispersive Raman spectrograph that operates with a 785-nm laser and a fiber optic probe that has

become successful for field analysis.[54] An explosives library has been developed for use with this instrument.[55]

Current developments in portable FT-IR instrumentation also show promise for field analysis of explosives. Recently, SensIR Technologies (Danbury, CT) introduced a portable instrument referred to as the TravelIR□, that uses a single reflection ATR arrangement for sample analysis.[56] Liquid and solid sample analysis is easily conducted in the field. A preliminary study of explosive samples has been conducted at the FBI Laboratory's FSRU. IR and Raman field methods are expected to complement one another.

6 SUMMARY AND FUTURE DIRECTION

Vibrational spectroscopy is used throughout forensic laboratories for many applications. IR analysis with FT-IR instrumentation has many applications in the areas such as polymers, drugs and explosives. With the exception of field analysis, where methods have just started to develop, IR has reached a level of maturity in forensic applications. Raman, on the other hand, is just beginning to develop. Both laboratory and field methods are anticipated to flourish in the next few years. The greatest developments are expected for field analysis using portable Raman spectrometers. The instruments will require small size designs providing the performance needed by specific sample types, and cost will be a major factor. The greatest challenge, with both Raman and IR field analysis, lies with the development of the software so that nontechnical law enforcement officials can quickly, conveniently, and accurately use the instruments to get the pertinent investigative information. Of great importance is that instrument operators do not obtain false information. A false positive identification of critical chemicals could result in unjust arrests. A false negative could place examiners in danger by contact with hazardous materials. If research continues at the same level, these challenges are expected to be met within the next few years.

ACKNOWLEDGMENTS

The author wishes to express his thanks to Robert Ollis of the Georgia Bureau of Investigation Crime Laboratory, (Decator, GA), Henry Blum of the Drug Enforcement Administration Laboratory (Washington, DC) and Dr. Edward Suzuki of the Washington State Patrol Crime Laboratory (Seattle, WA). All these gentlemen contributed their expertise and spectra for figures used in writing this manuscript.

ABBREVIATIONS AND ACRONYMS

DEA	Drug Enforcement Administration
FSL	Forensic Service Laboratories
GSCL	Georgia State Crime Laboratory
IRE	Internal Reflection Element
LSD	Lysergic Acid Diethylamide
RCMP	Royal Canadian Mounted Police

RDX	Hexahydro-1,3,5-trinitro-1,3,5-triazine
SEM/EDX	Scanning Electron Microscopy with Energy Dispersive X-ray Spectroscopy

REFERENCES

1. E. Locard, *Police J.*, **1**, 177 (1928).
2. E. Locard, *Am. J. Police Sci.*, **1**, 276 (1930).
3. R. Saferstein, 'Criminalistics, An Introduction to Forensic Science', 7th edition, Prentice Hall, Upper Saddle River, NJ (2001).
4. E.M. Suzuki, 'Forensic Applications of Infrared Spectroscopy', in "Forensic Science Handbook", ed. R. Saferstein, Prentice-Hall, New York, 71–195, Vol. III (1993).
5. E.G. Bartick and M.W. Tungol, 'Infrared Microscopy and its Forensic Applications', in "Forensic Science Handbook", ed. R. Saferstein, Prentice-Hall, New York, 196–252, Vol. III (1993).
6. C. Roux, P. Maynard and M. Dawson, *Chem. Aust.*, 11 (1999).
7. P.G. Rogers, R. Cameron, N.S. Cartwright, W.H. Clark, J.S.Deak and E.W.W. Norman, *Can. Soc. Forensic Sci. J.*, **9**, 1 (1976).
8. P.G. Rogers, R. Cameron, N.S. Cartwright, W.H. Clark, J.S.Deak and E.W.W. Norman, *Can. Soc. Forensic Sci. J.*, **9**, 49 (1976).
9. P.G. Rogers, R. Cameron, N.S. Cartwright, W.H. Clark, J.S.Deak and E.W.W. Norman, *Can. Soc. Forensic Sci. J.*, **9**, 103 (1976).
10. E.M. Suzuki and W.R. Gresham, *J. Forensic Sci.*, **31**, 931 (1986).
11. E.M. Suzuki and W.R. Gresham, *J. Forensic Sci.*, **31**, 1292 (1986).
12. E.M. Suzuki and W.R. Gresham, *J. Forensic Sci.*, **32**, 377 (1987).
13. E.M. Suzuki and W.R. Gresham, *J. Forensic Sci.*, **34**, 164 (1989).

14. E.M. Suzuki and W.R. Gresham, *J. Forensic Sci.*, **34**, 180 (1989).
15. W.D. Mazzella, C.J. Lenard and P.A. Margot, *J. Forensic Sci.*, **36**, 449 (1991).
16. W.D. Mazzella, C.J. Lenard and P.A. Margot, *J. Forensic Sci.*, **36**, 820 (1991).
17. R.A. Merrill and E.G. Bartick, *J. Forensic Sci.*, **37**, 528 (1992).
18. E.G. Bartick, *Appl. Spectrosc.*, **39**, 885 (1985).
19. E.G. Bartick, M.W. Tungol and J.A. Reffner, *Anal. Chim. Acta*, **288**, 35 (1994).
20. A.H. Kuptsov, *J. Forensic Sci.*, **39**, 305 (1994).
21. R.A. Nyquist, C.L. Putzig and M.A. Leugers, 'Handbook of Infrared and Raman Spectra of Inorganic Compounds and Organic Salts, Volume 1, Infrared and Raman Spectral Atlas of Inorganic Compounds and Organic Salts', Academic Press, New York (1997).
22. R.A. Merrill, E.G. Bartick and W.D. Mazzella, *J. Forensic Sci.*, **41**, 264 (1996).

23. E.G. Bartick and R.A. Merrill, 'The Development and Evaluation of a Photocopy Toner Spectral Database Obtained by Microscopical IR Analysis', Presented at the AAFS Annual Meeting, New York (1997).

24. M.W. Tungol, E.G. Bartick and A. Montaser, 'Forensic Examination of Synthetic Textile Fibers', in "Practical Guide to Infrared Microspectroscopy", ed. H. Humecki, Marcel Decker, New York, 245–286 (1995).

25. K.P. Kirkbride and M.W. Tungol, 'Infrared Microscopy of Fibres', in "Forensic Examination of Fibres", eds J. Robertson and M. Grieve, Taylor and Francis, Philadelphia, 179–222 (1999).

26. M.W. Tungol, E.G. Bartick and A. Montaser, *Appl. Spectrosc.*, **44**, 543 (1990).

27. M.W. Tungol, E.G. Bartick and A. Montaser, *Spectrochem. Acta Electron.*, **46B**, 1535E (1991).

28. M.W. Tungol, E.G. Bartick and A. Montaser, *J. Forensic Sci.*, **36**, 1027 (1991).

29. Federal Trade Commission Rules and Regulations under theTextile Products Identification Act, Title 15, US Code Section 70, 16 CFR 303.7.

30. M.C. Grieve, *Sci. Just.*, **35**, 179 (1995).

31. J.V. Miller and E.G. Bartick, 'Forensic Analysis of Synthetic Fibers Using Raman Spectroscopy', Presented at the AAFS Annual Meeting, Orlando, FL (1999).

32. J.V. Miller, 'Introduction of Raman Spectroscopy to the Forensic Analysis of Fiber', MS Dissertation, The George Washington University, Washington, DC (1999).

33. P.J. Hendra, W.F. Maddams, I.A.M. Royaud, H.A. Willis and V. Zichy, *Spectrochim. Acta*, **46A**, 747 (1990).

34. P.C. White, C.H. Munro and W.E. Smith, *Analyst*, **121**, 835 (1996).

35. P.C. White, C. Rodger, V. Rutherford, Y. Finnon, W.E. Smithand M. Fitzgerald, *SPIE*, **3576**, 77 (1998).

36. S.G. Ryland, 'Infrared Microscopy of Forensic Paint Evidence', in "Practical Guide to Infrared Microspectroscopy", ed. H. Humecki, Marcel Decker, Inc., New York, 163–244 (1995).

37. J.L. Buckle, D.A. Macdougall and R.R. Grant, *Can. Soc. Forensic Sci. J.*, **30**, 199 (1997).

38. G. Massonnet and W. Stoecklein, *Sci. Just.*, **39**, 181 (1999).

39. E.M. Suzuki, *J. Forensic Sci.* (in press).

40. R.A. Merrill and E.G. Bartick, *J. Forensic Sci.*, **45**, 93 (2000).

41. E.G. Bartick and R.A. Merrill, 'The Development of an Information Database for Duct Tapes', Presented at the AAFS Annual Meeting, Reno, NV (2000).

42. J.A. Seagal, 'Forensic Identification of Controlled Substances', in "Forensic Science Handbook', ed. R. Saferstein, Prentice-Hall, New York, 68–160, Vol. II (1988).

43. R.J. Ollis, Jr, J. Fitzpatrick and S. Ellis, 'Illicit Drug Identification Using a Multiple IRE in FTIR Spectroscopy', Presented at The Pittsburgh Conference, New Orleans, LA (2000).

44. C.V. Koulis, K.J. Hymes and J.L. Rawlins, *J. Forensic Sci.*, **45**, 876 (2000).

45. B. Eckenrode, E.G. Bartick, S.D. Harvey, M. Vucelick, R.W.Wright, R.A. Huff and D.M. Hickey, *Forensic Sci. Commun.* (in press).

46. S. Zitrin, 'Analysis of Explosives by Infrared Spectrometry and Mass Spectrometry', in "Forensic Investigation of Explosions", ed. A. Beverage, Taylor & Francis, Bristol, PA, 267–314 (1998).

47. R.O. Keto, *J. Forensic Sci.*, **31**, 241 (1986).

48. E.G. Bartick and R.A. Merrill, 'Proceedings of the International Symposium on the Forensic Aspects of Trace Evidence', US Government Printing Office, Washington, DC, 277–279 (1991).

49. I.R. Lewis, N.W. Daniel, Jr, N.C. Chaffin, P.R. Griffiths and M.W. Tungol, *Spectrochim. Acta*, *Part A*, **51**, 1985 (1995).

50. I.R. Lewis, N.W. Daniel, Jr and P.R. Griffiths, *Appl. Spectrosc.*, **51**, 1854 (1997).

51. I.R. Lewis, N.W. Daniel, Jr and P.R. Griffiths, *Appl. Spectrosc.*, **51**, 1868 (1997).

52. N.W. Daniel, Jr, I.R. Lewis and P.R. Griffiths, *Mikrokim. Acta*, (Suppl.), **14**, 281 (1997).

53. C. Cheng, T.E. Kirkbride, D.N. Bachelder, R.J. Lacey and T.G. Sheldon, *J. Forensic Sci.*, **40**, 31 (1995).

54. R.A. Huff and D.M. Hickey, 'A Portable Raman System for the Detection of Explosive Materials', 15th Triennial Meeting IAFS, Los Angeles, CA (1999).

55. N.T. Kawai and J.A. Janni, *Spectroscopy*, **15**(10), 32 (2000).

56. J. Coates and J. Reffner, *Spectroscopy*, **15**(4), 19 (2000).

RESUMEN

[18]

La aplicación de las técnicas espectroscópicas en el análisis de la evidencia forense es cada vez más frecuente debido la sensibilidad y confiabilidad de éstas. Se ha encontrado que cuando la evidencia consiste en fragmentos de pintura automotriz, las técnicas microscópicas de análisis visual en conjunto con las técnicas espectroscópicas, como la técnica Raman y el infrarrojo, pueden ayudar a identificar el vehículo del que proviene el fragmento. En este trabajo se demuestra que la técnica Raman resulta muy conveniente en el análisis de pequeños fragmentos de pintura, pues permite establecer su procedencia por comparación del perfil de los espectros, además, permite identificar algunos de los constituyentes de la pintura: matriz polimérica, pigmentos y otros componentes secundarios. En Costa Rica, el uso de la técnica de espectroscopía Raman, como parte de los análisis rutinarios en el Departamento de Ciencias Forenses del OIJ, está en proceso de desarrollo y por ello consideramos que los resultados de esta investigación pueden contribuir a su implementación.

Palabras clave: Pintura automotriz; evidencia forense; espectroscopia Raman

ABSTRACT

[22]

Nowadays, the application of spectroscopic techniques in the analysis of forensic evidence is increasingly common due to its sensitivity and reliability. When evidence consists of fragments of automotive paint, microscopic and visual analysis techniques, in conjunction with other techniques, such as Raman and infrared spectroscopy, can help to identify the vehicle from which the fragment comes from. This paper shows that using Raman spectroscopy is very favorable in the analysis of small fragments of paint, because it allows establishing its origin by comparing profiles of different spectra. In addition, by this technique the identification of some of the constituents of the automotive paint such as: the polymeric matrix, the pigments and, other minor components can be performed. In Costa Rica, the use of Raman spectroscopy technique as part of a routine analysis in the Department of Forensic Sciences of the Organismo de Investigación Judicial (OIJ) is under development; therefore, the results of this research could contribute to its implementation.

Keywords: Automotive paint; forensic evidence; Raman spectroscopy

INTRODUCCIÓN

Los estudios periciales que se realizan en los laboratorios de Ciencias Forenses requieren, cada vez más, el uso de técnicas analíticas modernas que apoyen los resultados obtenidos. Solo con una evidencia rigurosamente sustentada en pruebas estandarizadas y validadas, es posible que las conclusiones de los estudios sean de utilidad en los procesos judiciales. Algunas de las técnicas habituales en los análisis forenses son la microscopía óptica, la cromatografía, la microscopía electrónica, la espectroscopía infrarroja y la espectroscopía Raman [1][2][3]. En los laboratorios forenses de nuestro país se utiliza de forma habitual la espectroscopia infrarroja, mientras que la técnica Raman es relativamente reciente y todavía está en proceso de implementación en el análisis de evidencia forense.

La espectroscopia infrarroja (IR) por reflectancia total atenuada y la microespectroscopia Raman son dos técnicas de análisis con alta sensibilidad y especificidad, las cuales se pueden utilizar en el análisis e identificación de un gran número de sustancias líquidas y sólidas [4][5][6] . Aunque para ambas técnicas la preparación de las muestras es relativamente simple, para la técnica Raman es más sencilla porque se requiere menos tiempo y menor cantidad de muestra. Las características de estas dos técnicas analíticas han hecho que la mayoría de las pruebas estandarizadas que se aplican en el análisis de evidencias de casos forenses, las utilicen como pruebas de referencia primaria [7][3].

La sensibilidad de la espectroscopia IR y Raman se debe a que con poca cantidad de muestra es posible obtener suficiente señal para generar espectros bien definidos. En cuanto a su resolución, esta se debe a que los espectros IR y Raman están relacionados con las energías de vibración de los enlaces moleculares, es decir, con los enlaces presentes en las sustancias analizadas, los cuales suelen ser característicos, por lo tanto, permitiría diferenciar o identificar los componentes presentes en la muestra utilizando bases de datos de referencia [8][9].

En el caso de la espectroscopia IR el material tiene que presentar enlaces con momento dipolar. Cuando un enlace con momento dipolar interactúa con la radiación infrarroja, induce vibraciones que reducen la reflectancia o la transmitancia y es posible obtener el espectro IR. Por su parte, para que una sustancia genere señal Raman, debe inducirse una polarización momentánea del enlace con una radicación monocromática. Cuando un enlace no presenta momento dipolar, es más sencillo inducirlo con la radiación de excitación, esta propiedad se denomina polarizabilidad. En otras palabras, los enlaces que presentan mayor polarizabilidad son aquellos con menor carácter polar. Dicha interacción produce unos pocos fotones con diferente energía de la radiación incidente, la diferencia de energía de estos fotones está asociada con los estados vibracionales de la sustancia. Esta situación hace que ambas técnicas sean complementarias, pues una técnica funciona mejor con enlaces polares (IR) y la otra con enlaces no polares (Raman) [10][11]. En la mayor parte de los casos, una misma sustancia puede ser identificada con las dos técnicas, aunque es posible que con una de las dos se generen mejores resultados.

En los casos forenses donde participan vehículos automotores, es frecuente que una parte de las evidencias recolectadas correspondan a fragmentos de pintura multicapa. Habitualmente, estos fragmentos contienen varias capas de pintura de aspecto diferente, lo que permite caracterizar los mismos mediante el estudio del número, el grosor, el orden y el color de las capas. Si en el transcurso de una investigación se encuentra el vehículo del que se sospecha que proviene el fragmento, es posible realizar comparaciones con muestras obtenidas del vehículo sospechoso con estas propiedades físicas.

Pero también ocurre que cada capa puede tener una composición química particular, lo cual brinda otra posibilidad para establecer correspondencias o diferencias. Cuando se desea establecer la coincidencia de estas muestras con la pintura del vehículo sospechoso mediante la técnica de espectroscopia Raman e IR, se puede realizar un análisis de diferencias y similitudes de los espectros. En otros casos, por la naturaleza del análisis o por el tamaño del fragmento, lo que interesa es la caracterización o la identificación de algunas de las sustancias presentes en los fragmentos.

Las técnicas IR y Raman tienen la ventaja de que garantizan la integridad de la muestra lo que, en el caso de los análisis forenses, es un factor importante. Además, la técnica Raman que se utiliza en los análisis forenses, suele acoplarse con un microscopio confocal, lo cual hace posible el análisis de muestras muy pequeñas en diferentes planos focales. El microscopio permite analizar muestras con dimensiones de micrómetros y la confocalidad permite el análisis de la muestra en diferentes planos focales. Esta facilidad también brinda la posibilidad, en algunos casos, de obtener espectros a través de coberturas transparentes, tales como bolsas plásticas o botellas de vidrio, lo cual incrementa la utilidad de la técnica en el estudio de evidencia forense [12]. A diferencia de la espectroscopia IR, mediante la espectroscopia Raman se puede obtener el espectro de capas individuales de pintura automotriz, siendo que sus espesores típicos son de pocos micrómetros [13].

La técnica IR presenta algunos inconvenientes como lo es la presencia de humedad. El fenómeno más importante que afecta a la técnica Raman es la fluorescencia del material al ser iluminado con la luz del láser. No obstante, mediante el efecto SERS (Surface Enhanced Raman Spectroscopy) se puede incrementar en varios órdenes de magnitud la señal Raman que proviene de las moléculas, reduciendo la importancia relativa de la fluorescencia [14]. Este aumento de la intensidad se explica, principalmente, por la interacción electromagnética de la luz con los electrones de las nanopartículas metálicas y por el contacto cercano de las moléculas del material analizado con el metal. Estas condiciones resultan en un aumento del campo electromagnético que actúa sobre las moléculas a través de excitaciones conocidas como resonancias de plasmones [15] . Precisamente, las pinturas suelen presentar efecto de fluorescencia importante, por lo que con el uso de la metodología SERS es posible evitar algunas de estas dificultades y analizar muestras de pintura que en ciertas circunstancias y con otras técnicas, serían de difícil análisis.

En este artículo se presentan los resultados de los análisis de fragmentos de pintura automotriz multicapa realizados principalmente con espectroscopía Raman.

MATERIALES Y MÉTODOS

Muestras de pintura. Las muestras se obtienen a partir de pequeños fragmentos desprendidos del vehículo o extraídas mediante una hoja metálica afilada con la que se obtiene un segmento de pintura que se extiende desde la capa base, la cual se encuentra adherida al metal. Posteriormente, las muestras son seleccionadas para asegurar la integridad de las capas, pues algunos de los fragmentos presentan deformaciones importantes en el espesor de las capas o inclusive, el desprendimiento de alguna de ellas.

Microscopía Raman. Los espectros fueron obtenidos utilizando un microscopio Raman confocal, modelo DXR de la marca Thermo Scientific, equipado con láseres de diodos de 532 nm (Potencia máxima de 10 mW), 633 nm (Potencia máxima de 8 mW) y 780 nm (Potencia máxima de 24 mW); cada uno con potencias que pueden variar en pasos desde 0.1 mW hasta su valor máximo. El instrumento está equipado con un detector del tipo CCD. La resolución espectral del instrumento varía de 2 cm^{-1} a 5 cm^{-1}.

Microscopía Infrarroja. Los espectros de la muestra fueron obtenidos utilizando un espectrómetro infrarrojo FT-IR Nicolet 380 de la marca Thermo Scientific, equipado con ATR y cristal de diamante, con una resolución < 0.9 cm^{-1}. El rango espectral

utilizado fue de 3500 cm^{-1} a 400 cm^{-1}; además, los espectros fueron utilizados sin ningún procesamiento posterior de los datos.

Preparación de muestras para la espectroscopía Raman. Los fragmentos de pintura fueron lavados con agua jabonosa y posteriormente enjuagados varias veces con agua destilada en baño ultrasónico. De estos fragmentos se extraen pequeñas virutas, obtenidas mediante cortes longitudinales realizados con una hoja quirúrgica afilada. Las pequeñas virutas se colocan sobre un vidrio portaobjetos, lo que permite realizar mediciones transversales de cada una de las capas.

Preparación de los coloides de plata. Una solución coloidal consiste en una dispersión de pequeñas partículas en un medio. En este caso, las partículas dispersadas consisten de nanopartículas de plata (AgNP) o agregados de ellas, dispersas en agua.

Los coloides fueron preparados de acuerdo al método de Lee y Meisel [16][17]a partir de una disolución de nitrato de plata ($AgNO_3$) y citrato de sodio ($Na_3C_6H_5O_7$) como agente reductor. Se disolvieron 45 mg de $AgNO_3$ en 250 ml de agua, llevándose, bajo agitación constante, hasta el punto de ebullición. Luego se añadió 5 ml de una disolución de $Na_3C_6H_5O_7$ al 1 %. La disolución se mantuvo en el punto de ebullición por un periodo de 45 min, obteniéndose una solución amarillo-verdosa. De esta solución se toman 10 ml, a los que se elimina el sobrenadante previa centrifugación y se completa nuevamente con agua ultrapura al volumen inicial.

También se prepara una disolución en agua desionizada de 18,223 µg/ml de 1,2-Di(4Piridil) Etileno. Se mezclan en volúmenes iguales 1 µl de solución de nanopartículas y 1 µl de la disolución de Di-Etileno para determinar la actividad de las nanopartículas antes de la realización de los ensayos.

RESULTADOS Y DISCUSIÓN

En esta sección se detallan los resultados obtenidos al utilizar las técnicas de espectroscopía Raman convencional, metodología SERS y espectroscopía infrarroja.

Para obtener los espectros de las capas que componen la pintura se procura que el haz del láser incida dentro de los límites de cada capa, obteniendo así el espectro individual de cada una. La figura 1 muestra el espectro de dos capas internas de una pintura automotriz, cada capa tendrá un espectro Raman característico. En la Figura 1 se señalan algunas frecuencias que únicamente están presentes en una de las dos capas, también se observa que muchas de las frecuencias coinciden, esto se debe a que dentro de la composición general de las capas se encuentra la matriz, los solventes y diluyentes que generan los mismos picos Raman en los espectros de diferentes capas.

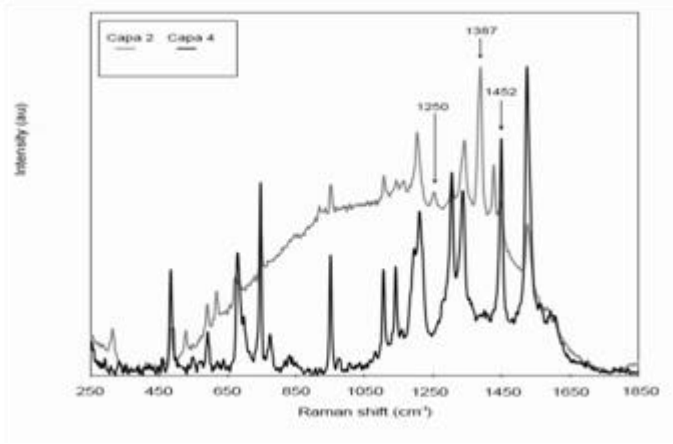

Figura 1 Espectro Raman de dos capas de una misma muestra de pintura automotriz cuyo color externo es negro. Los espectros se encuentran normalizados. La capa 2 presenta fluorescencia. *Laboratorio de Espectroscopía Raman, Tecnológico de Costa Rica*.

Para investigar los compuestos presentes en las muestras de pintura, los espectros obtenidos se comparan directamente con las líneas espectrales de los componentes que comúnmente se utilizan para fabricar pinturas automotrices. En la Figura 2 se identifican los picos característicos del violeta de dioxacina dentro del espectro de una de las capas de la muestra; aquí es posible ver que los picos de la dioxacina coinciden en posición y proporción con los picos del espectro de la capa 2, por lo que es posible asegurar que hay violeta de dioxacina en su composición, además se aprecia que la capa 4 no contiene este pigmento.

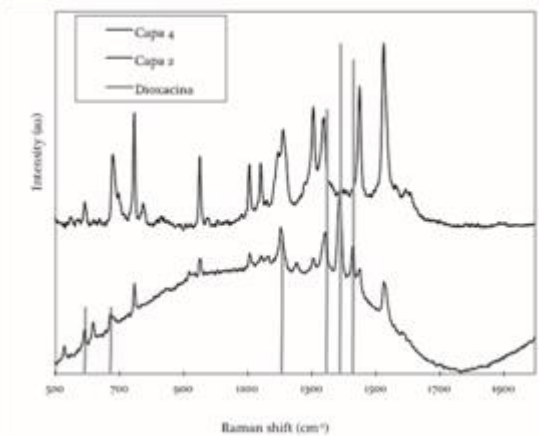

Figura 2 Espectro Raman de una muestra de color exterior negro comparada con las frecuencias características de la dioxacina. *Laboratorio de Espectroscopía Raman, Tecnológico de Costa Rica*.

Sin embargo, la pintura automotriz está formada de muchos otros componentes. En la Figura 3 se analiza la presencia del metacrilato en una muestra de pintura, en este caso es posible observar una buena coincidencia de los picos. Para confirmar esta inferencia, puede usarse el espectro infrarrojo de la muestra como fuente de información complementaria. En la Figura 4 se puede ver que para la muestra estudiada, el perfil del espectro es coincidente con el espectro del metacrilato [18], además varios de los picos corresponden a los grupos funcionales que están presentes

en el metacrilato. Con la información de ambos espectros (infrarrojo y Raman) es posible comprobar que la muestra de pintura estudiada contiene metacrilato.

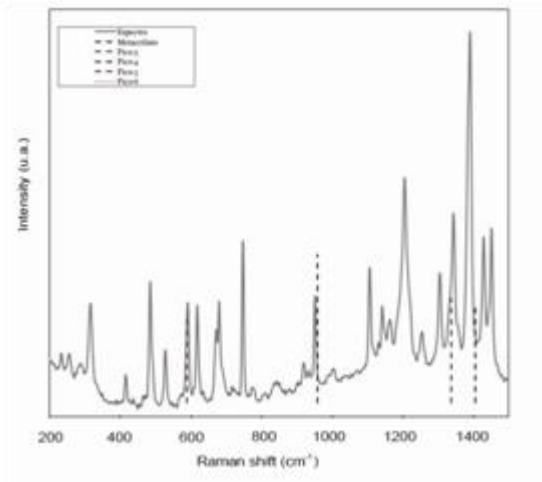

Figura 3 Espectro Raman de una muestra automotriz (color exterior azul). Se muestran los picos característicos del metacrilato. *Laboratorio de Espectroscopía Raman, TEC.*

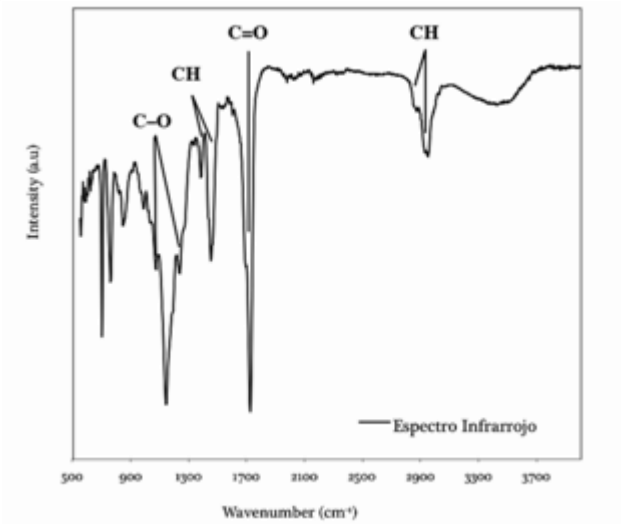

Figura 4 Espectro infrarrojo de una muestra de pintura color azul. También se señalan los grupos funcionales del metacrilato. *Laboratorio CEQUIATEC, TEC.*

La frecuencia Raman dispersada es independiente del láser utilizado, ésta característica se debe a que la frecuencia emitida corresponde a un estado vibracional específico de la molécula. Sin embargo, la intensidad de la dispersión Raman sí se verá afectada por el láser elegido. La Figura 5 muestra una pintura automotriz analizada con dos láseres de diferente longitud de onda, aquí se observa que la forma del espectro no cambia, es decir, la posición de los picos principales se mantiene, sin embargo, la intensidad sí varía, es decir, la altura de cada pico es diferente.

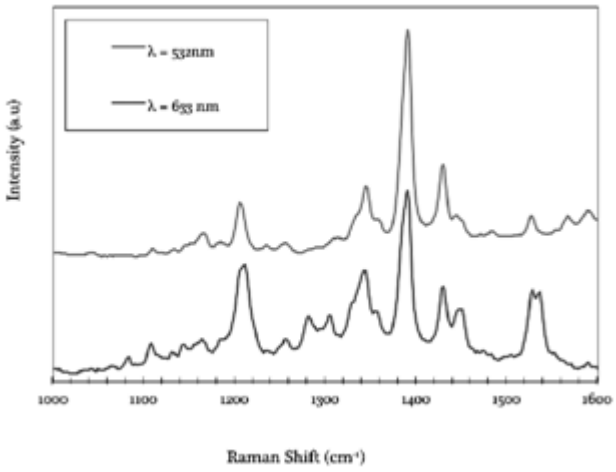

Figura 5 Espectro Raman de una pintura automotriz de color exterior gris. *Laboratorio de Espectroscopía Raman, Tecnológico de Costa Rica*.

Al utilizar diferentes láseres, el espectro obtenido podría presentar fluorescencia, por este motivo la posibilidad de utilizar más de un láser para caracterizar una muestra puede representar una ventaja. Podría ser que la emisión Raman con uno de los láseres sea muy débil o que la fluorescencia sea muy intensa para recolectar información, pero al cambiar de láser, estos problemas podrían disminuir. También puede ocurrir que aunque se utilicen distintos láseres con distintas potencias no se logre adquirir un espectro del que se pueda obtener información, en estos casos se puede acudir a la técnica SERS, la cual permite incrementar en varios órdenes de magnitud la señal Raman. Para lograr este efecto se debe contar con una solución de nanopartículas de plata. La solución de nanopartículas de plata se analizó mediante un microscopio electrónico de transmisión (Figura 6).

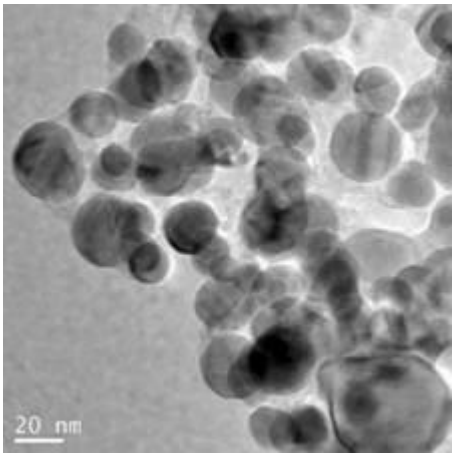

Figura 6 Micrografía TEM de las nanopartículas de plata obtenidas por el método Lee - Meisel.

Laboratorio de nanotecnología, TEC.

Se pueden observar nanopartículas con geometría esférica, mayoritariamente con diámetros entre 20 nm y 35 nm. La distribución de tamaños se puede variar mediante el tiempo del tratamiento térmico, produciendo un aumento del diámetro de las

nanopartículas con el incremento del tiempo de tratamiento. En la Figura 7 se observa el espectro Raman de la disolución 1,2-Di(4-Piridil) Etileno sin nanopartículas y con nanopartículas, lo cual indica que ocurre el efecto SERS.

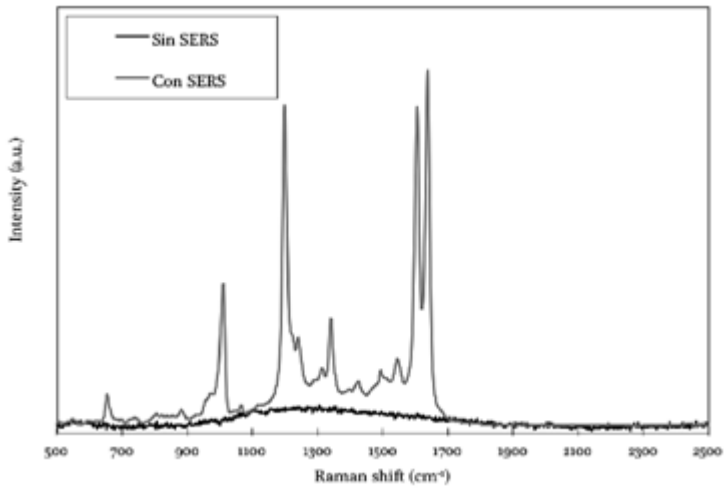

Figura 7 Espectro Raman de la disolución 1,2-Di(4-Piridil) Etileno con nanopartículas y sin nanopartículas de plata. *Laboratorio de Espectroscopía Raman, TEC*.

En la espectroscopía Raman se pueden utilizar las nanopartículas en diversas aplicaciones, en este caso, se deposita una gota de 2 µl de la solución de nanopartículas directamente sobre la superficie de una capa de pintura automotriz. Una vez seca se realiza el ensayo en las regiones cercanas al borde de la gota, pues ahí es donde se encuentra la mayor concentración de nanopartículas. La Figura 8 presenta el espectro Raman de una muestra de pintura automotriz, la cual no ha sido posible observar mediante la espectroscopía Raman convencional, pero sí mediante la metodología SERS.

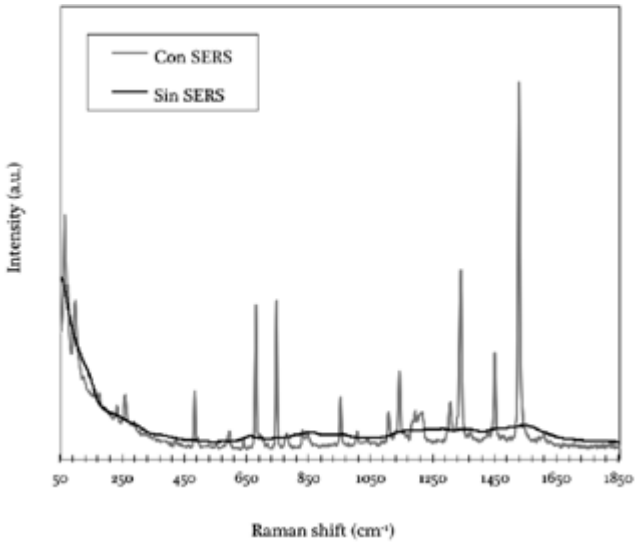

Figura 8 Espectro Raman de una muestra de pintura automotriz obtenido a) sin nanopartículas y b) mediante SERS. *Laboratorio de Espectroscopía Raman, TEC*.

CONCLUSIONES

En este trabajo se comprueba que es posible caracterizar pequeños fragmentos de pintura automotriz utilizando técnicas espectroscópicas. Además, es posible generar espectros de las capas individuales del fragmento, lo cual permite identificar distintos componentes en cada capa y por lo tanto, caracterizar el fragmento de manera precisa por las diferentes propiedades de sus capas.

El microscopio del equipo Raman permite enfocar adecuadamente el haz en un área pequeña, de este modo es posible generar el espectro Raman de cada capa, con lo que se puede analizar las diferencias de los espectros e identificar los componentes de éstas. El equipo permite utilizar distintos láseres lo que mejora la obtención de información referente a una muestra.

Las muestras de pintura automotriz fueron analizadas con técnicas de espectroscopía Raman e infrarroja. Estos análisis permitieron distinguir y comprobar la presencia de algunos de los componentes que comúnmente se encuentran en las pinturas. Ambas técnicas son complementarias porque permiten distinguir componentes diferentes en una muestra y también confirmar la presencia de los mismos.

Cuando el espectro de una muestra Raman presenta fluorescencia, puede ser tratado con la metodología SERS para incrementar la señal Raman, lo que permite caracterizar la muestra. En el Laboratorio de Espectroscopía Raman de la Escuela de Física del Tecnológico de Costa Rica se desarrolló la destreza para implementar la metodología SERS (incluida la preparación de las nanopartículas de Ag) que es un análisis de gran valor, porque aumenta la variedad de muestras que pueden ser estudiadas.

La rigurosidad de los resultados generados en nuestro laboratorio, pueden contribuir al desarrollo de la espectroscopía Raman en el ámbito de las Ciencias Forenses en Costa Rica.

AGRADECIMIENTOS

Agradecemos el apoyo del Consejo de la Escuela de Física y el respaldo y financiamiento de la Vicerrectoría de Investigación y Extensión (VIE) del Instituto Tecnológico de Costa Rica. También agradecemos la colaboración del Lic. Max Méndez de la Sección de Pericias Físicas del Departamento de Ciencias Forenses del OIJ, por su ayuda en el suministro de las muestras de pintura y en la explicación de las técnicas de caracterización visual de los fragmentos de pintura automotriz. Agradecemos además, la colaboración del Laboratorio de Nanotecnología del TEC por las imágenes del microscopio electrónico de transmisión, del CEQUIATEC por los espectros infrarrojos realizados por el investigador M.Sc. Allen Puente Urbina y del químico Lic. Oscar Lacy Mora. Finalmente, agradecemos a todos los estudiantes asistentes del TEC que participaron en este proyecto, por su valiosa colaboración.

REFERENCIAS

[1] J. DeGelder, P.Vandenabeele, F.Govaert y L.Moens, "Forensic analysis of automotive paints by Raman spectroscopy," *Journal of Raman Spectroscopy*, vol. 36, nº 11, pp. 1059-1067, 2005. [Links]

[2] M.Skenderovska, B.Minceva-Sukarova y L.Andreeva, "Application of micro-Raman and FT-IR spectroscopy in forensic analysis of automotive topcoats in the Republic of Macedonia," *Macedonian Journal of Chemistry and Chemical Engineering*, vol. 27, nº 1, pp. 9-17, 2008. [Links]

[3] J. M.Chalmers, H. G.Edwards y M. D.Hargreaves, Infrared and Raman spectroscopy in forensic science, John Wiley & Sons, 2012. [Links]

[4] A. C.Ferrari, "Raman spectroscopy of graphene and graphite: Disorder, electron-phonon coupling, doping and nonadiabatic effects," *Solid State Communications*, vol. 143, nº 1, pp. 47-48, 2007. [Links]

[5] M. S.Dresselhaus, G.Dresselhaus, R.Saito y A.Jorio, "Raman spectroscopy of carbon nanotubes," *Physics Reports*, vol. 409, nº 2, pp. 47-99, 2005. [Links]

[6] E.Smidt y K.Meissl, "The applicability of Fourier transform infrared (FT-IR) spectroscopy in waste management," *Waste Management*, vol. 27, nº 2, pp. 268-276, 2007. [Links]

[7] C.Muehlethaler, G.Massonnet y P.Esseiva, "The application of chemometrics on Infrared and Raman spectra as a tool for the forensic analysis of paints," *Forensic science international*, vol. 209, nº 1, pp. 173-182, 2011. [Links]

[8] E. G.Bartick, "Applications of vibrational spectroscopy in criminal forensic analysis," *Handbook of vibrational spectroscopy*, 2002. [Links]

[9] A. G.Ryder, G. M.O'Connor y T. J.Glynn, "Identifications and quantitative measurements of narcotics in solid mixtures using near-IR Raman spectroscopy and multivariate analysis," *Journal of Forensic Science*, vol. 44, nº 5, pp. 1013-1019, 1999. [Links]

[10] W. M.Tolles, J. W.Nibler, J. R.McDonaldy A. B.Harvey, "A Review of the Theory and Application of Coherent Anti-Stokes Raman Spectroscopy (CARS)," *Applied Spectroscopy*, vol. 31, nº 4, pp. 253-271, 1977. [Links]

[11] Y.Roggo, P.Chalus, L.Maurer, C.Lema-Martinez, A.Edmond y N.Jent, "A review of near infrared spectroscopy and chemometrics in pharmaceutical technologies," *Journal of Pharmaceutical and Biomedical Analysis*, vol. 44, nº 3, pp. 683-700, 2007. [Links]

[12] J. C.Carter, W. E.Brewer y S. M.Angel, "Raman spectroscopy for the in situ identification of cocaine and selected adulterants," *Applied Spectroscopy*, vol. 54, nº 12, pp. 1876-1881, 2000. [Links]

[13] Ž.Šmit, K.Janssens, K.Proost y I.Langus, "Confocal µ-XRF depth analysis of paint layers," *Nuclear Instruments and Methods in Physics Research Section B: Beam Interactions with Materials and Atoms*, vol. 219, pp. 35-40, 2004. [Links]

[14] P. L.Stiles, J. A.Dieringer, N. C.Shah y R. P. VanDuyne, "Surface-Enhanced Raman Spectroscopy," *Annual Review of Analytical Chemistry*, vol. 1, p. 601-626, 2008. [Links]

[15] K. A.Willets y R. P. VanDuyne, "Localized Surface Plasmon Resonance Spectroscopy and Sensing," *Annual Review of Physical Chemistry*, vol. 58, pp. 267-297, 2007. [Links]

[16] P.Lee y D.Meisel, "Adsorption and surface-enhanced Raman of dyes on silver and gold sols," *The Journal of Physical Chemistry*, vol. 86, nº 17, pp. 3391-3395, 1982. [Links]

[17] M.Monge, "Nanopartículas de plata: métodos de síntesis en disolución y propiedades bactericidas," *Anales de Química*, vol. 105, nº 1, pp. 33-41, 2009. [Links]

[18] G.Duan, C.Zhang, A.Li, X.Yang, L.Lu y X.Wang, "Preparation and characterization of mesoporous zirconia made by using a poly (methyl methacrylate) template.," *Nanoscale research letters*, vol. 3, nº 3, p. 118, 2008. [Links]

Received: August 10, 2016; Accepted: November 08, 2016

ABSTRACT

[22]

Nowadays, the application of spectroscopic techniques in the analysis of forensic evidence is increasingly common due to its sensitivity and reliability. When evidence consists of fragments of automotive paint, microscopic and visual analysis techniques, in conjunction with other techniques, such as Raman and infrared spectroscopy, can help to identify the vehicle from which the fragment comes from. This paper shows that using Raman spectroscopy is very favorable in the analysis of small fragments of paint, because it allows establishing its origin by comparing profiles of different spectra. In addition, by this technique the identification of some of the constituents of the automotive paint such as: the polymeric matrix, the pigments and, other minor components can be performed. In Costa Rica, the use of Raman spectroscopy technique as part of a routine analysis in the Department of Forensic Sciences of the Organismo de Investigación Judicial (OIJ) is under development; therefore, the results of this research could contribute to its implementation.

Keywords: Automotive paint; forensic evidence; Raman spectroscopy

INTRODUCCIÓN

Los estudios periciales que se realizan en los laboratorios de Ciencias Forenses requieren, cada vez más, el uso de técnicas analíticas modernas que apoyen los resultados obtenidos. Solo con una evidencia rigurosamente sustentada en pruebas estandarizadas y validadas, es posible que las conclusiones de los estudios sean de utilidad en los procesos judiciales. Algunas de las técnicas habituales en los análisis forenses son la microscopía óptica, la cromatografía, la microscopía electrónica, la espectroscopía infrarroja y la espectroscopía Raman [1][2][3]. En los laboratorios forenses de nuestro país se utiliza de forma habitual la espectroscopia infrarroja, mientras que la técnica Raman es relativamente reciente y todavía está en proceso de implementación en el análisis de evidencia forense.

La espectroscopia infrarroja (IR) por reflectancia total atenuada y la microespectroscopia Raman son dos técnicas de análisis con alta sensibilidad y especificidad, las cuales se pueden utilizar en el análisis e identificación de un gran número de sustancias líquidas y sólidas [4][5][6] . Aunque para ambas técnicas la preparación de las muestras es relativamente simple, para la técnica Raman es más sencilla porque se requiere menos tiempo y menor cantidad de muestra. Las características de estas dos técnicas analíticas han hecho que la mayoría de las pruebas estandarizadas que se aplican en el análisis de evidencias de casos forenses, las utilicen como pruebas de referencia primaria [7][3].

La sensibilidad de la espectroscopia IR y Raman se debe a que con poca cantidad de muestra es posible obtener suficiente señal para generar espectros bien definidos. En cuanto a su resolución, esta se debe a que los espectros IR y Raman están relacionados con las energías de vibración de los enlaces moleculares, es decir, con los enlaces presentes en las sustancias analizadas, los cuales suelen ser característicos, por lo tanto, permitiría diferenciar o identificar los componentes presentes en la muestra utilizando bases de datos de referencia [8][9].

En el caso de la espectroscopia IR el material tiene que presentar enlaces con momento dipolar. Cuando un enlace con momento dipolar interactúa con la radiación infrarroja, induce vibraciones que reducen la reflectancia o la transmitancia y es posible obtener el espectro IR. Por su parte, para que una sustancia genere señal Raman, debe inducirse una polarización momentánea del enlace con una radicación monocromática. Cuando un enlace no presenta momento dipolar, es más sencillo inducirlo con la radiación de excitación, esta propiedad se denomina polarizabilidad. En otras palabras, los enlaces que presentan mayor polarizabilidad son aquellos con menor carácter polar. Dicha interacción produce unos pocos fotones con diferente energía de la radiación incidente, la diferencia de energía de estos fotones está asociada con los estados vibracionales de la sustancia. Esta situación hace que ambas técnicas sean complementarias, pues una técnica funciona mejor con enlaces polares (IR) y la otra con enlaces no polares (Raman) [10][11]. En la mayor parte de los casos, una misma sustancia puede ser identificada con las dos técnicas, aunque es posible que con una de las dos se generen mejores resultados.

En los casos forenses donde participan vehículos automotores, es frecuente que una parte de las evidencias recolectadas correspondan a fragmentos de pintura multicapa. Habitualmente, estos fragmentos contienen varias capas de pintura de aspecto diferente, lo que permite caracterizar los mismos mediante el estudio del número, el grosor, el orden y el color de las capas. Si en el transcurso de una investigación se encuentra el vehículo del que se sospecha que proviene el fragmento, es posible realizar comparaciones con muestras obtenidas del vehículo sospechoso con estas propiedades físicas.

Pero también ocurre que cada capa puede tener una composición química particular, lo cual brinda otra posibilidad para establecer correspondencias o diferencias. Cuando se desea establecer la coincidencia de estas muestras con la pintura del vehículo sospechoso mediante la técnica de espectroscopia Raman e IR, se puede realizar un análisis de diferencias y similitudes de los espectros. En otros casos, por la naturaleza del análisis o por el tamaño del fragmento, lo que interesa es la caracterización o la identificación de algunas de las sustancias presentes en los fragmentos.

Las técnicas IR y Raman tienen la ventaja de que garantizan la integridad de la muestra lo que, en el caso de los análisis forenses, es un factor importante. Además, la técnica Raman que se utiliza en los análisis forenses, suele acoplarse con un microscopio confocal, lo cual hace posible el análisis de muestras muy pequeñas en diferentes planos focales. El microscopio permite analizar muestras con dimensiones de micrómetros y la confocalidad permite el análisis de la muestra en diferentes planos focales. Esta facilidad también brinda la posibilidad, en algunos casos, de obtener espectros a través de coberturas transparentes, tales como bolsas plásticas o botellas de vidrio, lo cual incrementa la utilidad de la técnica en el estudio de evidencia forense [12]. A diferencia de la espectroscopia IR, mediante la espectroscopia Raman se puede obtener el espectro de capas individuales de pintura automotriz, siendo que sus espesores típicos son de pocos micrómetros [13].

La técnica IR presenta algunos inconvenientes como lo es la presencia de humedad. El fenómeno más importante que afecta a la técnica Raman es la fluorescencia del material al ser iluminado con la luz del láser. No obstante, mediante el efecto SERS (Surface Enhanced Raman Spectroscopy) se puede incrementar en varios órdenes de magnitud la señal Raman que proviene de las moléculas, reduciendo la importancia relativa de la fluorescencia [14]. Este aumento de la intensidad se explica,

principalmente, por la interacción electromagnética de la luz con los electrones de las nanopartículas metálicas y por el contacto cercano de las moléculas del material analizado con el metal. Estas condiciones resultan en un aumento del campo electromagnético que actúa sobre las moléculas a través de excitaciones conocidas como resonancias de plasmones [15] . Precisamente, las pinturas suelen presentar efecto de fluorescencia importante, por lo que con el uso de la metodología SERS es posible evitar algunas de estas dificultades y analizar muestras de pintura que en ciertas circunstancias y con otras técnicas, serían de difícil análisis.

En este artículo se presentan los resultados de los análisis de fragmentos de pintura automotriz multicapa realizados principalmente con espectroscopía Raman.

MATERIALES Y MÉTODOS

Muestras de pintura. Las muestras se obtienen a partir de pequeños fragmentos desprendidos del vehículo o extraídas mediante una hoja metálica afilada con la que se obtiene un segmento de pintura que se extiende desde la capa base, la cual se encuentra adherida al metal. Posteriormente, las muestras son seleccionadas para asegurar la integridad de las capas, pues algunos de los fragmentos presentan deformaciones importantes en el espesor de las capas o inclusive, el desprendimiento de alguna de ellas.

Microscopía Raman. Los espectros fueron obtenidos utilizando un microscopio Raman confocal, modelo DXR de la marca Thermo Scientific, equipado con láseres de diodos de 532 nm (Potencia máxima de 10 mW), 633 nm (Potencia máxima de 8 mW) y 780 nm (Potencia máxima de 24 mW); cada uno con potencias que pueden variar en pasos desde 0.1 mW hasta su valor máximo. El instrumento está equipado con un detector del tipo CCD. La resolución espectral del instrumento varía de 2 cm^{-1} a 5 cm^{-1}.

Microscopía Infrarroja. Los espectros de la muestra fueron obtenidos utilizando un espectrómetro infrarrojo FT-IR Nicolet 380 de la marca Thermo Scientific, equipado con ATR y cristal de diamante, con una resolución < 0.9 cm^{-1}. El rango espectral utilizado fue de 3500 cm^{-1} a 400 cm^{-1}; además, los espectros fueron utilizados sin ningún procesamiento posterior de los datos.

Preparación de muestras para la espectroscopía Raman. Los fragmentos de pintura fueron lavados con agua jabonosa y posteriormente enjuagados varias veces con agua destilada en baño ultrasónico. De estos fragmentos se extraen pequeñas virutas, obtenidas mediante cortes longitudinales realizados con una hoja quirúrgica afilada. Las pequeñas virutas se colocan sobre un vidrio portaobjetos, lo que permite realizar mediciones transversales de cada una de las capas.

Preparación de los coloides de plata. Una solución coloidal consiste en una dispersión de pequeñas partículas en un medio. En este caso, las partículas dispersadas consisten de nanopartículas de plata (AgNP) o agregados de ellas, dispersas en agua.

Los coloides fueron preparados de acuerdo al método de Lee y Meisel [16][17]a partir de una disolución de nitrato de plata ($AgNO_3$) y citrato de sodio ($Na_3C_6H_5O_7$) como agente reductor. Se disolvieron 45 mg de $AgNO_3$ en 250 ml de agua, llevándose, bajo agitación constante, hasta el punto de ebullición. Luego se añadió 5 ml de una

disolución de $Na_3C_6H_5O_7$ al 1 %. La disolución se mantuvo en el punto de ebullición por un periodo de 45 min, obteniéndose una solución amarillo-verdosa. De esta solución se toman 10 ml, a los que se elimina el sobrenadante previa centrifugación y se completa nuevamente con agua ultrapura al volumen inicial.

También se prepara una disolución en agua desionizada de 18,223 µg/ml de 1,2-Di(4Piridil) Etileno. Se mezclan en volúmenes iguales 1 µl de solución de nanopartículas y 1 µl de la disolución de Di-Etileno para determinar la actividad de las nanopartículas antes de la realización de los ensayos.

RESULTADOS Y DISCUSIÓN

En esta sección se detallan los resultados obtenidos al utilizar las técnicas de espectroscopía Raman convencional, metodología SERS y espectroscopía infrarroja.

Para obtener los espectros de las capas que componen la pintura se procura que el haz del láser incida dentro de los límites de cada capa, obteniendo así el espectro individual de cada una. La figura 1 muestra el espectro de dos capas internas de una pintura automotriz, cada capa tendrá un espectro Raman característico. En la Figura 1 se señalan algunas frecuencias que únicamente están presentes en una de las dos capas, también se observa que muchas de las frecuencias coinciden, esto se debe a que dentro de la composición general de las capas se encuentra la matriz, los solventes y diluyentes que generan los mismos picos Raman en los espectros de diferentes capas.

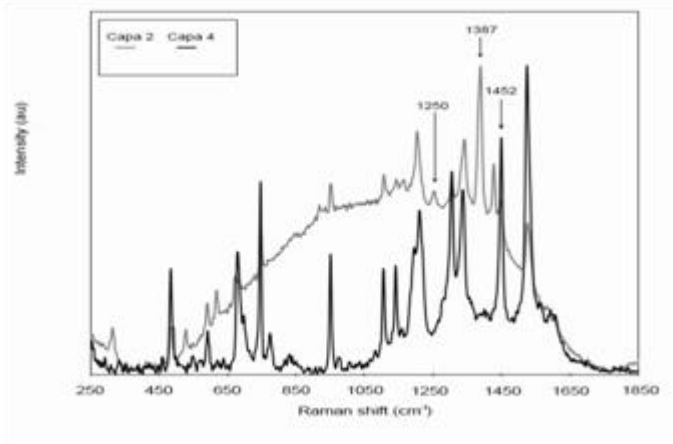

Figura 1 Espectro Raman de dos capas de una misma muestra de pintura automotriz cuyo color externo es negro. Los espectros se encuentran normalizados. La capa 2 presenta fluorescencia. *Laboratorio de Espectroscopía Raman, Tecnológico de Costa Rica*.

Para investigar los compuestos presentes en las muestras de pintura, los espectros obtenidos se comparan directamente con las líneas espectrales de los componentes que comúnmente se utilizan para fabricar pinturas automotrices. En la Figura 2 se identifican los picos característicos del violeta de dioxacina dentro del espectro de una de las capas de la muestra; aquí es posible ver que los picos de la dioxacina coinciden en posición y proporción con los picos del espectro de la capa 2, por lo que es posible asegurar que hay violeta de dioxacina en su composición, además se aprecia que la capa 4 no contiene este pigmento.

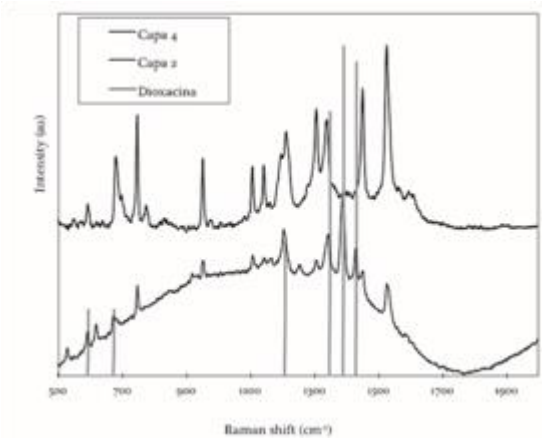

Figura 2 Espectro Raman de una muestra de color exterior negro comparada con las frecuencias características de la dioxacina. *Laboratorio de Espectroscopía Raman, Tecnológico de Costa Rica.*

Sin embargo, la pintura automotriz está formada de muchos otros componentes. En la Figura 3 se analiza la presencia del metacrilato en una muestra de pintura, en este caso es posible observar una buena coincidencia de los picos. Para confirmar esta inferencia, puede usarse el espectro infrarrojo de la muestra como fuente de información complementaria. En la Figura 4 se puede ver que para la muestra estudiada, el perfil del espectro es coincidente con el espectro del metacrilato [18], además varios de los picos corresponden a los grupos funcionales que están presentes en el metacrilato. Con la información de ambos espectros (infrarrojo y Raman) es posible comprobar que la muestra de pintura estudiada contiene metacrilato.

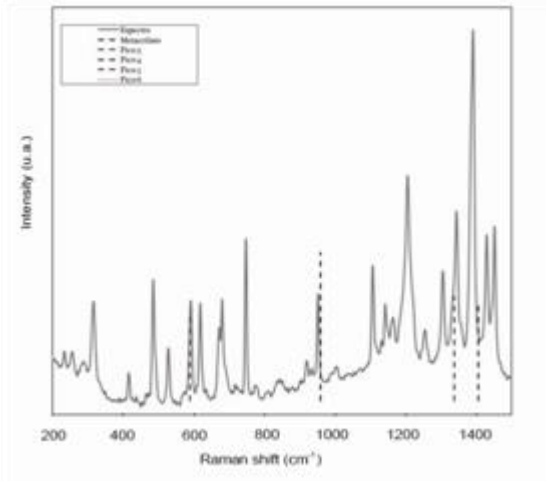

Figura 3 Espectro Raman de una muestra automotriz (color exterior azul). Se muestran los picos característicos del metacrilato. *Laboratorio de Espectroscopía Raman, TEC.*

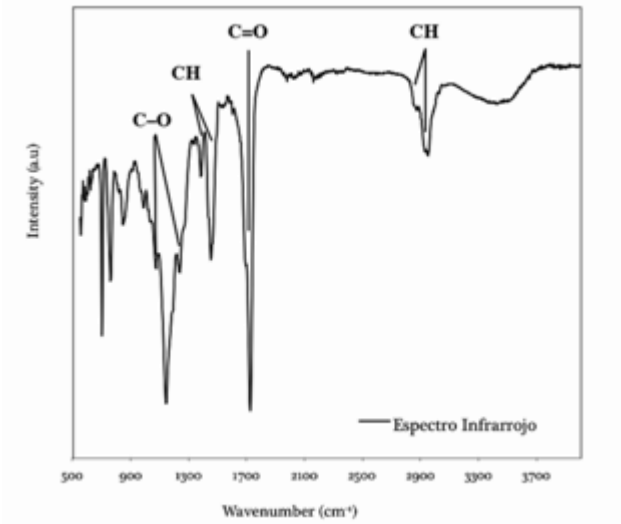

Figura 4 Espectro infrarrojo de una muestra de pintura color azul. También se señalan los grupos funcionales del metacrilato. *Laboratorio CEQUIATEC, TEC.*

La frecuencia Raman dispersada es independiente del láser utilizado, ésta característica se debe a que la frecuencia emitida corresponde a un estado vibracional específico de la molécula. Sin embargo, la intensidad de la dispersión Raman sí se verá afectada por el láser elegido. La Figura 5 muestra una pintura automotriz analizada con dos láseres de diferente longitud de onda, aquí se observa que la forma del espectro no cambia, es decir, la posición de los picos principales se mantiene, sin embargo, la intensidad sí varía, es decir, la altura de cada pico es diferente.

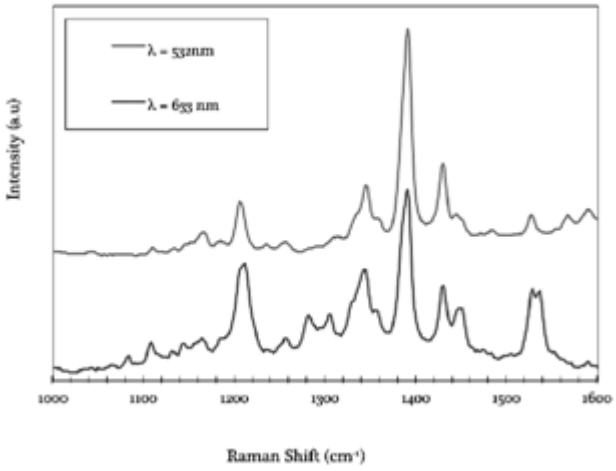

Figura 5 Espectro Raman de una pintura automotriz de color exterior gris. *Laboratorio de Espectroscopía Raman, Tecnológico de Costa Rica*.

Al utilizar diferentes láseres, el espectro obtenido podría presentar fluorescencia, por este motivo la posibilidad de utilizar más de un láser para caracterizar una muestra puede representar una ventaja. Podría ser que la emisión Raman con uno de los láseres sea muy débil o que la fluorescencia sea muy intensa para recolectar información, pero al cambiar de láser, estos problemas podrían disminuir. También

puede ocurrir que aunque se utilicen distintos láseres con distintas potencias no se logre adquirir un espectro del que se pueda obtener información, en estos casos se puede acudir a la técnica SERS, la cual permite incrementar en varios órdenes de magnitud la señal Raman. Para lograr este efecto se debe contar con una solución de nanopartículas de plata. La solución de nanopartículas de plata se analizó mediante un microscopio electrónico de transmisión (Figura 6).

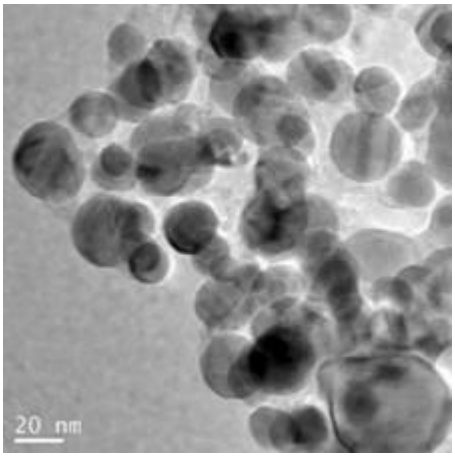

Figura 6 Micrografía TEM de las nanopartículas de plata obtenidas por el método Lee - Meisel.

Laboratorio de nanotecnología, TEC.

Se pueden observar nanopartículas con geometría esférica, mayoritariamente con diámetros entre 20 nm y 35 nm. La distribución de tamaños se puede variar mediante el tiempo del tratamiento térmico, produciendo un aumento del diámetro de las nanopartículas con el incremento del tiempo de tratamiento. En la Figura 7 se observa el espectro Raman de la disolución 1,2-Di(4-Piridil) Etileno sin nanopartículas y con nanopartículas, lo cual indica que ocurre el efecto SERS.

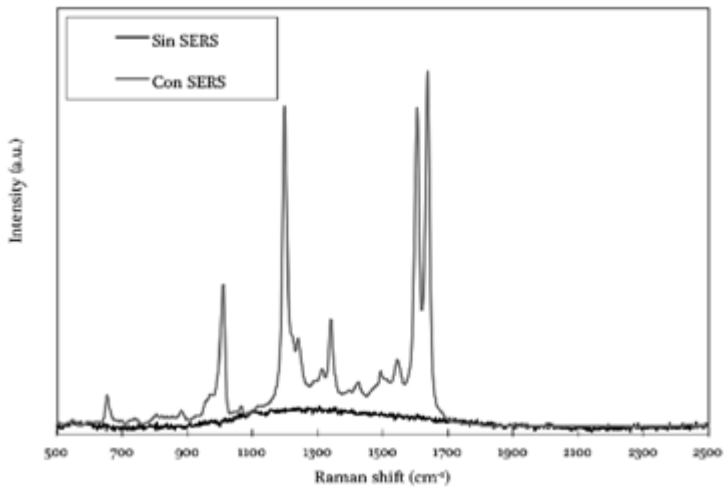

Figura 7 Espectro Raman de la disolución 1,2-Di(4-Piridil) Etileno con nanopartículas y sin nanopartículas de plata. *Laboratorio de Espectroscopía Raman, TEC*.

En la espectroscopía Raman se pueden utilizar las nanopartículas en diversas aplicaciones, en este caso, se deposita una gota de 2 µl de la solución de nanopartículas directamente sobre la superficie de una capa de pintura automotriz. Una vez seca se realiza el ensayo en las regiones cercanas al borde de la gota, pues ahí es donde se encuentra la mayor concentración de nanopartículas. La Figura 8 presenta el espectro Raman de una muestra de pintura automotriz, la cual no ha sido posible observar mediante la espectroscopía Raman convencional, pero sí mediante la metodología SERS.

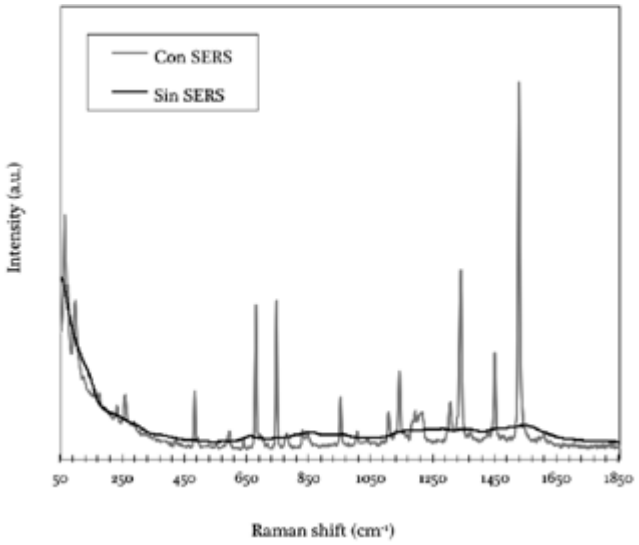

Figura 8 Espectro Raman de una muestra de pintura automotriz obtenido a) sin nanopartículas y b) mediante SERS. *Laboratorio de Espectroscopía Raman, TEC*.

CONCLUSIONES

En este trabajo se comprueba que es posible caracterizar pequeños fragmentos de pintura automotriz utilizando técnicas espectroscópicas. Además, es posible generar espectros de las capas individuales del fragmento, lo cual permite identificar distintos componentes en cada capa y por lo tanto, caracterizar el fragmento de manera precisa por las diferentes propiedades de sus capas.

El microscopio del equipo Raman permite enfocar adecuadamente el haz en un área pequeña, de este modo es posible generar el espectro Raman de cada capa, con lo que se puede analizar las diferencias de los espectros e identificar los componentes de éstas. El equipo permite utilizar distintos láseres lo que mejora la obtención de información referente a una muestra.

Las muestras de pintura automotriz fueron analizadas con técnicas de espectroscopía Raman e infrarroja. Estos análisis permitieron distinguir y comprobar la presencia de algunos de los componentes que comúnmente se encuentran en las pinturas. Ambas técnicas son complementarias porque permiten distinguir componentes diferentes en una muestra y también confirmar la presencia de los mismos.

Cuando el espectro de una muestra Raman presenta fluorescencia, puede ser tratado con la metodología SERS para incrementar la señal Raman, lo que permite caracterizar la muestra. En el Laboratorio de Espectroscopía Raman de la Escuela de Física del Tecnológico de Costa Rica se desarrolló la destreza para implementar la metodología SERS (incluida la preparación de las nanopartículas de Ag) que es un análisis de gran valor, porque aumenta la variedad de muestras que pueden ser estudiadas.

La rigurosidad de los resultados generados en nuestro laboratorio, pueden contribuir al desarrollo de la espectroscopía Raman en el ámbito de las Ciencias Forenses en Costa Rica.

AGRADECIMIENTOS

Agradecemos el apoyo del Consejo de la Escuela de Física y el respaldo y financiamiento de la Vicerrectoría de Investigación y Extensión (VIE) del Instituto Tecnológico de Costa Rica. También agradecemos la colaboración del Lic. Max Méndez de la Sección de Pericias Físicas del Departamento de Ciencias Forenses del OIJ, por su ayuda en el suministro de las muestras de pintura y en la explicación de las técnicas de caracterización visual de los fragmentos de pintura automotriz. Agradecemos además, la colaboración del Laboratorio de Nanotecnología del TEC por las imágenes del microscopio electrónico de transmisión, del CEQUIATEC por los espectros infrarrojos realizados por el investigador M.Sc. Allen Puente Urbina y del químico Lic. Oscar Lacy Mora. Finalmente, agradecemos a todos los estudiantes asistentes del TEC que participaron en este proyecto, por su valiosa colaboración.

REFERENCIAS

[1] J. DeGelder, P.Vandenabeele, F.Govaert y L.Moens, "Forensic analysis of automotive paints by Raman spectroscopy," *Journal of Raman Spectroscopy*, vol. 36, nº 11, pp. 1059-1067, 2005. [Links]

[2] M.Skenderovska, B.Minceva-Sukarova y L.Andreeva, "Application of micro-Raman and FT-IR spectroscopy in forensic analysis of automotive topcoats in the Republic of Macedonia," *Macedonian Journal of Chemistry and Chemical Engineering*, vol. 27, nº 1, pp. 9-17, 2008. [Links]

[3] J. M.Chalmers, H. G.Edwards y M. D.Hargreaves, Infrared and Raman spectroscopy in forensic science, John Wiley & Sons, 2012. [Links]

[4] A. C.Ferrari, "Raman spectroscopy of graphene and graphite: Disorder, electron-phonon coupling, doping and nonadiabatic effects," *Solid State Communications*, vol. 143, nº 1, pp. 47-48, 2007. [Links]

[5] M. S.Dresselhaus, G.Dresselhaus, R.Saito y A.Jorio, "Raman spectroscopy of carbon nanotubes," *Physics Reports*, vol. 409, nº 2, pp. 47-99, 2005. [Links]

[6] E.Smidt y K.Meissl, "The applicability of Fourier transform infrared (FT-IR) spectroscopy in waste management," *Waste Management*, vol. 27, nº 2, pp. 268-276, 2007. [Links]

[7] C.Muehlethaler, G.Massonnet y P.Esseiva, "The application of chemometrics on Infrared and Raman spectra as a tool for the forensic analysis of paints," *Forensic science international*, vol. 209, nº 1, pp. 173-182, 2011. [Links]

[8] E. G.Bartick, "Applications of vibrational spectroscopy in criminal forensic analysis," *Handbook of vibrational spectroscopy*, 2002. [Links]

[9] A. G.Ryder, G. M.O'Connor y T. J.Glynn, "Identifications and quantitative measurements of narcotics in solid mixtures using near-IR Raman spectroscopy and multivariate analysis," *Journal of Forensic Science*, vol. 44, nº 5, pp. 1013-1019, 1999. [Links]

[10] W. M.Tolles, J. W.Nibler, J. R.McDonaldy A. B.Harvey, "A Review of the Theory and Application of Coherent Anti-Stokes Raman Spectroscopy (CARS)," *Applied Spectroscopy*, vol. 31, nº 4, pp. 253-271, 1977. [Links]

[11] Y.Roggo, P.Chalus, L.Maurer, C.Lema-Martinez, A.Edmond y N.Jent, "A review of near infrared spectroscopy and chemometrics in pharmaceutical technologies," *Journal of Pharmaceutical and Biomedical Analysis*, vol. 44, nº 3, pp. 683-700, 2007. [Links]

[12] J. C.Carter, W. E.Brewer y S. M.Angel, "Raman spectroscopy for the in situ identification of cocaine and selected adulterants," *Applied Spectroscopy*, vol. 54, nº 12, pp. 1876-1881, 2000. [Links]

[13] Ž.Šmit, K.Janssens, K.Proost y I.Langus, "Confocal µ-XRF depth analysis of paint layers," *Nuclear Instruments and Methods in Physics Research Section B: Beam Interactions with Materials and Atoms*, vol. 219, pp. 35-40, 2004. [Links]

[14] P. L.Stiles, J. A.Dieringer, N. C.Shah y R. P. VanDuyne, "Surface-Enhanced Raman Spectroscopy," *Annual Review of Analytical Chemistry*, vol. 1, p. 601-626, 2008. [Links]

[15] K. A.Willets y R. P. VanDuyne, "Localized Surface Plasmon Resonance Spectroscopy and Sensing," *Annual Review of Physical Chemistry*, vol. 58, pp. 267-297, 2007. [Links]

[16] P.Lee y D.Meisel, "Adsorption and surface-enhanced Raman of dyes on silver and gold sols," *The Journal of Physical Chemistry*, vol. 86, nº 17, pp. 3391-3395, 1982. [Links]

[17] M.Monge, "Nanopartículas de plata: métodos de síntesis en disolución y propiedades bactericidas," *Anales de Química*, vol. 105, nº 1, pp. 33-41, 2009. [Links]

[18] G.Duan, C.Zhang, A.Li, X.Yang, L.Lu y X.Wang, "Preparation and characterization of mesoporous zirconia made by using a poly (methyl methacrylate) template.," *Nanoscale research letters*, vol. 3, nº 3, p. 118, 2008. [Links]

A Review of the Theory and Application of Coherent Anti-Stokes Raman Spectroscopy (CARS)

Article *in* Applied Spectroscopy · July 1977
DOI: 10.1366/000370277774463625

CITATIONS
509

READS
5,185

4 authors, including:

William M. Tolles
United States Naval Research Laboratory
33 PUBLICATIONS **1,663** CITATIONS
SEE PROFILE

Joseph W. Nibler
Oregon State University
141 PUBLICATIONS **3,224** CITATIONS
SEE PROFILE

feature article

A Review of the Theory and Application of Coherent Anti-Stokes Raman Spectroscopy (CARS)

W. M. TOLLES,* J. W. NIBLER,† J. R. McDONALD, and A. B. HARVEY
Physical Chemistry Branch, Chemistry Division, Naval Research Laboratory, Washington, D.C. 20375

Coherent anti-Stokes Raman spectroscopy (CARS) is a relatively new kind of Raman spectroscopy which is based on a nonlinear conversion of two laser beams into a coherent, laser-like Raman beam of high intensity in the anti-Stokes region. The emission is often many orders of magnitude greater than normal Raman scattering and, because of the coherent and anti-Stokes character of radiation, the method is very useful for obtaining Raman spectra of fluorescing samples, gases in discharges, plasmas, combustion, atmospheric chemistry. In this paper we outline the basic theory behind CARS and describe its unusual effects and drawbacks. We review the research to date on various materials, and indicate the possible future direction, utility and applications of CARS such as surface studies, fluctuation phenomena, reaction dynamics, photochemistry, kinetics, relaxation, and energy transfer.

Index Headings: **CARS; Raman spectroscopy; Nonlinear optics.**

INTRODUCTION

Coherent anti-Stokes Raman spectroscopy (CARS)‡ is one of a number of different Raman processes that have developed with the availability of lasers in recent years. Examples include:

Conventional, spontaneous Raman scattering[1]
Resonance Raman effect[2]
Inverse Raman effect[3]
Hyper-Raman effect[4]
Raman-induced Kerr effect[5]
Coherent anti-Stokes Raman spectroscopy (CARS)[6]

It is beyond the scope of this paper to discuss all of these Raman effects, but they are compared briefly in a recent review[7] and discussed in more detail in the references above. However, it is to be emphasized that each method is quite different from the others, and equipment required to carry out CARS can be readily adapted to conduct experiments based on the other techniques. It also may be stated that beyond normal Raman spectroscopy, CARS probably has the most general utility.

CARS is potentially a powerful technique because of its promise in obtaining analytical and spectroscopic information pertaining to Raman active resonances in gases, liquids, and solids. With this process, spectral resonances corresponding to vibrational transitions may be observed by mixing together two visible laser beams. Unlike second-order processes, CARS, a third-order effect, is generally applicable to isotropic, as well as anisotropic media, and the conversion efficiency to (coherently) generated photons is considerably higher then with conventional, spontaneous Raman scattering. As such, it appears to be a superior tool for obtaining spectra of luminescent samples (fluorescent materials, impurities, combustion systems, and electric discharges) and of certain solutes in solution.

By the CARS technique two relatively high-powered (typically pulsed) laser beams at angular frequencies ω_l and ω_s are focused together in a sample. As a result of mixing the two lasers, a coherent beam resembling a low intensity laser beam at frequency, $\omega_{as} = 2\,\omega_l - \omega_s$, is generated in the medium. The efficiency of the conversion to frequency ω_{as} depends critically upon the presence of molecular resonances at a frequency $\omega_l - \omega_s$, the laser intensities, the resonance line width, and the number density. Typically ω_s is varied to obtain a spectrum. As $\omega_l - \omega_s$ is swept over the molecular resonance, the intensity of the beam at ω_{as} changes. Recording this intensity as a function of $\omega_l - \omega_s$ constitutes a CARS spectrum.

The first observation of this particular nonlinear mixing process was reported by Terhune[8] as a by-product of stimulated Raman emission. Later Maker and Terhune[9] used a 0.1 J pulse from a ruby laser and a second beam produced by stimulated Raman emission in benzene to observe the effect in several samples. Since these initial experiments, a number of investigations demonstrating the application of CARS in solids,[10–16] liquids,[17–33] gases,[34–49] and for kinetics[50–56] have been reported. The high-powered, tunable, pulsed dye laser has made it possible to scan conveniently over a significant spectral region in order to observe the resonances. As we shall see, one of the most impressive properties of CARS is that very high conversion efficiencies are possible. Also, the process actually improves with higher resolution. Since lasers can be spectrally narrowed to rather small widths ($< 10^{-3}$ cm^{-1}, see Ref. 5) with only small sacrifices in laser output, high resolution spectra are readily attainable. Thus, it is safe to say that in the future CARS will be the preferred method of doing high resolution Raman spectroscopy. We shall also see that the coherent and anti-Stokes character of the emission

Received 15 April 1976.
* Present address: Department of Physics and Chemistry, Naval Postgraduate School, Monterey, CA 93950.
† On sabbatical leave from: Department of Chemistry, Oregon State University, Corvallis, OR 97330.
‡ Also referred to as coherent anti-Stokes Raman scattering.

makes the technique very useful for many applications where fluorescence is a problem or where only small viewing apertures are available.

In this paper we shall attempt to outline the basic theory behind CARS in order to explain its properties, to review some of the recent progress, and to project somewhat into the future in order to suggest problems that need solving and to point out applications.

I. OUTLINE OF THE DEVELOPMENT OF CARS THEORY

A brief discussion of the basic theory behind CARS is offered here in order to explain the process and describe its properties. A more complete account of the theory may be found elsewhere,[9, 33, 58-64] and a review on nonlinear effects including CARS may be found in a recent account by Shen.[65] Conversion of two laser beams into the anti-Stokes component at $\omega_{as} = 2\omega_l - \omega_s$ is a direct consequence of the nonlinear dielectric properties of materials. The efficiency of this process is considered for both plane wave and focused beam cases and an expression is developed which relates this efficiency to the normal Raman cross section.

A. Nonlinear Mixing. The polarization of a medium in an electric field may generally be expressed as a power series:

$$\vec{\mathbf{P}}(\omega) = \chi^{(i)}(\omega)\,\vec{\mathbf{E}}(\omega) + \chi^{(2)}(\omega)\,\vec{\mathbf{E}}^2(\omega) + \chi^{(3)}(\omega)\,\vec{\mathbf{E}}^3 \tag{1}$$

where $\vec{\mathbf{P}}$ is the macroscopic polarization vector, $\chi^{(i)}$ is the dielectric susceptibility tensor of rank $i + 1$ associated with the ith order of the electric field, and $\mathbf{E}$ is the applied electric field. The subscripts denoting the tensor properties of the susceptibility have been eliminated for simplicity. Under low intensity fields, only the first-order term is important and is the basic for classical, linear optics including normal Raman scattering. The higher order terms become important as the field strengths approach very high levels, a fact which explains why the whole field of nonlinear optics achieved exponential growth immediately following the advent of the laser. The first nonlinear term depends on the square of the field strength and is responsible for second harmonic generation (doubling of laser frequencies), sum and difference frequency generation, hyper-Raman effect and parametric oscillation. The third-order term is responsible for third harmonic generation ($3\omega_1 \rightarrow \omega_3$) and other processes, e.g., $2\omega_1 + \omega_2 \rightarrow \omega_3$, $2\omega_1 - \omega_2 \rightarrow \omega_3$, etc. It is the last mentioned process, namely, $2\omega_1 - \omega_2 \rightarrow \omega_3$, which is designated as CARS. An isotropic medium such as a liquid or gas exhibits inversion symmetry in its macroscopic dielectric properties. Examination of Eq. (1) under the inversion operation reveals that $\chi^{(2)}$ must be identically equal to zero for such a medium. Hence, the lowest order nonlinearity which may be present in a liquid or gas is due to the third-order susceptibility, $\chi^{(3)}$.

The electric field is, of course, a vector. In what follows, we shall assume that the direction of all electric fields involved are along the same axis and treat each field as a scalar quantity. Using complex notation, we may express the magnitude of the electric field at angular frequency ω_i ($= 2\pi c/\lambda_i$) as:

$$E_i(\omega_i) = \frac{1}{2}\left[\mathscr{E}_i e^{i(k_i z - \omega_i t)} + \text{c.c.}\right] \tag{2}$$

where $\mathscr{E}_i$ is the amplitude, k_i is the momentum vector equal to $\omega_i n_i/c$, t is time, z is distance along the direction of propagation, n_i is the index of refraction at ω_i and c.c. is the complex conjugate. In general, E may consist of a sum of a number of different frequencies. For the process designated as CARS, only two frequencies at ω_1 and ω_2 are introduced, and the consequent polarization at frequency $2\omega_1 - \omega_2$ will be examined. Conventions differ in the literature regarding the introduction of a factor of 3 at this point. If $E = E_1 + E_2$, the third-order term in Eq. (1) has a component of magnitude $3E_1^2E_2$. The reader is cautioned that this factor of 3 is the source of some confusion when relating results from various articles. For clarity, the relationships derived here explicitly show this factor of 3 as a multiplicative coefficient associated with the value for susceptibility. Thus, retaining only those terms in which the polarization varies by $\omega_3 = 2\omega_1 - \omega_2$,

$$P^{(3)} = \frac{1}{8}\left[3\,\chi^{(3)}(-\omega_3, \omega_1, \omega_1, -\omega_2)\right] \{\mathscr{E}_1^2\,\mathscr{E}_2^*\,e^{i[2k_1 - k_2]z - (2\omega_1 - \omega_2)t} + \text{c.c.}\}\,, \tag{3}$$

where the usual notation of Bloembergen[60] is used such that $\chi^{(3)}(-\omega_a, \omega_b, \omega_c, \omega_d)$ represents the susceptibility for the process in which $\omega_a = \omega_b + \omega_c + \omega_d$.

Substituting Eq. (3) into Maxwell's equations gives the gain equation for plane waves;[45, 46]

$$d\mathscr{E}_{as} = \frac{-i\,\pi\,\omega_{as}}{2\,cn_{as}}\,\mathscr{E}_l^2\,\mathscr{E}_s^*\,(3\,\chi^{(3)})\,e^{i(2k_l - k_s - k_{as})Z}\,dZ \tag{4}$$

where the previous subscripts 1, 2, and 3 are replaced by l, s and as to represent the laser frequency, Stokes frequency, and the anti-Stokes frequency, respectively. Introducing the usual relationship between electric field and intensity [$I_i = (c/8\pi)\,|\mathscr{E}_i|^2$], integration of Eq. (4) gives:

$$\epsilon = \frac{I_{as}}{I_s} = \frac{P_{as}}{P_s} = \left(\frac{4\,\pi^2\,\omega_{as}}{n_{as}\,c^2}\right)^2 |3\,\chi^{(3)}|^2\,I_l^2\,L^2\left[\frac{\sin(\Delta kL/2)}{(\Delta kL/2)}\right]^2 \tag{5}$$

where ϵ is the efficiency of the process, P is the power of the respective beams, L is the length over which the beams are mixed through the sample and $\Delta k = 2k_l - k_s - k_{as}$. The momentum mismatch Δk is a direct result of the fact that the propagating waves move in and out of phase because of dispersion in the medium. As can be seen from Fig. 1, conversion efficiency for a length of path L is much higher for $\Delta k = 0$, the phase-matched condition. Since dispersion in gases is usually quite small, particularly for low-pressure conditions, phase matching over moderate path lengths (many centimeters) is readily achieved. For condensed media, $\Delta k \neq 0$ even over small paths. In this case, phase matching is achieved, however, if the beams are crossed at angle θ,

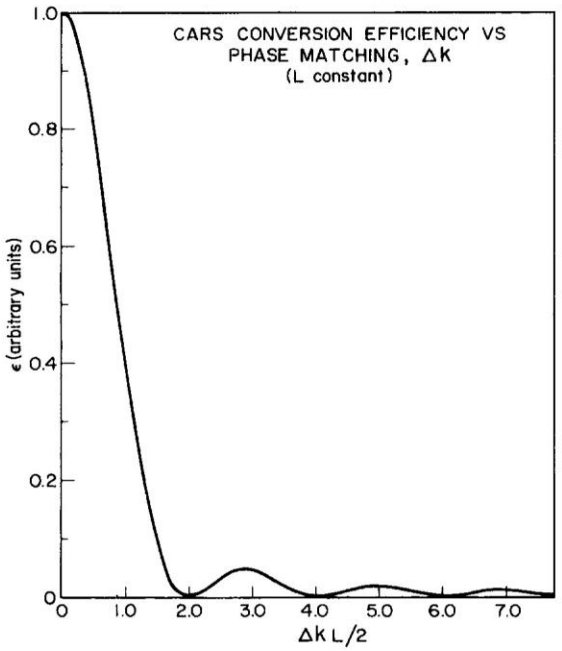

FIG. 1. CARS conversion efficiency vs phase matching (Δk) for constant interaction length.

the phase matching angle. This angle is determined from the geometry illustrated in Fig. 2. Note that when this is done, the CARS beam emerges at a second angle θ', which aids in spatial filtering. Of course, if the beams are crossed, the interaction length is now limited by the beam walk-off. The phase matching angle, θ, is usually quite small ($\sim 1°$ for benzene at 992 cm^{-1}) but increases rapidly with Raman shift or for conditions near electronic absorption as encountered in resonance CARS enhancement.

If the beams are not crossed and $\Delta k \neq 0$, then according to Eq. (5), the CARS signal will vary sinusoidally with path length. The path length to reach maximum conversion efficiency we define as the coherence length, $L = L_c$ which occurs when $\Delta k L_c/2 = \pi/2$ or $\Delta k = \pi/L_c$. In Fig. 3, we show how conversion efficiency varies with path length for collinear beams and various coherence lengths. It should be mentioned that some authors[66, 67] define coherence length as the path length between successive maxima ($L_c = 2\pi/\Delta k$).

We should now consider the question of the effects of focusing on conversion efficiency. In one treatment[48] the focal region is assumed to be a cylinder of plane waves and because of fortuitous cancellation of terms, the resulting expression ($\Delta k = 0$) for the efficiency is independent of focal length:

$$\epsilon = \left(\frac{2}{\lambda_l}\right)^2 \left(\frac{4\pi^2 \omega_{as}}{n_{as} c^2}\right)^2 |3\chi^{(3)}|^2 P_l^2 \qquad (6)$$

In another approach to the problem, one assumes a functional form for the beam area but maintains the plane wave approximation for the field. The beam diameter $d(z)$ can then be expressed in usual gaussian form[68] as:

$$d(z)^2 = d_0^2 \left[1 + \left(\frac{4\lambda z}{\pi d_0^2}\right)^2\right] \qquad (7)$$

where z is the longitudinal distance from the focal point and d_0 is the minimum diameter of the beam waist. For a lens of focal length f and an unfocused beam diameter d and wavelength λ, it can be shown[68] that:

$$d_0 = 4\lambda f/\pi d \qquad (8)$$

The beam diameter described here represents the $1/e$ value of the electric field or $1/e^2$ value of the intensity. If the intensity is considered to be a constant in a beam profile of diameter $d(z)$, an approximate solution to Eq. (4) may be obtained for the conversion efficiency:

$$\epsilon = \frac{P_{as}}{P_s} \approx \left[\frac{2\tan^{-1}\left(\frac{2L\lambda}{\pi d_0^2}\right)}{\lambda n_{as}}\right]^2 \left(\frac{4\pi^2 \omega_{as}}{c^2}\right)^2 |3\chi^{(3)}|^2 P_l^2 \qquad (9)$$

where λ is some average wavelength taken to be λ_l. This relation indicates that 71% of the maximum conversion takes place over length L equal to $2\pi d_0^2/\lambda$. Implicitly

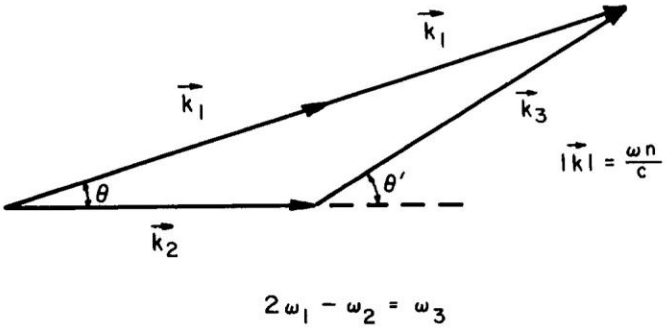

FIG. 2. Wave vector diagram for phase matching ($\Delta k = 0$).

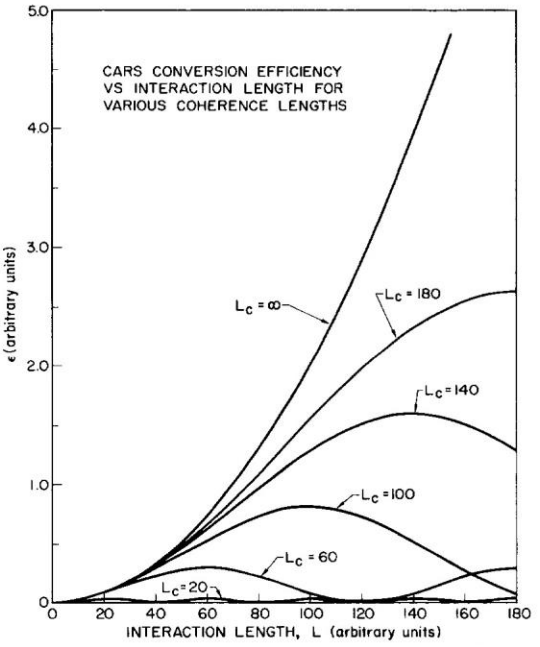

FIG. 3. CARS conversion efficiency as a function of interaction length for various coherence lengths.

assumed in this derivation is the plane wave approximation and a beam at ω_{as} which has the same spatial distribution as that of the beam at ω_l and ω_s. A rigorous derivation of conversion efficiency for focused beams has been carried out by Regnier,[45] Bjorklund,[69–71] and Shaub.[72] In Fig. 4 the functional form of Eq. (9) is compared with a numerical solution obtained by Regnier. Because Regnier's results include an undefined scale factor, an absolute comparison of his calculation with Eq. (9) is not possible. Nonetheless, Fig. 4 shows that both have the same general form and that the same maximum is reached regardless of the focal length (for shorter focal length lens, this maximum is reached in a shorter mixing path, L). The more rigorous calculations [69–72] show significant increase in conversion efficiency for tighter focusing.

B. Magnitude of $\chi^{(3)}$. The effect of an intense field on matter is to polarize it in a nonlinear fashion. The magnitude of the third-order nonlinear coefficient or susceptibility shown in Eq. (1) is a measure of the conversion efficiency of the process $2\omega_l - \omega_s = \omega_{as}$. This conversion of laser power into anti-Stokes radiation takes place in any medium, including noble gases. However, when there is a vibrational resonance present, the conversion efficiency increases rapidly when $\omega_l - \omega_s = \omega_v$. The total susceptibility is then a sum of a frequency-dependent resonant part and a nearly frequency-independent nonresonant part:

$$\chi^{(3)} \equiv \chi = \chi^{\text{res}} + \chi^{\text{NR}} \tag{10}$$

where for simplicity the superscript "3" has been removed, and throughout this text it is assumed that we are concerned with the third-order susceptibility associated with the process $2\omega_l - \omega_s = \omega_{as}$. It is to be emphasized that when χ^{res} is relatively small because there are no nearby resonances or if the number density of resonant materials is very low, then the CARS emission is governed by the nonresonant susceptibility, which usually arises from the solvent or diluent gas. It is the presence of this nonresonant term χ^{NR}, which limits the sensitivity of the technique, because one can record Raman spectra only to an extent that χ^{res} exceeds χ^{NR}. We shall return to this point later when we discuss the limits of sensitivity for the technique. For now, however, we shall show how χ^{res} is related to spectral properties of normal Raman transitions.

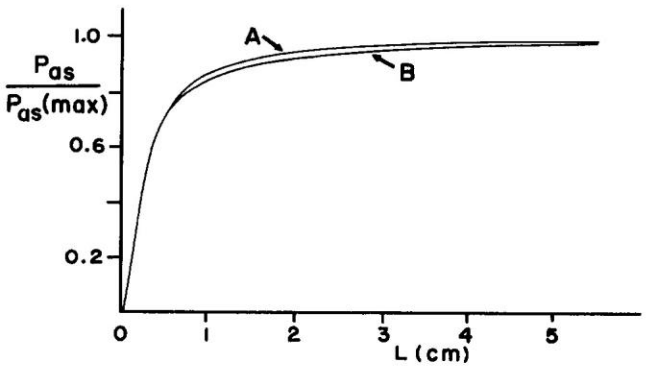

FIG. 4. Effects of focusing laser beams using plane wave approximation. The ratio of power in the CARS beam to maximum conversion is plotted as a function of cell length, L. The upper curve, A, represents computed data of Regnier.[45] The lower curve, B, is calculated from Eq. (9).

Expressions for the resonant part of χ may be derived from classical or quantum mechanical developments. The results allow χ to be expressed in terms of the normal Raman cross section. In addition, the various resonances present in χ are explicitly demonstrated in the quantum mechanical results.

The harmonic oscillator serves as a model for the classical approach. Placzek's development[73] relates the polarizability, α, of a molecule to a bond stretching coordinate, q:

$$\alpha = \alpha_0 + \left(\frac{\partial \alpha}{\partial q}\right)_0 q + \ldots \tag{11}$$

The force produced on the oscillator by a field because of this polarizability is:

$$F = \frac{1}{2}\left(\frac{\partial \alpha}{\partial q}\right)_0 E^2 \tag{12}$$

The equation of motion for the simple damped harmonic oscillator is thus:[63]

$$\ddot{q} + \Gamma \dot{q} + \omega_v^2 q + \frac{1}{2m}\left(\frac{\partial \alpha}{\partial q}\right)_0 E^2 \tag{13}$$

where Γ is a damping constant and ω_v the resonant frequency. With the application of the field $E = E_l + E_s$, where E_i has the form given in Eq. (2), it is seen that q is driven not only at ω_l and ω_s but also at $\omega_l - \omega_s$. The solution of Eq. (13) for $q(\omega_l - \omega_s)$ gives rise to a polarization at the anti-Stokes frequency due to the relation: $P = \chi E = N(\partial\alpha/\partial q)_0\, q(\omega_l - \omega_s)\, E_l$, where N is the molecular number density. A direct comparison of these relations then yields the following expression for the susceptibility:[23]

$$3\chi^{(3)}(\omega_{as}) = \frac{N}{m}\left(\frac{\partial \alpha}{\partial q}\right)_0^2 \frac{\Delta_j}{\omega_v^2 - (\omega_l - \omega_s)^2 - i\Gamma(\omega_l - \omega_s)} \tag{14}$$

where $N\Delta_j$, the difference in population in the lower and upper states for a particular transition j, has been introduced to account for statistical distribution (see Refs. 40, 42, and 74), that is, $\Delta_j = 1$ for low temperature, $\Delta_j = 0$ for infinite temperature. The factor, Δ_j, is an integral part of the quantum mechanical approach by density matrix methods.[59]

Electromagnetic scattering theory gives the differential scattering cross section, $d\sigma/d\Omega$, of a molecule exposed to electromagnetic radiation:[74, 75]

$$\frac{d\sigma}{d\Omega} = (\alpha')^2 \left(\frac{\omega}{c}\right)^4 \tag{15}$$

where, for the Raman Stokes frequency:

$$(\alpha')^2 = \left(\frac{\partial \alpha}{\partial q}\right)^2 < q^2 > \tag{16}$$

This relation ignores contributions to $d\sigma/d\Omega$ from anisotropic scattering, for which a 5 to 10% correction can be included when desired.[75]

The elementary quantum mechanical expression of $< q^2 >$ for a harmonic oscillator is:

$$< q^2 > = \frac{\hbar}{2\, m\, \omega_v} \tag{17}$$

By combining the three previous expressions, we get:

$$\frac{d\sigma}{d\Omega} = \frac{\hbar}{2\, m\, \omega_v} \left(\frac{\partial \alpha}{\partial q}\right)^2 \frac{\omega^4}{c^4} \tag{18}$$

The polarizability derivative in this expression may be substituted into Eq. (14) to obtain $\chi^{(3)}$ in terms of the normal Raman differential cross section:

$$3\,\chi^{(3)} = \frac{2\, N\, c^4}{\hbar\, \omega_s{}^4} \left(\frac{d\sigma}{d\Omega}\right) \frac{\omega_v\, \Delta_j}{\omega_v{}^2 - (\omega_l - \omega_s)^2 - i\, \Gamma\, (\omega_l - \omega_s)} \tag{19}$$

Note that the resonant third-order susceptibility is a complex quantity which can be separated into a real and an imaginary part. These characteristics, the added nonresonant contribution, and the squared dependence of susceptibility on CARS signals produce unusual spectral properties compared with normal, spontaneous Raman effect. These features are discussed further in Section IIB.

If we define $\Delta\omega \equiv \omega_v - (\omega_l - \omega_s)$ and assume that $\Delta\omega/\omega_v \ll 1$, which is usually a very valid approximation in the vicinity of a resonance, then Eq. (19) simplifies to:

$$3\,\chi^{(3)} = A \left[\frac{1}{2\Delta\omega - i\, \Gamma}\right]$$

where

$$A = \frac{2\, N\, c^4}{\hbar\, \omega_s{}^4} \left(\frac{d\sigma}{d\Omega}\right) \Delta_j \tag{20}$$

According to Eqs. (5), (6), and (9), the CARS signal or efficiency is proportional to the square of the modulus of $\chi^{(3)}$ or:

$$|3\,\chi^{(3)}|^2 = \frac{A^2}{4\Delta\omega^2 + \Gamma^2} \tag{21}$$

For the integrated area over the CARS band, Eq. (21) becomes

$$\int |3\,\chi^{(3)}|^2\, d\,(\Delta\omega) = \frac{\pi\, A^2}{2\, \Gamma} \tag{22}$$

While at the peak of the emission ($\Delta\,\omega = 0$), the relation is:

$$|3\,\chi^{(3)}|^2_{\Delta\omega=0} = \frac{A^2}{\Gamma^2} \tag{23}$$

In an alternative approach, one derives an expression for $\chi^{(3)}$ from quantum mechanical considerations. Armstrong *et al.*[58] and Maker and Terhune[9] obtain expressions using a third-order perturbation development. DeWitt *et al.*[59] have derived expressions for the third-order susceptibility by the density matrix method. From all of these developments, it is apparent that there are resonant denominators which show that $\chi^{(3)}$ is enhanced as the anti-Stokes signal or the laser frequency spectrally approaches an electronic resonance. Such an effect is analogous to resonance Raman effect in conventional Raman spectroscopy.[2, 76] From the theory,[59] however, it is also clear that resonance enhancement is very complex and may not be a benefit in every case. In Section IIIC, we refer to a recent experiment where such enhancement has been observed and was of definite advantage.

C. Saturation Effects. The basic relation for conversion efficiency Eqs. (6) and (9) indicates higher conversion into the anti-Stokes component with increasing power. This is true until various saturation effects become important. The derivation of Eq. (9) was based on an assumption that the power at ω_{as} was sufficiently small that it had negligible effect on the beams at ω_l and ω_s and that the power of the beams at ω_l and ω_s was not attenuated in the medium or in the conversion process. This approximation is valid if the power at ω_{as} is less than about 1% of the power of either of the other two beams.

In addition to this limitation, at high-power levels the population of the energy states involved in the CARS process may be altered significantly from equilibrium values. This saturation process has been discussed by Maier *et al.*[74] From the harmonic oscillator model used in obtaining differential Eq. (13), it follows that the presence of two electric fields at frequencies ω_l and ω_s will drive the oscillator at a frequency equal to $\omega_l - \omega_s$. This effect may, in fact, be used to populate upper vibrational levels of homonuclear diatomic molecules and has been used in studies of relaxation times between excited species and admixed gases. If $\omega_l - \omega_s = \omega_v$, the equation describing the time dependence of the population difference, Δ, between the two lowest vibration levels is:

$$\frac{\partial \Delta}{\partial t} = \frac{8\, \lambda^4}{h^2\, c^2\, \Gamma} \left(\frac{d\sigma}{d\Omega}\right) I_l\, I_s\, \Delta + \ldots = -\tau^{-1}\, \Delta \tag{24}$$

where additional terms including relaxation effects have been excluded in the first approximation.

The intensity, I, or power density at the focus of a diffraction-limited gaussian beam can be obtained from Eq. (8):

$$I \approx \frac{\pi\, P}{4\, \lambda^2\, (f/d)^2} \tag{25}$$

where f/d is the ratio of focal length to beam diameter and P is the power of the laser. The power density at the focus will be of the order of 10^{10} W/cm^2 for modest powers (100 kW) and a typical value of 30 for f/d. The value of τ for H_2 gas is then of the order of 10^{-9} s, indicating rapid equilibration of the $v = 0$ and $v = 1$ levels (> 99% after $t = 6\,\tau$). Since the CARS experiment is typically 10 to 15 nsec, τ must be kept as large as possible to avoid saturation effects. To an extent, this can be done by increasing the f/d ratio, although the sample length must be concurrently increased to maintain the same CARS signal (Eq. (9)). At relatively high laser powers ($P_l > 1.0$ MW, $P_s = 0.1$ MW) for H_2 and for spectral laser widths comparable to the H_2 line widths, saturation becomes certain over much of the focal volume. From Eq. (24), one sees that the $v = 0$ number density is halved (in the absence of further resonant pumping from $v = 1$ or rotational relaxation into $v = 0$ or out of $v = 1$). In addition, the appearance of Δ_j in Eqs. (14 and 19) means

that there is a limit to the amount of CARS signal which can be generated in a region of saturation. The surrounding nonsaturated regions of the focal zone thus contribute a greater proportionate share of the total CARS signal than is the case for a low-power, nonsaturated experiment. This means that a more complicated analysis will be required for number density measurements at high laser powers. In particular, care must be taken in interpreting relative intensities in terms of vibrational or rotational temperatures since according to Eq. (24) the saturation level will vary for lines of different χ values, which depend on Raman cross section and line width.

It is important to note that the total magnitude of CARS signal will continue to increase with laser power even under saturation conditions due to the effective increase in sampling volume. Thus, for frequency measurements at low pressures or concentrations, the use of high laser powers is desirable. Some broadening of CARS lines would be expected under saturation conditions. Thus, plots of line widths (as well as CARS power) vs $P_l^2 P_s$ might serve to identify power regions in which saturation effects are occurring.

II. COMPARISON OF CARS WITH NORMAL RAMAN SCATTERING

As was shown in Section IB, CARS is related to the normal Raman cross section and, therefore, all molecular vibrations which are active in normal Raman spectroscopy are CARS active. However, there are several differences between CARS and normal Raman spectroscopy which need to be discussed.

A. Efficiencies. First, it is useful to compare the efficiency of normal Raman scattering with CARS. In principle, this should be a straightforward exercise, but in practice the comparison is difficult since normal Raman scattering is usually performed with cw sources, whereas CARS is better carried out with intense, pulsed sources. However, for simplicity, let us assume that both Raman and CARS experiments use the same laser, i.e., a 5 MW, pulsed (20 ns), Nd:YAG laser operating on the second harmonic (532 nm and 0.03 cm^{-1} line width) at 10 pps. This laser yields an average power of about 1 W or about the same cw laser power used in many normal Raman experiments. If a portion of this laser is used to pump a dye laser and dye laser amplifier, then typical laser powers for CARS experiments might be: 2 MW at 532 nm and ~0.2 MW of dye laser power. A CARS arrangement similar to this is used for studying gases at the Naval Research Laboratory (NRL) (see Section IIIB and Fig. 18). These power levels are probably high enough to saturate the CARS signal in certain gases (see previous section), but for the purposes of this comparison, we shall neglect this effect. Now, combining Eq. (23) for the peak CARS conversion with Eq. (9) for CARS efficiency (with long paths and focused beams), we get for anti-Stokes power:

$$P_{as} = \left(\frac{16\pi\lambda_s^4}{hc\lambda_l\lambda_{as}}\right)^2 \left[\frac{N\Delta_i}{\Gamma}\left(\frac{d\sigma}{d\Omega}\right)\right]^2 P_l^2 P_s \qquad (26)$$

where centimeter-gram-second units are used and Γ is full width at half-maximum in circular measure. For normal Raman emission the power scattered in the laser beam is:

$$P_{\text{Raman}} = NL\Omega\left(\frac{d\sigma}{d\Omega}\right) P_l \qquad (27)$$

where, as before, N is the number density, L is the length of the focal region, Ω is the solid angle collected, and $(d\sigma/d\Omega)$ is the differential Raman cross section. These equations indicate that CARS signals climb rapidly with laser power (cubic dependence on laser power), whereas normal Raman scattering increases linearly with laser power. These equations also indicate that CARS output drops rapidly with number density, an effect which can be counterbalanced with increased laser power to the point of saturation.

We are now prepared to calculate the efficiency of a CARS signal in some typical laboratory cases to be compared with normal Raman scattering using the same laser source. Suppose the gas to be detected is H_2 at 0.1 Torr. Let us also assume that the laser power is typical of the apparatus described earlier (2 MW at 532 nm, 0.2 MW of dye laser power). Normal Raman cross sections and, particularly, line widths are not precisely known; however, we shall assume that for H_2, $\Gamma = 0.03$ cm^{-1} and $d\sigma/d\Omega \approx 2 \times 10^{-30}$ cm^2/sr for Q_{01}.[1] Using Eq. (26) we calculate a CARS, single-pulse output of ~3 kW. If it is assumed that the CARS pulse narrows to ~10 ns, this output corresponds to an average power of $\sim 3 \times 10^{-4}$ W for 10 pps repetition rate. This enormous signal compares with $\sim 2 \times 10^{-8}$ W single pulse, or $\sim 4 \times 10^{-15}$ W average power for normal Raman scattering calculated from Eq. (27), where we have assumed a laser power of 5 MW, scattering into 1 sr and a 1 cm long focal region.

Thus, CARS produces signals in 0.1 Torr of H_2 which are $\sim 10^{11}$ times greater than normal Raman signals. Of course, at high laser powers, saturation effects will reduce the CARS efficiency as determined in Section IC. Inhomogeneities in the laser beams, unoptimized spatial and temporal overlap, etc. will also adversely affect the CARS output. Moreover, other gases with smaller scattering cross sections which are distributed among a complicated set of transitions or with broader line widths will result in lower CARS emission. Nonetheless, under favorable conditions CARS efficiencies close to theoretical have been observed.[18, 34] For low pressure gases (<0.1 Torr), CARS is clearly superior, since normal Raman detection at this low pressure has already begun to fail (4×10^{-15} watts average power is equivalent to $\sim 10^4$ photons/s, not considering spectrometer throughput, detection efficiency, etc.

It should also be pointed out that the CARS emission is calculated for 0.03 cm^{-1} line width, whereas normal Raman scattering is typically detected at 1 to 10 cm^{-1} spectral width. In fact, high resolution Raman spectra (0.03 cm^{-1}) at low pressures of 0.1 Torr are essentially unknown, because the spectrometer throughput decreases markedly for small spectral widths. CARS emission actually improves rapidly as both laser and molecular line widths decrease. Unlike spectrometers, laser line widths can be reduced substantially, often with only modest loss in laser output. Thus, Wallenstein and Hansch[57] have recently produced a N_2 laser-pumped dye

laser with $<10^{-3}$ cm^{-1} width and 50 kW output, which has a power only about half of the broader band (0.3 cm^{-1}) output. Dye laser widths of 0.3 to 0.03 cm^{-1} are already available commercially.

B. Band Shapes, Interferences, and Dependences. We shall now show that coherent anti-Stokes signals develop unique band shapes and interferences which arise from background nonresonant susceptibility and neighboring resonances. It will also be evident that CARS is not only a measure of molecular energy levels but is also a property of the bulk medium (like refractive index).

As shown earlier the total third-order nonlinear susceptibility is a complex quantity, consisting of a real and an imaginary part associated with the resonant susceptibility and an added nonresonant term:

$$\chi^{(3)} = \chi' + i\chi'' + \chi^{NR} \tag{28}$$

The real and the imaginary parts of the resonant susceptibility and their squares are plotted in Fig. 5. With no χ^{NR} contribution, a plot of $|\chi^{(3)}|^2$ or equivalently the CARS signal has a lorentzian line shape similar to a normal Raman resonance. Moreover, it may be stated that the real part of the susceptibility is related to the nonlinear refractive index, and the imaginary part is associated with the normal Raman transition.[63, 78] Thus, outside of the fact that the relative intensities of distant resonances have different dynamic ranges because of the squared dependence on number density and cross section, a single, coherent anti-Stokes resonance reveals no unusual spectral features. However, as soon as a significant amount of nonresonant susceptibility (from the solvent or the resonant material itself) is introduced or when another resonance is situated nearby, the band shapes are appreciably distorted. The reasons for this effect can be seen from the following relation for $|\chi^{(3)}|^2$ which is a measure of CARS signal:

$$\begin{aligned} |\chi^{(3)}|^2 &= (\chi' + \chi^{NR})^2 + (\chi'')^2 \\ &= (\chi')^2 + 2\chi'\chi^{NR} + (\chi^{NR})^2 + (\chi'')^2 \end{aligned} \tag{29}$$

The mixing of nonresonant susceptibility arising from the cross term $\chi'\chi^{NR}$ adds an asymmetric shape to the band contour. In Fig. 6, we plot CARS intensity vs frequency for varying amounts of a resonant material while maintaining a constant background susceptibility. The asymmetry is very apparent even for relatively large resonant contribution. Note also that the frequency of the maximum shifts slightly and a minimum develops as the resonant component decreases. In the limit as the concentration of the resonant species is very small with respect to the nonresonant part, the CARS output takes on the shape of the real part of the susceptibility with the center of the resonance exactly between the maximum and the minimum. This effect comes about because the only appreciable frequency dependent term left in Eq. (29) is the cross term $\chi'\chi^{NR}$. Because of this cross term, the CARS signal (taken to be the maximum) does not follow the N^2 dependence when the resonant contribution to the susceptibility approaches that of the nonresonant part (Fig. 7 and Refs. 6 and 18). However, Moya *et al.* (42) have shown that if the square root of the CARS signal, which is proportional to $|\chi^{(3)}|$ is

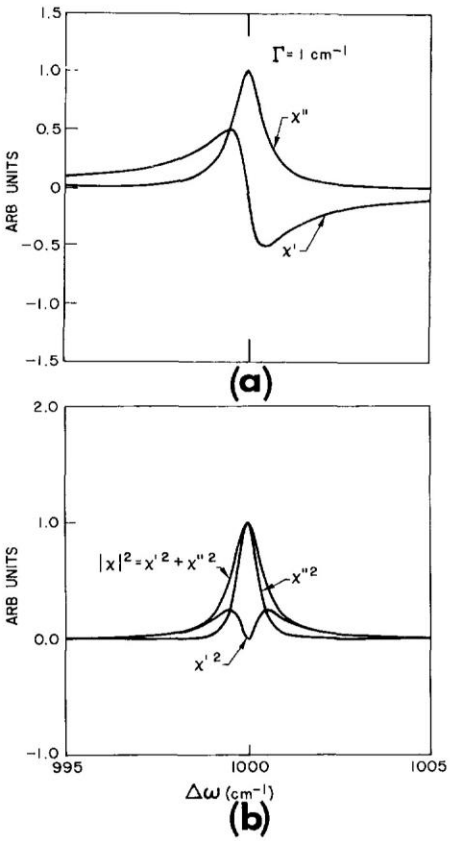

FIG. 5. a. This trace is a plot of the real (χ') and imaginary (χ'') parts of the third-order susceptibility for a resonance centered at 1000 cm^{-1} Raman shift and a line width of 1.0 cm^{-1}. Note the fact that χ' is negative in one-half of the frequency domain. b. The curves plotted here are the squares of the quantities in Fig. 5a. $|\chi|^2$ is directly proportional to the CARS signal. Note that at the center of the resonance the real part of the susceptibility vanishes.

plotted, the difference between the maximum and minimum value of $|\chi^{(3)}|$ varies linearly with number density. This can be best seen if the real and imaginary parts of the susceptibility are plotted as vectors in the complex plane (Fig. 8). In this figure χ' is plotted along the abscissa and χ'' along the ordinate. Note that χ' and χ'' are not independent quantities and describe a circle with diameter equal to A/Γ, as determined from Eq. (20) at $\Delta\omega = 0$. χ^{NR} linearly displaces the circle along the abscissa. The modulus of $\chi^{(3)}$ or $|\chi^{(3)}| = [(\chi')^2 + (\chi'')^2]^{1/2}$ is a vector drawn from the origin to some point on the circle. Note that the difference between the maximum and minimum value of $|\chi^{(3)}|$ or the difference between the length of the vector at its maximum and its minimum value is also equal to the diameter of the circle or A/Γ. Therefore, since A is linearly related to number density, a plot of $[P_{CARS}\ (max)]^{1/2}$ minus $[P_{CARS}\ (min)]^{1/2}$ varies linearly with number density.

Interferences can also occur among neighboring resonances which add a frequency-dependent background to the susceptibility. This mixing allows the two overlapping peaks to be better "resolved" by CARS than by normal Raman spectroscopy. This is because the negative part of one resonance cancels or partially cancels

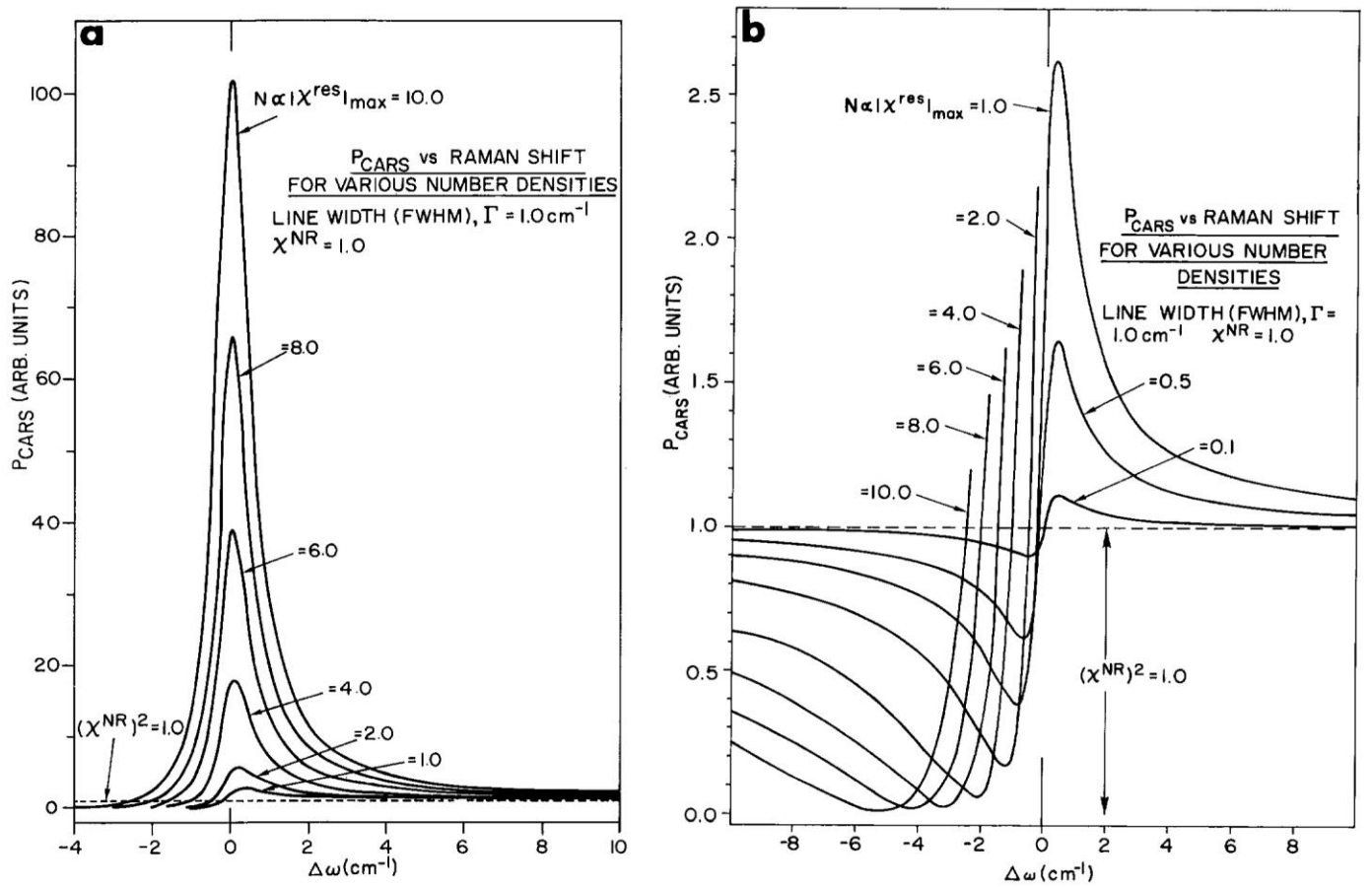

FIG. 6. a. A linear plot of CARS signal intensity vs frequency for a resonance of 1.0 cm^{-1} line width and a background (solvent) susceptibility, χ^{NR}, of 1.0 for a series of concentrations of resonant material. $|\chi^{res}|$, which is proportional to number density of the resonant material, varies from 10.0 to 1.0. Note the asymmetry in the peaks and the frequency shift even when the resonant susceptibility is tenfold longer than the nonresonant susceptibility. b. This figure is an extension of Fig. 6a. The illustration shows the effect of mixing the nonresonant susceptibility with the real part of the resonant susceptibility giving rise to a definite minimum. Note that at low concentrations ($|\chi^{res}| = 0.1$ or where χ^{NR} is 10 times the resonant part) the spectrum takes on the shape of χ' illustrated in Fig. 5a.

the positive part of the other, creating less overlap between adjacent peaks. This point is more clearly demonstrated in Fig. 9 where, as stated before, χ'' is a measure of the normal Raman band shape, while $|\chi^{(3)}|^2$ is proportional to CARS signal, which contains *both* real and imaginary components.

Another unusual feature of CARS is apparent from Fig. 9b, where the overlapping bands are of unequal intensity. By normal Raman effect, the cross sections are in a ratio of 2:1 (lower curve in Fig. 9b). Because of the squared dependence on cross section, the CARS spectrum is expected to have a relative intensity ratio of 4:1. However, the cross terms like those in Eq. (29) cause the intensity ratio to approach that of a normal Raman spectrum. An extreme case of this is found in β-ionone, which is discussed in Section IIIC (Fig. 21). In this case, the band system in the neighborhood of 1600 cm^{-1} is a region of several overlapping components. The CARS spectrum is remarkably like the normal, spontaneous Raman spectrum. If these components were not overlapped, the normal Raman and the CARS spectra would not look alike, with the CARS spectrum favoring the stronger lines and discriminating against the weaker components. It is these properties which make CARS a very unusual kind of spectroscopy. Therefore, as a first approximation, normal Raman spectroscopy is simply a sum of all resonances, i.e.

$$P_{\text{normal Raman}} \propto \Sigma_i \chi_i'' \tag{30}$$

whereas CARS is the square of a sum:

$$P_{\text{CARS}} \propto |\Sigma_i \chi_i^{(3)}|^2 \tag{31}$$

Eq. (31) for CARS signal power creates many cross terms resulting in strong interferences from background and neighboring resonances. These effects often go unnoticed if the CARS emission is plotted vs frequency. However, interferences become very pronounced in a logarithmic plot of P_{CARS} (Fig. 10). In fact, Levenson *et al.*[12, 26–28] had used such distorted plots to accentuate the minimum because the difference in frequency between the maximum and minimum is related to the nonresonant part of the susceptibility. From the combination of Eqs. (10) and (20), this frequency difference is:

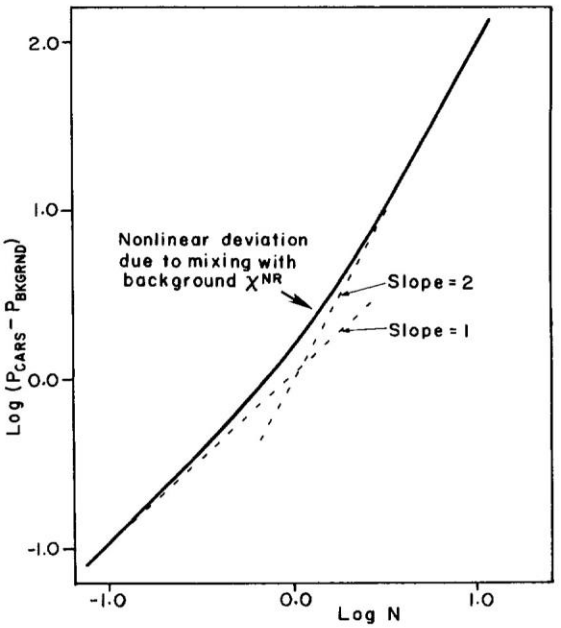

FIG. 7. This is a plot of the log of the resonant CARS signal vs log of concentration or number density for the spectra illustrated in Fig. 6 a and b. Note that at high concentrations the curve has a slope of nearly 2.0 as expected from the N^2 squared dependence in Eq. (26). At low concentrations the curve approaches a linear dependence on number density as indicated from examination of Eq. (29).

$$\Delta\omega_{max} - \Delta\omega_{min} = \frac{\sqrt{A^2 + 4(\chi^{NR})^2\Gamma^2}}{2\chi^{NR}} \qquad (32)$$

where A is defined in Eq. (20). Thus, the nonresonant susceptibility can be computed from the value of $\Delta\omega_{max} - \Delta\omega_{min}$, provided the spontaneous Raman cross sections and line widths are known (see Section IIID). Another example of how a logarithmic plot accentuates the interferences is in the CARS spectrum of H_2 by Moya *et al.* (40). This spectrum is reproduced in Fig. 11. Even though neighboring Q branches are several wavenumbers away, the presence of the neighbors is strongly evident by the deep depressions in the log plot. On a regular linear plot, these perturbations are hardly perceptible; also the lines are much sharper (more like normal Raman spectra).

Although the log plot amplifies the interferences and presents the spectrum in a display that is somewhat unusual to those unfamiliar with the technique, there are some good reasons for doing it. First, the large dynamic range of intensities created by the strong number density and cross section dependences is more easily controlled. Second, there is information in the minima which would be lost in the linear plot. Third, in a log plot the magnitude of the noise is comparable at peak and baseline. Of course, a square root plot has its advantages, as already mentioned. For example, the relative intensities of the CARS bands are more like normal Raman spectra (although line widths are not), and even in the presence of background nonresonant susceptibility, the plot of the square root of CARS intensity (maximum minus minimum) yields a straight line with number density.

C. Reduction of Background Interference. One of the most serious drawbacks of CARS as an analytical tool for trace analysis is the presence of background, nonresonant susceptibility. The sensitivity of the technique is limited by the extent to which the nonresonant signal can be distinguished from the background. Since liquids and solids have relatively broad line widths, concentrations of <1% (depending on the characteristics of both solute and solvent) are near the limit of detection.[6] For gases the lower limit of detection is somewhat better, >10 ppm.[45–48] It should be remembered that the problems we are addressing concern the detection of trace concentrations, not low absolute pressure, for in the absence of a solvent or buffer gas, the detection of low number densities (e.g., <1 mTorr) is quite realizable.[46, 48]

There are a number of schemes designed to either enhance the CARS signal over background or reduce the background susceptibility. One of these schemes was reported recently by Lynch *et al.* (29). The method makes the CARS experiment more complicated in that it introduces a second tunable source, but it offers the hope of markedly reducing background interference. The CARS signal at ω_3 is formed from the other frequencies by the following relation:

$$\omega_3 = \omega_0 + \omega_1 - \omega_2 \qquad (33)$$

Note that the process is identical to normal or single resonance CARS when $\omega_0 = \omega_1$. Now, suppose one wishes to detect a trace amount of gas in air, then $\omega_0 - \omega_2$ is then tuned to a major component in air, say, N_2, such that the negative part of the susceptibility (slightly off resonance, see Fig. 5a) cancels the real portion of background nonresonant susceptibility. At this point $\omega_1 - \omega_2$ (ω_1 variable) is tuned across the resonance in the material at low concentration. By this method, Lynch *et al.* (29) state that at least an order of magnitude in reducing background generation improvement is possible. The reason that improvement in background reduction is not much better than an order of magnitude is due to the fact that resonance arising from the imaginary part of the susceptibility at $\omega_0 - \omega_2$ is substituted for background generation through χ^{NR}.

III. REVIEW OF EXPERIMENTAL RESULTS

A. Experimental Techniques. A variety of experi-

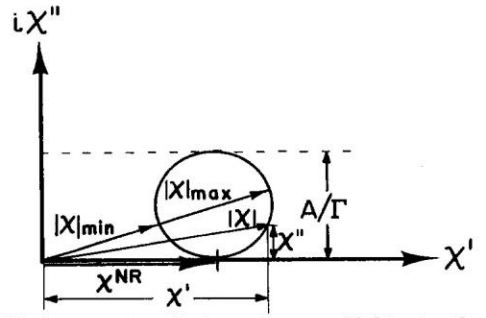

FIG. 8. This is a vector display of susceptibility in the complex plane. A vector drawn from the origin to a point on the circle represents the modulus of the susceptibility. The quantity A is defined in Eq. (20) and is proportional to the normal Raman cross section and number density.

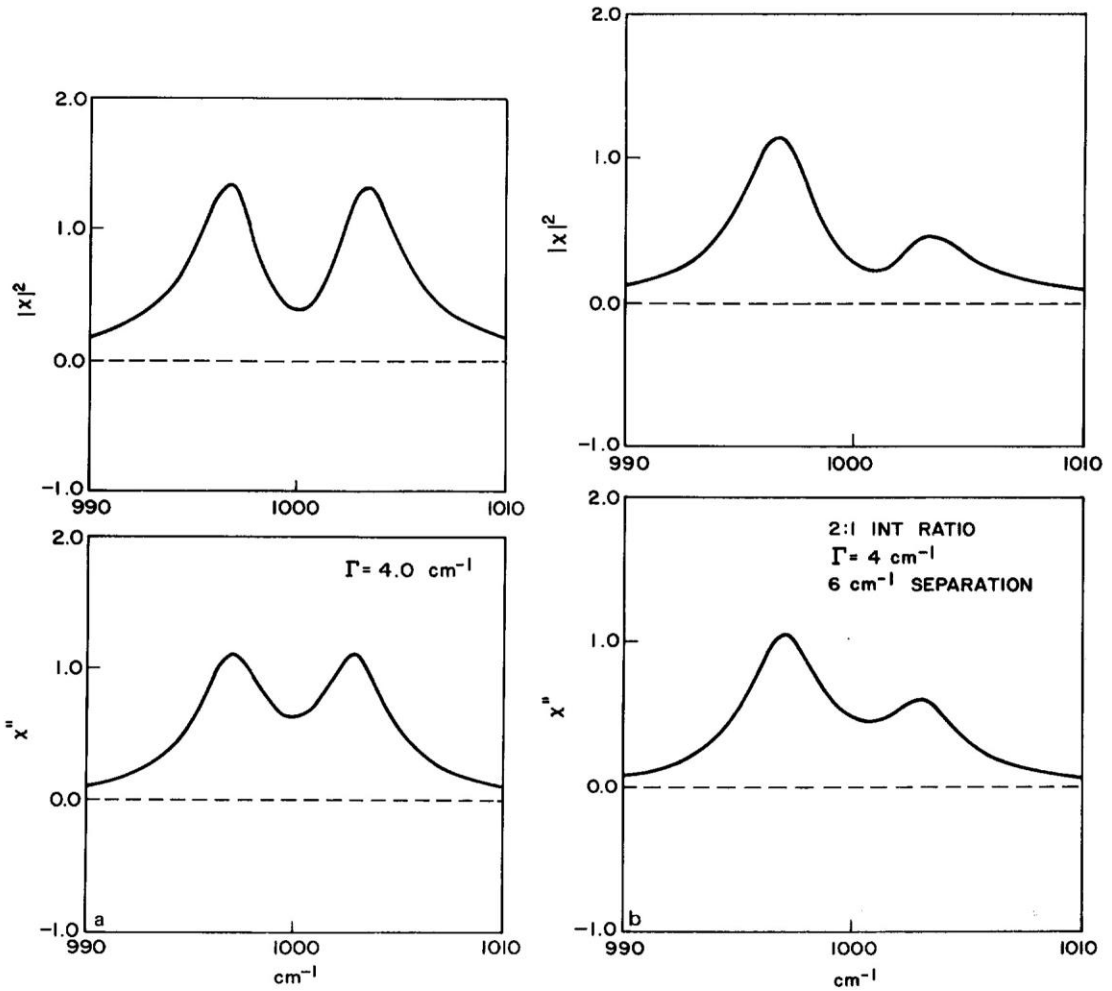

FIG. 9. These synthetically drawn curves illustrate the slightly better "resolving" power inherent in CARS. a. Two overlapping resonances of equal normal Raman cross section, number density, line width (4 cm^{-1}), and separated by 4 cm^{-1} are drawn as they are expected in a normal Raman spectrometer, where the signal is proportional to χ'' compared with the upper curve which represents the expected CARS trace. b. The traces in Fig. 9a are redrawn for an unequal number density or normal Raman cross section (2:1). Note the slight improvement in discerning the two overlapped peaks by CARS brought about by the negative contribution of the real part of the susceptibility not present in normal Raman mechanisms. Note also the fact that cross terms in the CARS process moderate the squared dependence on number density and cross section for strongly overlapped peaks.

mental arrangements have been used to generate coherent anti-Stokes signals. Early experiments[9, 32, 36-39, 44-48] utilized stimulated Raman scattering to create a Stokes beam which could be mixed with the pump laser beam. With the development of the dye laser, the ability to scan continuously the wavelength of one of the beams enabled spectra to be measured.[6, 12-16, 18-22, 26-29, 40-43, 49]

The pioneering work of Maker and Terhune[9, 33] made use of two fixed frequency beams, one from a ruby laser and the second generated by stimulated Raman scattering in benzene giving a Stokes shifted beam. These two beams, separated by 992 cm^{-1}, were useful only for measuring resonant CARS signals from benzene or nonresonant cross sections of other materials. Other liquids were employed to generate stimulated Stokes beams at frequencies appropriate for specific studies. Obviously, however, this was not a very convenient means of recording spectra. The method utilizing stimulated Raman scattering has also been used many times in the study of hydrogen gas.[36-39, 44-48] A diagram of such an experimental setup is shown in Fig. 12. The stimulated Raman generation cell, C, contains hydrogen at 10 to 20 atm. The filter, F, blocks the stimulated anti-Stokes line, leaving the frequencies ω_l and ω_s. The combined beam is split, half being focused into the sample under investigation, the remaining half is focused into a reference called RC. With suitable filters and detectors the frequency ω_{as} due to the sample is detected. Because amplitude fluctuations and spatial inhomogeneities of the ruby laser introduce considerable fluctuation in the magnitude of the CARS signal, the reference cell is used to generate a reference signal at a nonresonant frequency of some reference gas. What is measured rather than the CARS signal, P(CARS), then is the ratio, $R = P(\text{CARS})/P$ (Ref) of the CARS and reference signals. This ratio is approximately independent of the $P_l^2P_s$ (pump and Stokes shifted) intensity fluctuations and reduces effects of filter factors, etc.

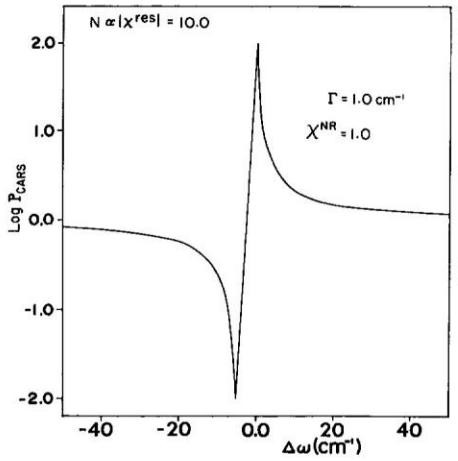

FIG. 10. This curve is a log plot of the curve illustrated in Fig. 6a for $N \alpha |\chi^{(3)}| = 10.0$. Note that this type of plot accentuates the minimum which goes almost unnoticed in the linear plot except where this region is expanded as in Fig. 6b. The difference in frequency between the maximum and minimum is a measure of χ^{NR}.

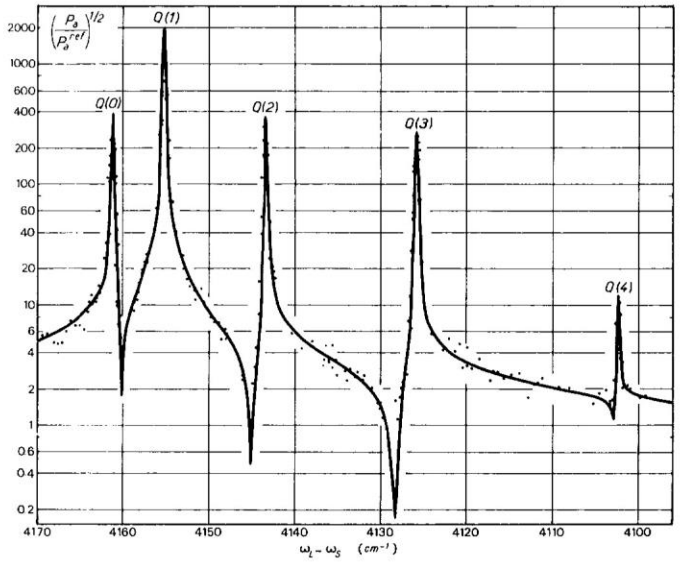

FIG. 11. Spectrum of the susceptibility of pure H_2 at STP; the quantity $(P_a/P_a^{ref})^{1/2}$ is plotted in arbitrary units; the solid line is theoretical, calculated after Eq. (2), assuming $\chi^{NR} = 4 \times 10^{-18}$ esu,[16] $d\sigma/d\Omega = 9.7 \times 10^{-31}$ cm²/sr, $\gamma/2\pi c = 2 \times 10^{-2}$ cm^{-1}, a monochromatic ruby laser, and a gaussian dye laser line of width 0.3 cm^{-1}; this curve has been normalized to give a good fit with the experimental data between the $Q(1)$ and $Q(2)$ lines (taken from Moya *et al.*[40] by permission of the publisher, North-Holland Publishing Company).

An experimental arrangement employing two dye lasers pumped by a single nitrogen laser generates two beams of individually tunable wavelengths at power levels of from 10 to 100 kW in each dye beam. This arrangement, as used by Wynne,[13, 14] Levenson *et al.*,[26-28] Itzkan and Leonard,[25] Begley *et al.*,[6] Chabay *et al.*,[20] and Klauminzer,[22] is illustrated in Fig. 13. The two dye laser beams can be split, forming a double, nonlinear mixing arrangement to generate a reference signal for the purpose of reducing amplitude fluctuations. The introduction of two orthogonal knife edges, which may be translated into the beam, aids in the alignment of the coincident beams. The use of nitrogen laser-pumped dye lasers has both advantages and disadvantages. Among the advantages is the fact that all the components needed can be obtained commercially and will operate perhaps with less attention than current high-power solid state lasers. Also, nitrogen lasers can operate at higher repetition rates which can make experiments easier to perform and allow spectra to be recorded in short periods of time. On the other hand, because of the need for transverse pumping, the spatial quality of the nitrogen laser-pumped dye laser beams is invariably less than ideal. Such dye laser beams, tailored sufficiently to be acceptable for narrow band width

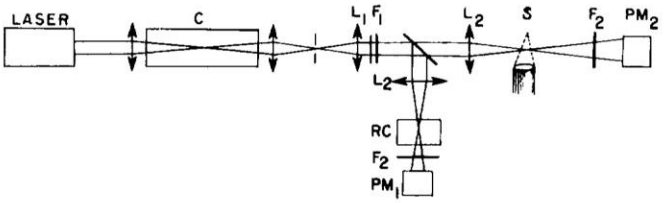

FIG. 12. Experimental arrangement; the ruby laser emits a diffraction-limited signal t-frequency pulse; strong Raman-shifted sidebands are generated in the high-pressure stimulated Raman cell C filled with H_2. Filters F_1 (4-mm-thick Schott OG 590 + 1-cm-thick water cell) cut off the anti-Stokes lines and the second Stokes line, in that order; filters F_2 (interference filter + Schott VG 14 glass) admit the anti-Stokes into photomultipliers PM_1 and PM_2 with S-11 photocathodes. RC is the reference cell; S is the gas sample (here, a flame) (taken from Regnier and Taran[47] with permission of the publisher, American Institute of Physics).

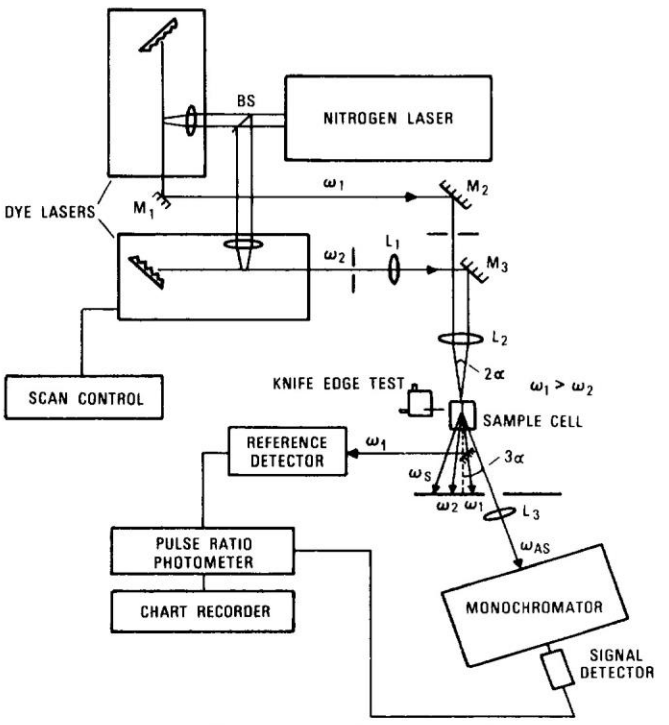

FIG. 13. CARS optical schematic, M_1, M_2, and M_3 are mirrors; L_1, L_2, and L_3 are lenses; BS is a beam splitter which reflects 33% of the light. The focal length of L_1 is 500 to 800 mm, that of L_2 is 200 mm. The crossing angle is 2α (taken from Chabay *et al.*[20] with permission from the publisher, American Institute of Physics).

(0.03 cm^{-1}) and high spatial quality needed for gas phase applications, will have at most <30 kW peak power without an amplifier (it is difficult to increase the nitrogen laser power over 2 MW). Such beams are usable for medium and high-pressure gas phase and condensed phase applications. Moreover, because of the poor beam quality, the nitrogen laser cannot be used as one of the lasers for the nonlinear excitation scheme. Hence, it must pump two lasers.

Another common arrangement utilizes a doubled Nd:YAG laser at 532 nm. Part of the beam is used to pump a dye laser which is then recombined with the 532 nm beam.[6, 18, 19, 21, 43] This configuration has the advantage that only one dye laser is required, and the power of the beam at ω_l may readily be on the order of a few megawatts, leading to higher conversion efficiencies, necessary in the study of gases at reduced pressure. YAG lasers can be used at high repetition rates and are amenable to longitudinally pumping dye lasers. The higher repetition rates and better beam quality available make YAG lasers more attractive compared to ruby. Also, for large Raman shifts, the dye laser for the ruby system must operate in the infrared region making the apparatus more difficult to align.

The type of dye laser utilized for experiments depends on the spectral properties of the sample to be studied and the type of laser available for pumping. In general, spectra in solution and in the solid state have widths on the order of a few cm^{-1} or greater. A Hansch-type dye laser,[79] typically employed with a nitrogen laser pump, a low-power beam expander and grating, readily gives line widths of 0.3 to 1.0 cm^{-1}. An amplifier stage may be added if higher powers are required in the dye beam.[57] The widths of the resonances in diatomic gas molecules, however, are typically on the order of 0.01 to 0.2 cm^{-1}, making a reduction in the width of the dye laser desirable if the true line width is to be observed. In general, dye lasers operating in a high gain configuration cannot be satisfactorily narrowed to less than 0.1 cm^{-1} with a single active tuning element. Several different techniques have been employed which gang multiple tuning elements. All are more or less inconvenient because of the necessity of synchronously tuning them. One technique introduces an etalon into the cavity, requiring synchronous sweeping of grating and etalon.[79] Alternatively, two etalons may be used for the tuning elements in conjunction with passive elements such as dielectric filters.[40] Another alternative is the use of a pressure-tuned dye laser cavity[80] in which the introduction of a gas tunes the grating and air gapped etalon together, simplifying the task of tracking two elements synchronously.

Finally, it should be mentioned that CARS need not be performed with narrow band lasers. If one of the lasers is fixed in frequency and spectrally narrow, the other laser may be broad band. CARS signals will be formed only with the spectral portions of the broad dye laser output that correspond to Raman shifts. However, the resulting CARS lines will need to be separated and analyzed by means of a monochromator. Using an optical multichannel analyzer (OMA), Schreiber *et al.*[49] have pointed out the advantages of this method for making real time measurements of temperature and concentrations on a single laser shot. Such an arrangement is useful for measuring turbulence in combustion systems,[81] in aerodynamic flows, e.g., wind tunnels,[82] and in analyzing the products of flash photolysis, explosions, etc.

B. Detection and Spectra of Gases. In order to obtain CARS spectra of gases, especially at reduced pressure, relatively high powers are required. Except for the notable exception of methane which has been observed using cw lasers, pulsed powers of greater than 1 kW have been used to observe CARS spectra in gases in all cases reported to date.

The first report of the CARS process in gases was by Rado.[44] Utilizing an arrangement similar to that in Fig. 12 with hydrogen gas, he measured the magnitude of the nonresonant susceptibility of a number of gases by measuring nonresonant conversion efficiencies relative to the resonance susceptibility of H_2 of 2.1×10^{-13} cm^3/erg at pressures greater than 10 atm. These data were obtained from electric field induced absorption measurements.[83] These results and those of Ward and New on third-harmonic generation[84] give some idea of the background level created by materials used as buffer gases (see Section IIID and Table I).

DeMartini *et al.*[35-39] have observed that $J = 1$ line of hydrogen gas, again utilizing a ruby laser and stimu-

TABLE I. Nonresonant values of $\chi^{(3)}$ for various substances.

Material	λ_1 (nm)	$\omega_1 - \omega_2$ (cm^{-1})	$\chi^{(3)}$ ($cm^{(3)}$/erg)	Ref.
LiF	694.3	992	0.20×10^{-14}	9
KI	694.3	992	0.25	9
CaF_2	694.3	992	0.35	9
MgO	694.3	992	1.0	9
KCl	694.3	992	1.9	9
NaCl	694.3	992	1.7	9
KBr	694.3	992	3.0	9
Fused SiO_2	694.3	992	0.7	9
$C_6H_5CH_3$	694.3	992	4	9
C_6H_5Br	694.3	992	6	9
LiF	496.3	1100	0.34 ± 0.06	26
CaF_2	496.3	1100	0.55 ± 0.06	26
Fused SiO_2	496.3	1100	0.70 ± 0.12	26
Sapphire	496.3	1100	1.14 ± 0.15	26
YAG	496.3	1100	2.18 ± 0.15	26
C_6H_6	555	~1000	1.75 ± 0.15	27
C_6H_5Cl	555	~1000	3.0 ± 1.0	27
$C_6H_5NO_2$	555	~1000	4.0 ± 2.0	27
CS_2	555	~1000	8.7 ± 0.8	27
CCl_4	555	~1000	1.1 ± 0.1	27
C_6H_6	545	···	1.84 ± 0.15	28
Diamond	545	···	4.60 ± 0.6	28
CaF_2	545	···	0.43 ± 0.16	38
SrF_2	545	···	0.44 ± 0.13	28
CdF_2	545	···	1.45 ± 0.32	28
BaF_2	545	···	0.83 ± 0.16	28
He (1 atm)	694.3	4153	0.087×10^{-18}	44
Ar (1 atm)	694.3	4153	1.55	44
D_2 (1 atm)	694.3	4153	1.30	44
N_2 (1 atm)	694.3	4153	1.35	44
O_2 (1 atm)	694.3	4153	1.30	44
CO (1 atm)	694.3	4153	1.80	44
NO (1 atm)	694.3	4153	4.20	44
CH_4 (1 atm)	694.3	4153	2.95	44
SiF_4 (1 atm)	694.3	4153	2.25	44
C_2H_6 (1 atm)	694.3	4153	6.2	44
SF_6 (1 atm)	694.3	4153	2.50	44
CO_2 (1 atm)	694.3	4153	2.00	44

lated Raman scattering to generate the Stokes-shifted beam at ω_s. The frequency ω_s was varied by changing the pressure of the H_2 gas in the stimulated Stokes cell used to generate ω_s in order to make measurements of the line shape.

In a series of experiments, Regnier, Moya, Druet, Pealat, and Taran[40–42, 45–48] have demonstrated some of the analytical and diagnostic capabilities of the CARS technique. With the use of stimulated Raman scattering in H_2 with a ruby laser (Fig. 12), the CARS signal as a function of hydrogen concentration was obtained (Fig. 14). As this figure illustrates, hydrogen gas in nitrogen (1 atm) may be detected by this method down to levels of 10 to 100 ppm. The limitation at the lower levels of hydrogen concentration is due to the contribution from the nonresonant susceptibility of bulk gas (N_2). With their apparatus, these authors were able to obtain a profile of the concentration of H_2 gas in a Bunsen burner flame (Fig. 15).

Utilizing a ruby-pumped dye laser narrowed with etalons (Fig. 16), Moya *et al.*[40] have measured the spectrum of H_2 gas, presented in Fig. 10. By measuring the relative intensities of several rotational lines, temperatures in a flame were measured to within ±30°K. With this same apparatus, recent efforts[41, 42] have produced the CARS spectra of N_2 and O_2 gas (Fig. 17). They also report temperature and concentration profiles of CO, O_2 and N_2 in a spherical flame burner.[42]

Other experiments with gases include the observation of methane using two cw lasers by Barrett and Begley.[34] With photon counting equipment, ~9000 photons per s were detected for CH_4 at STP as the difference frequency was swept over the Q branch of the ν_1 symmetri-

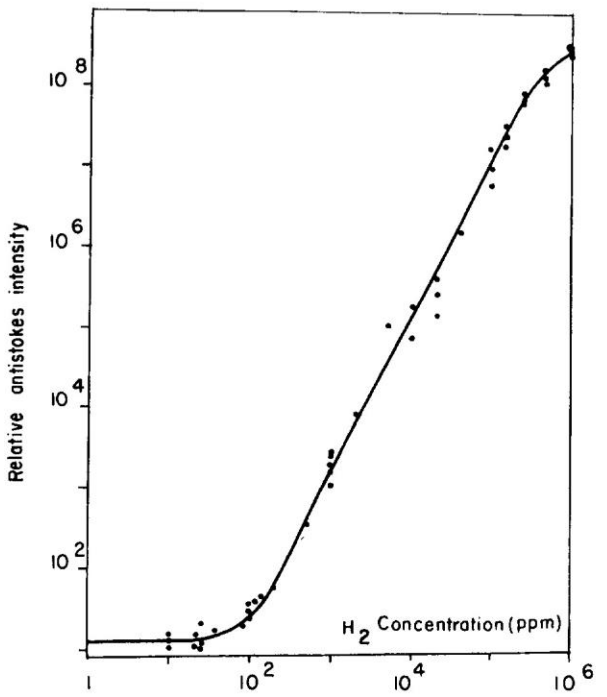

FIG. 14. Normalized anti-Stokes signal vs H_2 concentration in N_2 (taken from Regnier and Taran[47] with permission from the publisher, American Institute of Physics).

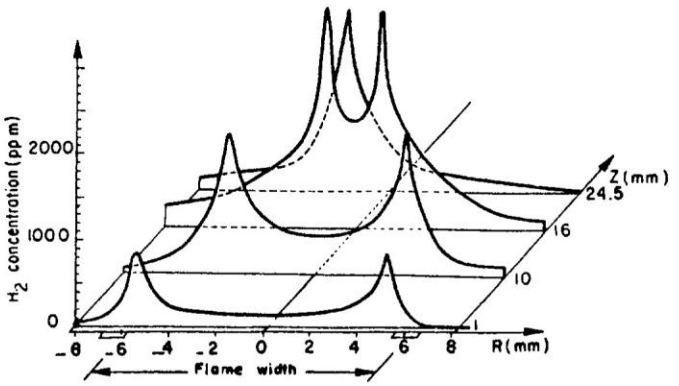

FIG. 15. H_2 distribution in a horizontal natural gas flame. R is the distance from the burner axis; Z is the distance along the axis; coordinate R is vertical, pointing downward. (These data were taken from Regnier and Taran[47] with permission from the publisher, American Institute of Physics.)

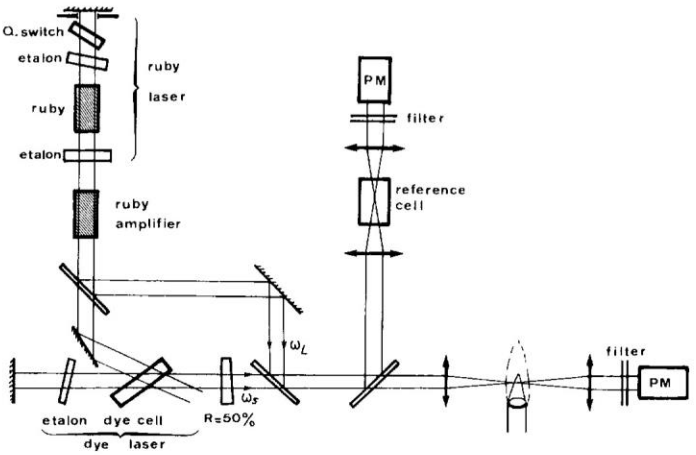

FIG. 16. Experimental arrangement of the CARS apparatus used by Moya *et al.*[40] to record the spectrum of H_2 displayed in Fig. 11 (by permission of the publisher, North-Holland Publishing Co.).

cal stretching resonance. For practical purposes cw laser experiments in gases will probably be limited to the high-pressure regime and to strong Raman scatterers, since the power levels are so low.

The apparatus for conducting CARS experiments in gases at NRL is described in Fig. 18. Several dye laser configurations have been tried, but it is too early to make recommendations. However, the simplest method utilizes a grating (tuned by a Burleigh PZT Inchworm, PZ-501) and telescope. This configuration yields a dye laser line width of about 0.3 cm^{-1}. The Inchworm has the capability of tuning the dye laser over a few hundred wave numbers in a large, dynamic range of scanning speeds. With this apparatus we are able to record spectra over the entire range of dye laser output in just a few minutes (the scanning speed being limited by the 10 pps pulse rate of the YAG laser). Instantaneous spectra based on a single shot can be achieved by using a broad band dye laser, monochromator and OMA.[49]

As pointed out earlier, the CARS method not only produces much larger Raman signals which are generated in the form of a collimated beam, but also the

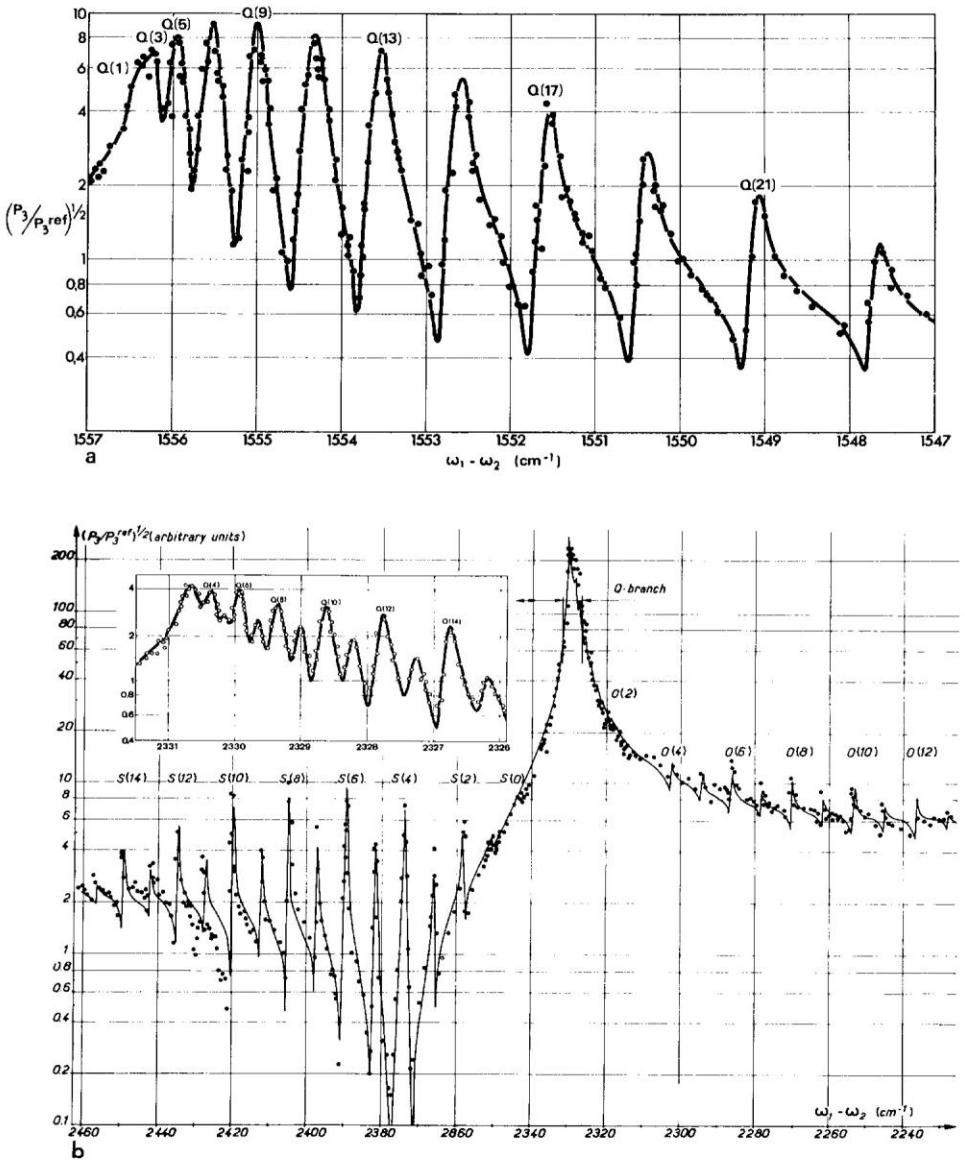

FIG. 17. a. The high resolution (0.15 cm^{-1}) CARS spectrum of O_2 (taken from Moya *et al.*[42] by permission of the publisher, American Institute of Aeronautics and Astronautics). b. Spectrum of atmospheric N_2. The main curve is a best fit to the experimental data and was obtained with a 0.8 cm^{-1} dye laser line width. The inset plot is the main Q-branch taken with higher resolution; the solid curve is theoretical, based on 300°K Boltzman equilibrium, with experimental line widths given by Fletcher (private communication) and assuming a gaussian 0.16 cm^{-1} dye laser line. From two to four shots were averaged for each data point. (This figure was taken from Moya *et al.*[42] by permission of the publisher, American Institute of Aeronautics and Astronautics).

technique strongly discriminates against laser fluorescence and other spontaneous luminescence. For example,[43] we have focused the laser beams at the center of an electrical discharge through 43 Torr of D_2. The resulting spectral scan of the CARS emission appears in Fig. 19. The separate manifolds of Q branches arising from ground and excited ($v = 1$) state D_2 are clearly detected even without the benefit of ratioing out the noise created by the jitter in the laser amplitude. The relative intensity of the Q branches in $v = 0$ compared with those in $v = 1$ yields a vibrational temperature of about 1050°K within the discharge region. The relative intensity of Q branches within each manifold is a measure of the rotational (translational) temperature which appears to be near ambient (~400°K). This disparity in temperatures of gases in discharges is well known and is a result of preferential electron pumping of the vibrational levels and relatively slow vibrational relaxation. In N_2 it is the basis for energy storage in the CO_2 laser.

In Fig. 20 we show the CARS spectrum of CH_4. The very strong Q branch is that of ν_1, the totally symmetric stretching vibration. The other lines are associated with ν_3, the triply degenerate stretching vibration. At 1 atm pressure, the CARS emission from CH_4 is strong enough

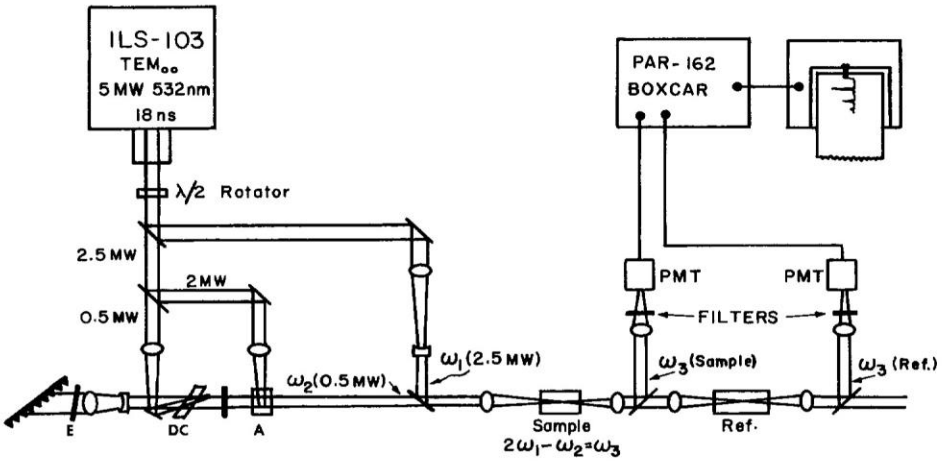

FIG. 18. Apparatus used at NRL to record CARS spectra of gases. The YAG laser has a line width of 0.03 cm^{-1} and a repetition rate of 10 pps. The dye laser with grating and telescope has a line width of ~0.3 cm^{-1}. With an added etalon the width narrows to ~0.03 cm^{-1}. High power from the dye laser is achieved with the amplifier, pumped by 2 MW of 532 nm.

to project around the laboratory as a low-power laser beam, readily visible as scattered reflection off a white card.

C. Results in Condensed Phase. With CARS Raman spectra may be obtained from optically transparent liquids and solids. The results of studies in the solid state yield information on phonons, magnons, and electron excitations. These studies are mentioned only briefly in this review. The results in liquids are considered in more detail. It is in this medium that electronic resonance enhancement in CARS has been recently demonstrated.[20]

Maker and Terhune in their original investigation[9] measured the nonresonant susceptibility of a number of solid materials by measuring the conversion efficiency to CARS photons. A measure of the nonresonant susceptibility may also be obtained by interpreting the shape of a molecular resonance of known magnitude in the presence of the unknown nonresonant susceptibility as mentioned in Section IIB. Levenson *et al.*[12] utilized this method to determine the electronic susceptibility in diamond. In this sample they observed an optical phonon resonance at 1332 cm^{-1} in which the relative number of CARS photons fluctuate by 5 orders of magnitude over the width of the resonance. In addition to diamond, the nonresonant contribution of a number of solids and organic liquids have been measured[26-28] by these methods (Table I).

When the electric fields from ω_l and ω_s are not parallel, additional effects may be observed in the conversion to ω_{as}. In general, the nonlinear polarizability may be written[28] with the third-order susceptibility as a tensor of rank 4:

$$P_i = \sum_{j,k,l} \chi^{(3)}_{ijkl} E_j E_k E_l \qquad (34)$$

where i, j, k, and l may be x, y, or z. The value of $\chi^{(3)}$ utilized throughout this review is $\chi^{(3)}_{1111}$. In a medium of isotropic symmetry, only two independent constants are permissible: $\chi^{(3)}_{1111}$, $\chi^{(3)}_{1122}$, and $\chi^{(3)}_{1221}$ with the constraint:

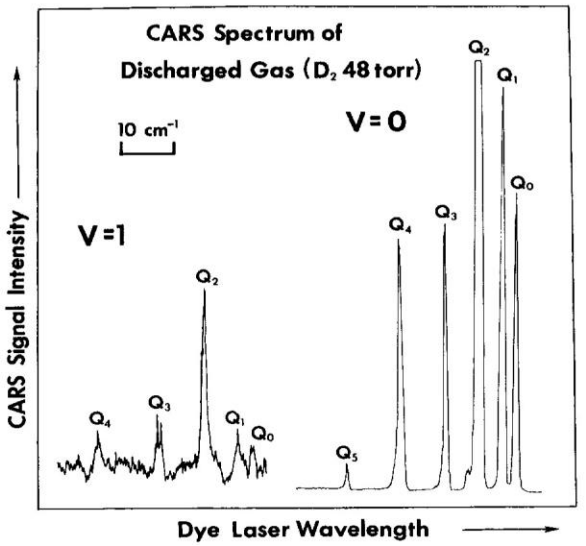

FIG. 19. The CARS spectrum of D_2 in an electrical discharge taken with the apparatus described in Fig. 18 with no etalon in the dye laser and no reference cell. The vibrational temperature calculated from these spectra is ~1050°K, while the rotational temperature is ~400°K.

$$2\chi^{(3)}_{1122} = \chi^{(3)}_{1111} - \chi^{(3)}_{1221} \qquad (35)$$

Levenson and Bloembergen[28] has investigated the effects of different polarization directions for ω_l, ω_s, and ω_{as}, with resulting estimates for the various values of $\chi^{(3)}_{ijkl}$ above.

Wynne[14] has observed resonances in lithium niobate between 50 cm^{-1} and 700 cm^{-1} using two dye lasers. Kramer *et al.* (11) and Lynch *et al.*[29] observed CARS in CuCl. Landau level excitations have been studied in the conduction band of InSb.[13, 16] Coffinet and DeMartini[10] have investigated gallium phosphide. Using two synchronized CO_2 lasers, Yablonovitch *et al.*[15] observed and measured anisotropic interference in beams generated by $\chi^{(2)}$ and $\chi^{(3)}$ processes in GaAs. Levenson and Bloem-

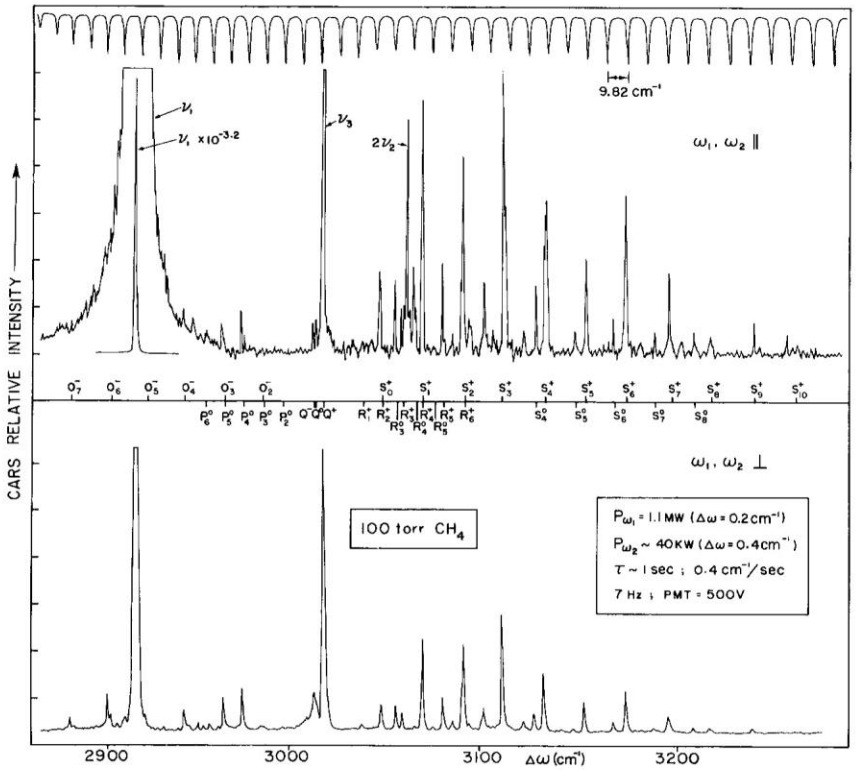

FIG. 20. A CARS spectrum of methane near 3000 cm^{-1}. The upper trace is recorded with parallel polarized laser beams, the lower with perpendicularly polarized beams. Notice the sharp reduction in signal intensity for the strongly polarized bands ν_1 and $2\nu_2$. As a means of identification an incomplete assignment based on literature information is provided at the center of the figure. At the top of the figure is a trace of Fabry-Perot fringes of the dye laser output. This trace serves as both an accurate relative frequency marker and an indicator of dye laser amplitude.

bergen[28] describe CARS measurements in calcite, SrF_2, CdF_2, and BaF_2.

As was described earlier, CARS resonances in various compounds were observed as early as 1965 by Maker and Terhune.[9, 33] Using tunable sources, Begley *et al.*[6, 18] reported a CARS resonance in benzene. With 1 kW of pump beam at $\omega_l = 532$ nm, a conversion efficiency of 1.2×10^{-3} was observed, within experimental error of 2.0×10^{-3} calculated with the bulk susceptibility value for benzene of 1.2×10^{-12} cm^3/erg at resonance. With the use of a 50 kW beam at ω_l, the efficiency increased to 1%.[6] The expected square law dependence between signal intensity and sample concentration was observed at high concentrations, and in dilute solutions first-order dependence was observed (Fig. 7). First-order dependence is expected when the nonresonant contribution from the solvent is significantly greater than that for the solute.

In addition to the observation of the benzene resonance, the advantage of using CARS when measuring Raman spectra for fluorescent samples was demonstrated. The spectrum of β-ionone, a strong fluorescer, was obtained in the 1600 cm^{-1} region.[6, 19] This spectrum and a comparison taken with a conventional Raman spectrometer are shown in Fig. 21. The coherent beam output of CARS affords a high degree of spatial discrimination against luminescence from a sample.

The spectrum of water was recorded by Itzkan and Leonard[25] between 2000 and 4000 cm^{-1} utilizing two nitrogen laser-pumped dye lasers. They point out the difficulty of the water background signal in discerning the resonance of a solute species.

A significant advance in obtaining spectra in solution has been reported by Chabay *et al.*[20, 24] in which they demonstrate the importance of resonance enhancement. If the value of ω_l is close to the angular frequency of an electronic resonance, the value of $\chi^{(3)}$ increases considerably. Resonance enhancement may be important as it increases the magnitude of the resonance due to a solute species relative to the background signal from the solvent. This was demonstrated with a 0.001 *M* solution of diphenyloctatetraene in benzene. The instrument used for this purpose consisted of two Molectron dye lasers with ω_l at 480.2 nm. The resulting spectrum, obtained with an integration time constant of 1 s, is shown in Fig. 22. The corresponding spectrum obtained by conventional Raman methods with a 3s integration time constant is shown in the same figure for comparison. In addition to the CARS signal observed at $\omega_1 + \Delta$ ($\Delta = \omega_1 - \omega_2$), other coherent beams generated by the process at frequencies $\omega_1 + 2\Delta$, $\omega_2 - \Delta$, and $\omega_2 - 2\Delta$ were observed. These "higher-order Raman spectral excitation studies" indicate that the additional beams at $\omega_1 + 2\Delta$ and $\omega_2 - 2\Delta$ are a consequence of the $\omega_1 + \Delta$ and $\omega_2 - \Delta$ beams interacting with ω_1 and ω_2.

D. Experimental Determination of Third-Order Sus-

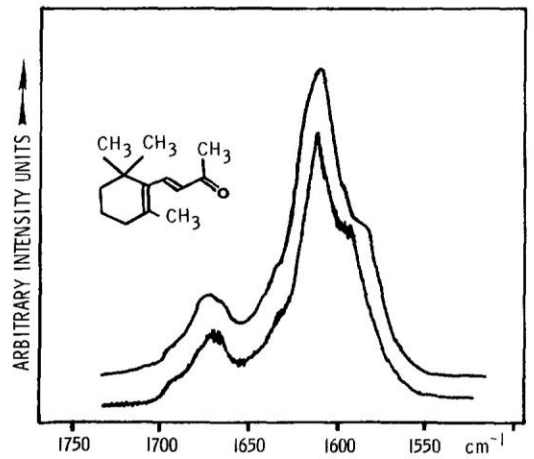

FIG. 21. Raman spectrum of β-ionone in the 1600 cm^{-1} region. The upper curve is the anti-Stokes spectrum, taken with ~1 mW average power in each beam; the lower spectrum is taken on a commercial Raman instrument using a double monochromator and 647 nm excitation (200 mW average power). The upper curve was traced at twice the rate of the lower. With the possible exception of an additional component discernible in the anti-Stokes spectrum near 1600 cm^{-1}, the two traces look remarkably alike. (This figure was taken from Begley *et al.*[19] with permission of the publisher, American Institute of Physics.)

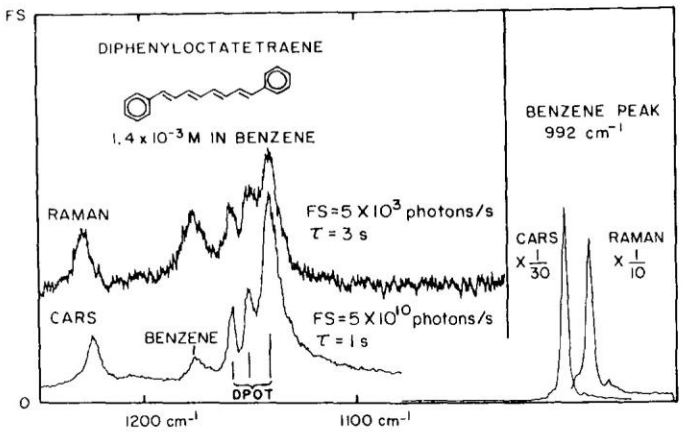

FIG. 22. CARS and Raman spectra of diphenyloctatetraene in benzene. The Raman spectrum is on a wavenumber scale; the CARS spectrum is on wavelength scale. The spectra are aligned at the 1140 cm^{-1} peak of diphenyloctatetraene. A 1 cm^{-1} bandwidth applies to the Raman spectrum and 0.3 cm^{-1} to the CARS. For CARS, ω_1 was 480.2 nm, as compared to 488.0 nm for the Raman. Nonresonant susceptibility, rather than fluorescence as for Raman, is the primary source of background signal for CARS. *FS* denotes full scale which for the Raman signal was 500 counts per s with a 10% quantum efficiency; for CARS it was 3 V from a photodiode. (This figure was taken from Chabay *et al.*[20] with permission of the publisher, American Institute of Physics.)

ceptibilities. For a number of years, physicists[61, 62, 65, 66] have been concerned with measuring third-order susceptibilities. As already described, this nonlinear coefficient gives rise to the CARS effect. The resonant part, χ^{res}, is responsible for the intensity of the vibrational (CARS) spectrum, while the nonresonant part sets a limit on the level of detection. Therefore, a list of accurate resonant and nonresonant susceptibilities would be very useful. Unfortunately, reliable data are rather difficult to acquire, since they depend on the knowledge of normal Raman cross sections, line widths, etc. (see Section IIB). In some cases, very accurate intensity measurements with well characterized laser beams must be carried out. Nonetheless, we have attempted to tabulate a list of nonresonant susceptibilities of various materials so that a best choice of solvent or buffer gas can be made in cases where background generation limits detection (Table I).

Because of the serious problems associated with untested theoretical models, uncertainties in normal Raman cross section measurements, and, especially, the lack of data on line widths, we have not listed a table of resonant susceptibilities. Instead, we have endeavored to tabulate a series of normal Raman cross sections of a few selected gases together with their Raman shifts (Table II). Further data on normal Raman cross sections may be found elsewhere.[75, 85, 86]

It is indeed very unfortunate that information on these nonlinear susceptibilities is so inadequate. However, in a very recent report,[87] a new method of determining these coefficients by a nonlinear interferometric technique offers the hope of making very accurate determinations of both resonant and nonresonant susceptibilities.

E. Selection Rules and Depolarization Ratios. Because of the nonlinear behavior of the CARS technique involving four photons, it has been suggested[88] that CARS has slightly relaxed selection rules from normal Raman spectroscopy. However, it appears that this conclusion is not correct.[89] On the other hand, there may be important information in the fact that one has greater flexibility in making polarization measurements with four photons.[88] Thus, one may be able to distinguish between some or all of the nontotally symmetric Raman transitions if one can make accurate measurements of various combinations of depolarization ratios.

F. Summary and Future Applications and Research. In the previous sections we have outlined the basis for the theory behind coherent anti-Stokes Raman spectroscopy and have shown the unusual features of the resulting spectra which are clearly unique as compared with conventional spectroscopy. CARS spectra really involve measurements of both bulk and molecular (microscopic) properties. The intensities one

TABLE II. Vibrational frequencies of some gases, with corresponding Raman scattering cross sections measured at 514.5 nm (Ref. 48) based on $\sigma_{N_2} = (4.4 \pm 1.7) \times 10^{-31}$ cm^2/sr.

Gas	ω_γ (cm^{-1})	$\sigma_{gas}/\sigma_{N_2}$
O_3	1103	4.0
CH_4	2914	8.0
	3020	0.79
NO	1877	0.55
H_2	4160	2.2
O_2	1556	1.2
N_2	2330	1.0
CO	2143	1.2
CO_2	1388	1.5
	1286	1.0
N_2O	1287	2.7
	2223	0.53

TABLE III.

Advantages of CARS

1. High Raman conversion efficiencies (as much as 1% or $>10^5$ greater than normal Raman conversion) are readily obtained.
2. Collection efficiencies are excellent because CARS is generated in a laser-like beam.
3. Monochromator is not necessary and spectral width determined by the laser line width.
4. Moderately high resolution (~ 0.03 cm^{-1}) is routine by CARS because lasers of such line widths are readily attainable (commercially). Very high resolution ($<10^{-3}$ cm^{-1}) at modestly high powers (50 kW) is feasible with lasers already devised.[57]
5. Laser-induced fluorescence and spontaneous emission from flames, plasmas, discharges, etc. are usually not interferences by CARS because of the coherency and spectral properties of the phenomenon.
6. Sensitivity for gases at low pressures (calculated to be $\sim 10^{-10}$ atm for very high-powered lasers[48]) is high.
7. Because of the higher conversion efficiencies and the need to use pulsed sources, new and interesting experiments in photochemistry, kinetics and molecular relaxation, and fluid dynamics seem possible.
8. Since CARS is a process involving four waves, there appears to be more information potentially available in measuring polarization ratios. Hence, it may be possible to make better assignments of normal modes to their correct irreducible representations.

Disadvantages of CARS

1. One of the most serious problems with CARS as an analytical tool appears to be the generation of background radiation due to the nonresonant part of the susceptibility which limits, at present, detection $\sim 1\%$ for aqueous solution and about 10 ppm in gases. Lynch *et al.*[29] have already been successful in reducing some of the background susceptibility in their experiments. Further research in this area is badly needed.
2. The method is probably not useful for media with large losses, e.g., opaque, strongly absorbing or (Mie) scattering materials.
3. Equipment costs are high, and no completed packaged commercial units are available.
4. Tunability over the entire vibrational region and the observation of small Raman shifts are not routine operations.
5. There is always the possibility of sample damage with high-power lasers.
6. There are strong dependences of CARS signal or laser power, number density, and line width.
7. Interactions with neighboring resonances, background and electronic transitions may cause strong perturbation of the CARS spectrum.

achieves with this method, however, can be truly astounding compared with normal Raman spectroscopy. For high-pressure gases (~ 1 atm) with narrow lines and for some liquids, the efficiencies are very high ($\sim 1\%$) with watts to kilowatts of peak power in the form of a coherent laser-like beam in the anti-Stokes region. These properties clearly make the method ideally suited for recording Raman spectra of fluorescent samples (as are often encountered with biological samples and natural products) and in situations where background luminescence is a problem (photochemistry, plasmas, discharges, etc.). High-resolution spectroscopy is another area where CARS is clearly advantageous. These points and other advantages are listed in Table III. Also listed in the table are the disadvantages of CARS. One of the most serious problems with CARS is background generation via the nonresonant susceptibility. The background is, in some respects, similar to fluorescence in normal Raman spectroscopy and at present limits the sensitivity.

Fertile and extremely useful areas of research in CARS will surely include means for reducing or eliminating background susceptibility, investigation into the use of depolarization measurements, effects of pressure and neighboring resonances on band shapes, studies in electronic resonance enhancement, problems associated with saturation and the effects of turbulence and Mie scattering, etc. on CARS efficiencies. With regard to future applications, CARS has already been shown to be useful in profiling temperatures and number densities in flames.[40-42] Such studies will certainly increase as the demand for new diagnostic tools for combustion applications increases.[90-92] Other areas of research for which CARS has applications are in laser diagnostics,[93] analysis of discharges,[43] plasmas, and atmospheric chemistry. The method is already finding utility in obtaining spectra on biological samples.[6, 20] Future research into the use of CARS for studying surfaces, fluctuation phenomena, reaction dynamics, photochemistry, kinetics, relaxation, and energy transfer is just a partial list. CARS will clearly be a valuable method for making measurements in a wide variety of chemical, physical, and engineering applications.

1. A. Anderson, Ed., *The Raman Effect*, (Dekker, New York, 1971), Vols. 1 and 2.
2. W. Kiefer and H. J. Bernstein, Mol. Phys. **23**, 31 (1972).
3. E. S. Yeung, J. Mol. Spectrosc. **53**, 379 (1974).
4. J. F. Verdieck, S. H. Peterson, C. M. Savage, and P. D. Maker, Chem. Phys. Lett. **7**, 219 (1970).
5. D. Herman, R. W. Hellwarth, M. D. Levenson, and G. Martin, Phys. Rev. Lett. **36**, 1, 189 (1976).
6. R. F. Begley, A. B. Harvey, R. L. Byer, and B. S. Hudson, Am. Lab. **6**, 11 (1974).
7. A. B. Harvey, J. R. McDonald, and W. M. Tolles, "Analytical applications of a new spectroscopic tool: coherent anti-Stokes Raman spectroscopy (CARS)," in *Progress in Analytical Chemistry* (Plenum, New York, 1976), Vol. 8, p. 211.
8. R. W. Terhune, Bull. Am. Phys. Soc. **8**, 359 (1963).
9. P. D. Maker and R. W. Terhune, Phys. Rev. **137**, A801 (1965).
10. J. P. Coffinet and F. DeMartini, Phys. Rev. Lett. **22**, 60 (1969).
11. S. D. Kramer, F. G. Parsons, and N. Bloembergen, Phys. Rev. **9**, B1853 (1974).

12. M. D. Levenson, C. Flytzanis, and N. Bloembergen, Phys. Rev. 6, B3962 (1972).
13. J. J. Wynne, IEEE J. Quantum El. 8, 607 (1972).
14. J. J. Wynne, Phys. Rev. Lett. 29, 650 (1972).
15. E. Yablonovitch, C. Flytzanis, and N. Bloembergen, Phys. Rev. Lett. 29, 865 (1972).
16. E. Yablonovitch, N. Bloembergen, and J. J. Wynne, Phys. Rev. 3, B2060 (1971).
17. S. A. Akhmanov and N. I. Koroteev, Sov. Phys. Jetp. 40, 650 (1975).
18. R. F. Begley, A. B. Harvey, and R. L. Byer, Appl. Phys. Lett. 25, 387 (1974).
19. R. F. Begley, A. B. Harvey, R. L. Byer, and B. S. Hudson, J. Chem. Phys. 61, 2466 (1974).
20. I. Chabay, G. Klauminzer, and B. S. Hudson, Appl. Phys. Lett. 28, 27 (1976).
21. S. E. Harris and B. S. Hudson, "(CARS) coherent anti-Stokes Raman spectroscopy," Chromatix Application Note No. 6 (1975).
22. "Coherent anti-Stokes Raman spectroscopy (CARS)," Molectron Corp. Applications Note No. 111.
23. G. Hauchecorne, F. Kerherve, and G. Mayer, J. Phys. 32, 47 (1971).
24. B. S. Hudson, W. Heatherington, S. Cramer, I. Chabay, and G. Klauminzer, Proc. Natl. Acad. Sci. U.S. 73, 3798 (1976).
25. I. Itzkan and D. A. Leonard, Appl. Phys. Lett. 26, 106 (1975).
26. M. D. Levenson, IEEE J. Quant. El. QE-10, 110 (1974).
27. M. D. Levenson and N. Bloembergen, J. Chem. Phys. 60, 1323 (1974).
28. M. D. Levenson and N. Bloembergen, Phys. Rev. 10, B4447 (1974).
29. R. T. Lynch, Jr., S. D. Kramer, H. Lotem, and N. Bloembergen, Opt. Commun. 16, 372 (1976).
30. G. M. Krochik and Yu, G. Khronopulo, Sov. J. Quant. El. 5, 917 (1975).
31. J. E. Moore and L. M. Frass, Anal. Chem. 45, 2009 (1973).
32. A. Nabara and K. Kubota, Jap. J. Appl. Phys. 6, 1105 (1967).
33. R. W. Terhune and P. D. Maker, in *Nonlinear Optics*, A. K. Levine, Ed. (Dekker, New York, 1968, Vol. 2, p. 295.
34. J. J. Barrett and R. F. Begley, Appl. Phys. Lett. 27, 129 (1975).
35. F. Capasso and F. DeMartini, Opt. Commun. 9, 172 (1973).
36. F. DeMartini, "High Resolution Nonlinear Spectroscopy of Molecular Vibrational Resonances in Gases," Lecture-Esfahan Symposium on Fund and Applied Laser Physics, Esfahan, Iran (1971).
37. F. DeMartini, G. P. Giuliani, and E. Santamato, Opt. Commun. 5, 126 (1972).
38. F. DeMartini, E. Santamato, and F. Capasso, IEEE J. Quant. El. QE-8, 542 (1972).
39. F. DeMartini, F. Simoni, and E. Santamato. Opt. Commun. 9, 176 (1973).
40. F. Moya, S. A. J. Druet, and J-P. E. Taran, Opt. Commun. 13, 169 (1975).
41. F. Moya, S. A. J. Druet, and J-P. E. Taran, in *Laser Spectroscopy*, S. Haroche, J. C. Pebay-Peyroula, T. W. Hansch and S. E. Harris, Eds. (Springer-Verlag, New York, 1975), p. 66.
42. F. Moya, S. Druet, M. Pealat, and J-P. E. Taran, "Flame investigation by coherent anti-Stokes Raman scattering," AIAA Paper No. 76-29, Presented at the AIAA 14th Aerospace Sciences Meeting and 12th Annual Meeting Aerospace 1976, Washington, D.C., 26–30 January 1976.
43. W. M. Shaub, J. W. Nibler, and A. B. Harvey, J. Chem. Phys. in press.
44. W. G. Rado, Appl. Phys. Lett. 11, 123 (1967).
45. P. Regnier, "Application of coherent anti-Stokes Raman scattering to gas concentration measurements and to flow visualization," Office National D'Etudes Et De Recherches Aerospatiales, Technical Note No. 215, 92320 Chatillon, France (1973).
46. P. Regnier, F. Moya, and J-P. E. Taran, AIAA J. 12, 826 (1974).
47. P. Regnier and J-P. E. Taran, Appl. Phys. Lett. 23, 240 (1973).
48. P. Regnier and J-P. E. Taran, in *Laser Raman Gas Diagnostics*, (M. Lapp and C. M. Penney, Eds. (Plenum, New York, 1974), p. 87.
49. W. B. Roh, P. W. Schreiber, and J-P. E. Taran, Appl. Phys. Lett. 29 (1976).
50. H. Matsui, E. L. Resler, Jr., and S. H. Bauer, J. Chem. Phys. 63, 4171 (1975).
51. J. Lukasik and J. Ducuing, J. Chem. Phys. 60, 331 (1974).
52. R. Frey, J. Lukasik, and J. Ducuing, Chem. Phys. Lett. 14, 514 (1972).
53. F. DeMartini and J. Ducuing, Phys. Rev. Lett. 17, 117 (1966).
54. M. M. Audibert, C. Joffrin, and J. Ducuing, Chem. Phys. Lett. 25, 158 (1974).
55. M. M. Audibert, C. Joffrin, and J. Ducuing, Chem. Phys. Lett. 19, 26 (1973).
56. R. G. Miller and J. K. Hancock, J. Chem. Phys. in press.
57. R. Wallenstein and T. W. Hansch, Opt. Commun. 14, 353 (1975).
58. J. A. Armstrong, N. Bloembergen, J. Ducuing, and P. S. Pershan, Phys. Rev. 127, 1918 (1962).
59. R. W. DeWitt, A. B. Harvey, and W. M. Tolles, "Theoretical development of third-order susceptibility as related to coherent anti-Stokes Raman spectroscopy," NRL Memorandum Report, No. 3260 (April 1976).
60. N. Bloembergen, *Nonlinear Optics*, (Benjamin, New York, 1965).
61. C. Flynzanis, in *Quantum Electronics – A Treatise*, H. Rabin and C. Tang, Eds. (Academic Press, New York, 1975), Vol. 1, p. 9.
62. R. W. Minck, R. W. Terhune, and C. C. Wang, Appl. Opt. 5, 1595 (1966).
63. R. H. Pantell and H. E. Putoff, *Fundamentals of Quantum Electronics*, (Wiley, New York, 1969).
64. A. Yariv, *Quantum Electronics*, (Wiley, New York, 1975), 2nd Ed.
65. V. R. Shen, Rev. Mod. Phys. 48, 1 (1976).
66. F. Zernike and J. E. Midwinter, *Applied Nonlinear Optics*, (Wiley, New York, 1973).
67. A. Yariv, *Introduction to Optical Electronics*, (Holt, Rinehart and Winston, New York, 1971).
68. H. Kogelnik and T. Li, Proc. IEEE 54, 1312 (1966).
69. G. C. Bjorklund, IEEE J. Quantum El. QE-11, 287 (1975).
70. G. C. Bjorklund, "Effects of focusing on third-order nonlinear processes in isotropic media," Bell Laboratories TM 74-1313-23 (1974).
71. G. C. Bjorklund, "Vacuum ultraviolet holography," Microwave Laboratory Report 2339, Stanford University (1974).
72. W. M. Shaub, A. B. Harvey, and G. C. Bjorklund, J. Chem. Phys. in press.
73. G. Placzek, in *Handbook Der Radiologie*, Erich Marx, Ed. (Akademische Verlagsgellschaft, Leibig, 1934), Vol. 6, p. 209.
74. M. Maier, W. Kaiser, and J. A. Giordmaine, Phys. Rev. 177, 580 (1969).
75. W. F. Murphy, W. Holzer, and H. J. Bernstein, Appl. Spectrosc. 23, (1969).
76. D. L. Jeanmaire, M. R. Suchanski, and R. P. VanDuyne, J. Am. Chem. Soc. 97, 1699 (1975).
77. J. S. Rayside and W. H. Fletcher, "Linewidth and profiles of some simple gases at high resolution," paper presented at the Fourth International Conference on Raman Spectroscopy, 25–29 August 1974, Brunswick, ME, Paper 1.2.14 and private communication.
78. P. Lallemand, in *The Raman Effect*, A. Anderson, Ed. (Dekker, New York, 1971), vol. 1, p. 287.
79. T. W. Hansch, Appl. Opt. 11, 895 (1972).
80. R. Wallenstein and T. W. Hansch, Appl. Opt. 13, 1625 (1974).
81. M. Lapp and C. M. Penney, Eds., *Laser Raman Gas Diagnostics* (Plenum, New York, 1974).
82. A. R. Bandy and M. E. Hillard, Jr., "Theoretical predictions of the performance of the Raman scattering technique for measuring temperature and molecular number density," LWP-1020, Langley Research Center, NASA (1971).
83. E. E. Hagenlocker, R. W. Minck, and W. G. Rado, Phys. Rev. 154, 226 (1967).
84. J. F. Ward and G. H. C. New, Phys. Rev. 185, 57 (1969).
85. D. G. Fouche and R. K. Chang, Appl. Phys. Lett. 18, 579 (1971).
86. C. M. Penney, R. L. St. Peters, and M. Lapp, J. Opt. Soc. Am. 64, 712 (1975).
87. A. Owyoung, Opt. Commun. 16, 266 (1976).
88. B. Hudson, J. Chem. Phys. 61, 5461 (1974).
89. B. Hudson, private communication.
90. D. L. Hartley, "The role of physics in combustion," American Physical Society Study (1974).
91. D. Hartley, M. Lapp, and D. Hardesty, Phys. Today 37 (Dec. 1975).
92. R. Goulard, Ed., *Proceedings of a Project Squid Workshop on "Combination Measurements in Jet Propulsion Systems,"* held at Purdue University, West Lafayette, IN, 22–23 May (1975).
93. J. W. Nibler, J. R. McDonald, and A. B. Harvey, "Development of a diagnostic tool for measuring temperature and number density in the EDGDL," Semiannual Technical Report for DARPA Order No. 2062.